POPULATION DISTRIBUTION OF THE COPEPOD CALANUS FINMARCHICUS IN THE LABRADOR SEA: A MODELLING STUDY

DEREK TITTENSOR

Your file Votre référence
ISBN: 0-612-84044-1
Our file Notre référence
ISBN: 0-612-84044-1

POPULATION DISTRIBUTION OF THE COPEPOD *CALANUS FINMARCHICUS* IN THE LABRADOR SEA: A MODELLING STUDY

By

© Derek Tittensor

A thesis submitted to the School of Graduate Studies in partial fulfillment of the requirements for the degree of Master of Science

Computational Science

Memorial University of Newfoundland

March, 2002

St. John's **Newfoundland** **Canada**

Abstract

Calanus finmarchicus is a zooplankter that forms a critical part of the North Atlantic ecosystem, and provides a key link in the transfer of energy between trophic levels. The Labrador Sea contains a large population of *Calanus finmarchicus*, but existing data for the central and northern parts of this region are sparse. There are, as yet, few wintertime observations due to the difficulties of data collection. Modelling studies provide a useful method to assess ecological and oceanographic processes and can give insight into the spatial structure of populations. This study couples a biological model of *Calanus finmarchicus* with a circulation model of the Labrador Sea and its environs in an attempt to understand interactions between the physical oceanographic transport processes of the region and zooplankton behaviour, life-history and distribution. The study aims to produce a large-scale, comprehensive picture of the spatial distribution of *Calanus finmarchicus* in the Labrador Sea, along with an exploration of the timing of diapause, and an examination of transport processes and their effect on population sustainability. The modelled population structure matches reasonably well to temporal and spatial patterns in the Labrador Sea derived from available data sets. During an annual cycle, surface currents can cause a population to be advected onto shelf and slope regions from the deeper ocean. A latitudinally-dependent diapause emergence scheme with early emergence to the south of Newfoundland provides the best fit to data.

Acknowledgements

I would like to thank Brad deYoung for guiding me through a stimulating and rewarding degree program, providing me with a challenging research project, and instilling in me a valuable sense of intellectual independence. Dr. deYoung and the School of Graduate Studies also provided me with financial support without which this degree would not have been possible. A number of people at the Department of Fisheries and Oceans made helpful contributions: Pierre Pepin switched me on to the SeaWiFS data set which aided immensely during the course of my research, and Glen Harrison kindly generated new SeaWiFS data boxes at very short notice. Charles Tang provided the results from the physical model, Brendan deTracey support and assistance with said model, and Piotr Trela the biological model. Geoff Evans provided useful commentary during the early stages of my work.

I would like to thank Danielle Finney and Daniel Jubainville for accompanying me through this process; each provided support in their own special way, and a refuge from the rigours of academic life. My family, Ralph, Ruth, Rosemary and Andrew Tittensor, have always helped me in whatever I am doing, and kept me pointed in the right direction.

I am grateful to all.

Table of Contents

List of tables

List of figures

List of Abbreviations

CPR	Continuous Plankton Recorder
DFO	Department of Fisheries and Oceans
NAO	North Atlantic Oscillation
NASA	National Aeronautics and Space Administration
NCAR	National Center for Atmospheric Research
NCEP	National Centers for Environmental Prediction
NOAA	National Oceanic and Atmospheric Administration
NPZ	Nutrient-Phytoplankton-Zooplankton
OWS-B	Ocean Weather Station Bravo
POM	Princeton Ocean Model
SeaWiFS	Sea-viewing Wide Field-of-view Sensor
SST	Sea Surface Temperature

Chapter 1

Introduction

1.1 Overview

Plankton are oceanic organisms that drift with the current, with a size range spanning several orders of magnitude from micrometres (picoplankton) to millimetres (zooplankton) to centimetres or metres (jellyfish). Many fish species have planktonic larval forms. Plankton play a critical role in the marine food-web as primary producers (phytoplankton), by providing a food source for the larvae of higher trophic levels (Mann & Lazier, 1996; Balino *et al.*, 2000) - including economically important species such as cod and haddock – and as remineralizers of detritus (bacteria) and organic matter (zooplankton). Detailed information about their spatial distribution, life-history and production is therefore essential to improve understanding of ecosystem fluctuations and to aid in fisheries resource management.

Most plankton have developed the ability to change their vertical position within the water column, though they are typically passive drifters in response to horizontal currents and consequently their distributions are strongly influenced by physical oceanic

transport processes. The coupling of biological and physical models is therefore a useful technique for exploring the influence of circulation on biomass distributions.

Phytoplankton are one of the dominant groups of primary producers in the oceans, microscopic plants that photosynthesise and form the base of the marine food webs. Studies such as the Joint Global Ocean Flux Study (JGOFS) have highlighted the importance of phytoplankton as part of the 'biological pump', a cycle which exchanges carbon between the atmosphere, surface ocean, and deep ocean (Ducklow *et al.*, 2001). The biological and physical pumps are part of the global carbon cycle, and may provide a sink for anthropogenic CO_2 (Feely *et al.*, 2001).

In the temperate waters of the North Atlantic, there is a pronounced increase in phytoplankton productivity during the spring (Mann & Lazier, 1996). A decrease in wind mixing and an increase in solar heating during the spring often cause a shallowing of the mixed layer that leads to phytoplankton being concentrated in nutrient-rich, sunlight-rich waters and a large amount of photosynthetic activity and production known as the spring bloom takes place (Mann & Lazier, 1996). The spring bloom does not occur in all temperate regions; for example, large areas of the North Pacific have no spring bloom (Mann & Lazier, 1996). Tropical latitudes tend to be less productive than temperature regions as well as showing less variability in seasonal phytoplankton productivity, since meteorological differences between seasons are less pronounced. Coastal regions, however, may be more productive due to high nutrient concentrations from river run-off.

Figure 1.1 shows a global picture of 2001 chlorophyll *a*. The concentration of chlorophyll *a* in the water column can be used as a proxy for phytoplankton abundance and biomass, since the ratio of chlorophyll to phytoplankton biomass is a relatively constrained parameter. Values of chlorophyll *a* are lower in tropical areas than at higher latitudes (except around coastal regions where river run-off can add nutrients to the water). This picture is derived from the satellite-borne SeaWiFS remote colour sensor (Hooker *et al.*, 1992).

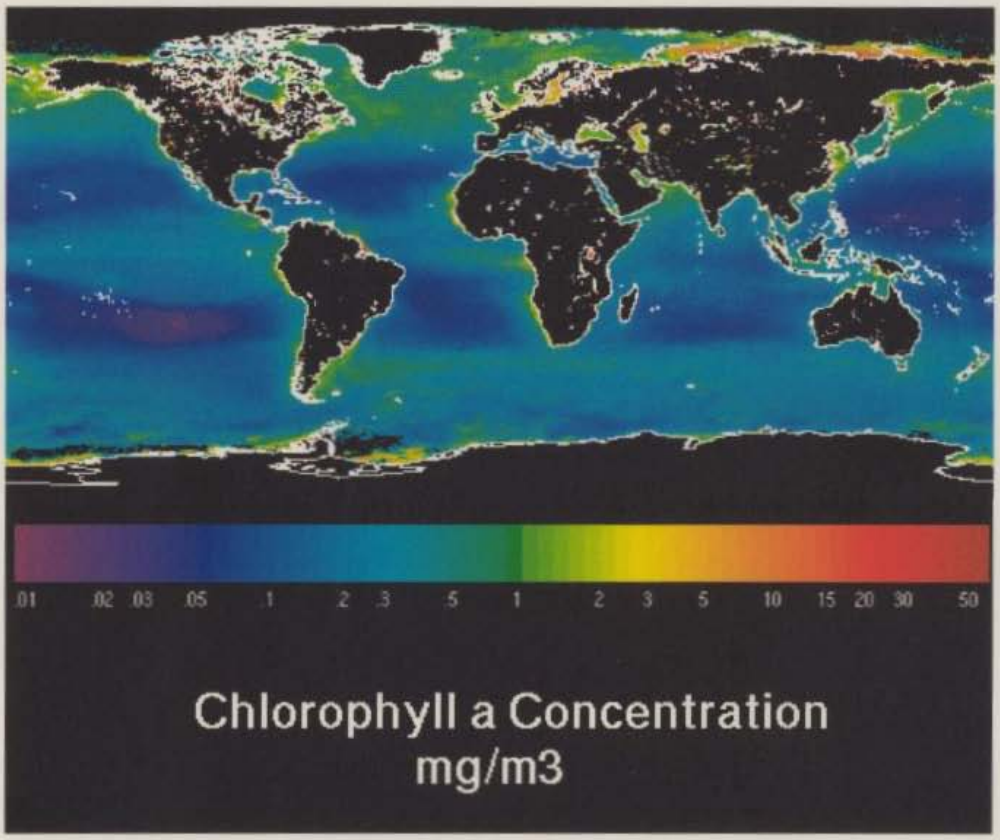

Figure 1.1: Global composite of 2001 chlorophyll *a* concentration; NASA, SeaWiFS.

Zooplankton are small animals (generally in the millimetre size range) that graze primarily upon phytoplankton (Marshall & Orr, 1955), though the larger meso- and macrozooplankton may also predate on microzooplankton. One of the key zooplankton species of the northern hemisphere is *Calanus finmarchicus*, an important member of the zooplankton community in the North Atlantic (Jashnov, 1970; Planque *et al.*, 1997) North Sea (Gallego *et al.*, 1999; Heath *et al.*, 1999), Norwegian Sea (Slagstad & Tande, 1996), and Labrador Sea (Kielhorn, 1952; ICNAF, 1968; Huntley *et al.*, 1983; Head *et al.*, 2000). *Calanus finmarchicus* holds an important position in the marine food web and helps to facilitate the transfer of primary production (phytoplankton) to higher trophic levels (e.g. fish, marine mammals).

Zooplankton of the order *Copepoda* (to which *Calanus finmarchicus* belongs) may be the most numerous multicellular organisms on earth (Mauchline, 1998). Figure 1.2 represents some of the important physical and biological oceanographic features that affect *Calanus finmarchicus* growth and distributions. In general, the surface layer is warmer than at depth (except during the winter at high latitudes), receives more light, and thus has a higher spring and summer phytoplankton production. This provides more food for zooplankton, though predation is also higher in this layer. At depth, the water is cooler and darker, with much less food availability, but correspondingly lower predation. Many zooplankton exhibit seasonal overwintering behaviour, migrating to depth in the autumn and reducing their metabolism, a behaviour known as diapause. This may aid in

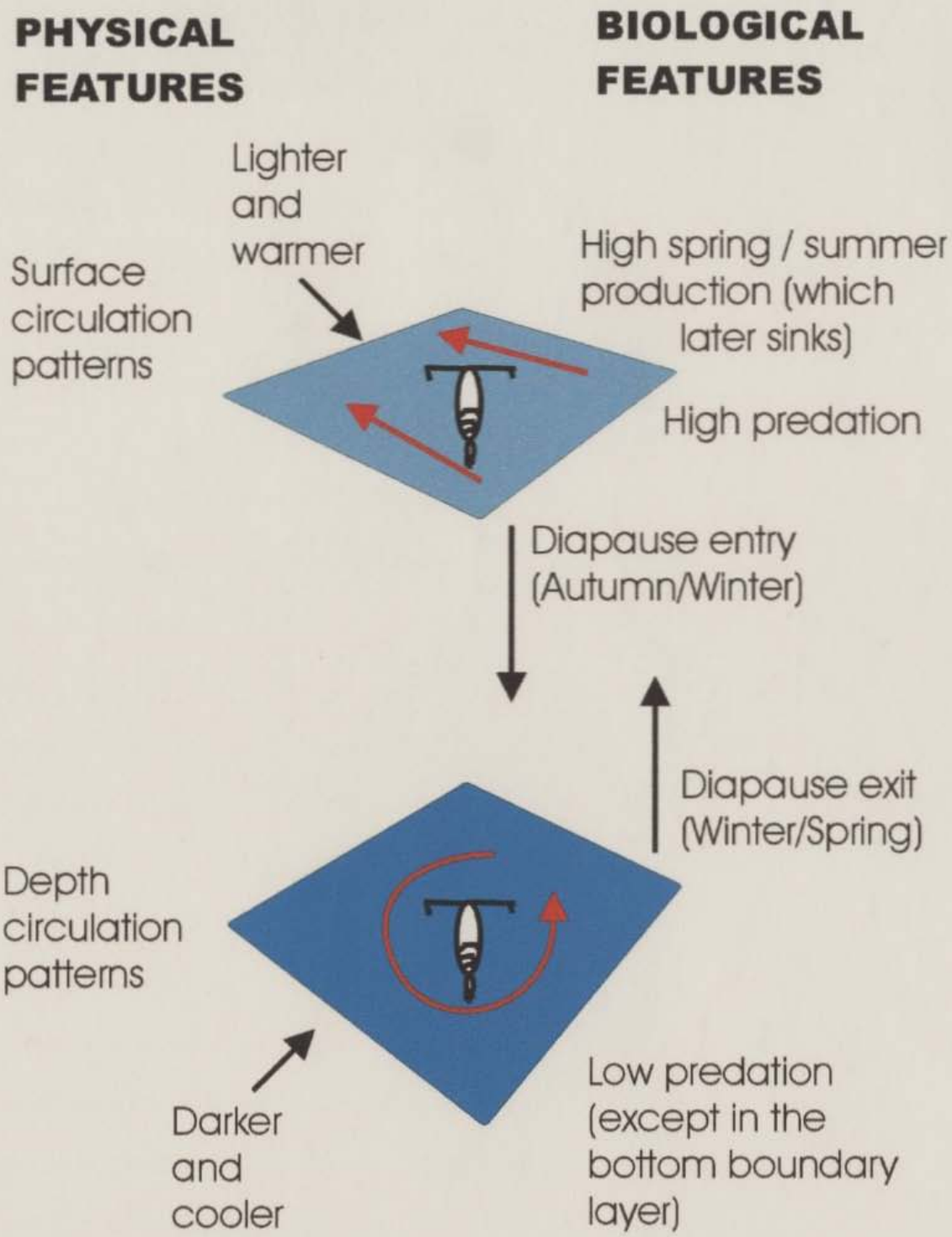

Figure 1.2: Interaction between zooplankton and physical oceanographic features.

survival during the low-temperature low-food periods that are characteristic of high-latitude winter, and could also help to reduce predation during these periods (Hirche, 1996). The migration to depth can cause the zooplankton to pass through, and reside in, different oceanic transport regimes; this is an example of how biology (seasonal behaviour) and physics (vertically differentiated transport and stratification) can interact to have an impact upon population distributions. Migrations at both daily and annual time-scales may have substantial ecological implications (Leggett, 1977; Angel, 1989).

Calanus finmarchicus distributions have been measured for almost 50 years by the Continuous Plankton Recorder (CPR) survey. The CPR survey consists of boxes that are towed behind merchant ships in the North Atlantic, which collect plankton on a silk spool to be counted and identified in the laboratory. The distribution of *Calanus finmarchicus* as derived from CPR data (Planque, 1997) shows considerable spatial heterogeneity, with three regions of high abundance - the southern part of the Labrador Sea and the waters between southwest Greenland and Newfoundland, the area to the west coast of Norway, and Georges Bank – which are separated by areas of lower concentration (Figure 1.3). CPR data, however, is dependent upon ships of opportunity, which rarely venture into the mid and northern Labrador Sea, especially when it is ice-covered during the winter, so long-term, detailed data sets for these locations are not available. The data does also not take into account vertical shifts in the position of zooplankton, many of which migrate into and out of the surface layer on a daily basis. Additionally, during the winter *Calanus finmarchicus* are often located at depth during

diapause (Hirche, 1996), and since the CPR comprises tow data from the top 10 metres or so it only represents surface population features and activity.

Figure 1.3 clearly shows the importance of *Calanus finmarchicus* in the Labrador Sea. This is confirmed by other surveys (Kielhorn, 1952; ICNAF, 1968; Huntley *et al.*, 1983) in which *Calanus finmarchicus* is the dominant zooplankton in the region. The need for a comprehensive depiction of seasonal distributions throughout the entire Labrador Sea is thus clear.

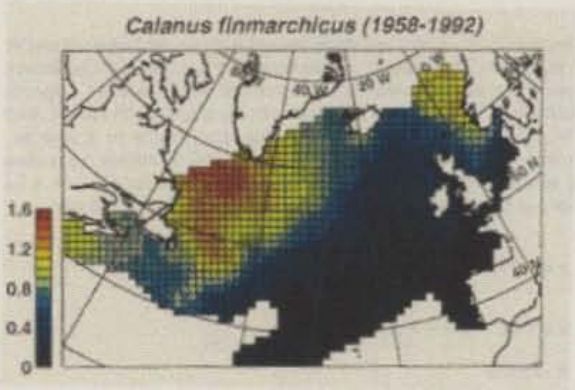

Figure 1.3: Spatial distribution of *Calanus finmarchicus*, January 1958 to December 1992, compiled CPR data. Abundance is indicated by the colour scale and is given in $Log_{10}(x+1)$ where x is the number of organisms per sample. Only pixels with at least 36 months of data are shown. From Planque (1997).

As previously mentioned, *Calanus finmarchicus* is also important in the North Atlantic as a whole (Planque, 1997). An approach to modelling and sampling within this

region is to consider the population as inhabiting three gyres (Head *et al.*, 2001) which are depicted schematically in Figure 1.4; a Norwegian Sea gyre, a Western North Atlantic Gyre, and a Labrador/Irminger Sea Gyre. It has been proposed that exchange between these gyres is restricted relative to intra-gyre exchange (Head *et al.*, 2001). Given the importance of *Calanus finmarchicus* in the Labrador Sea, and that this region is part of a large, enclosed gyre, I propose to study populations in this location.

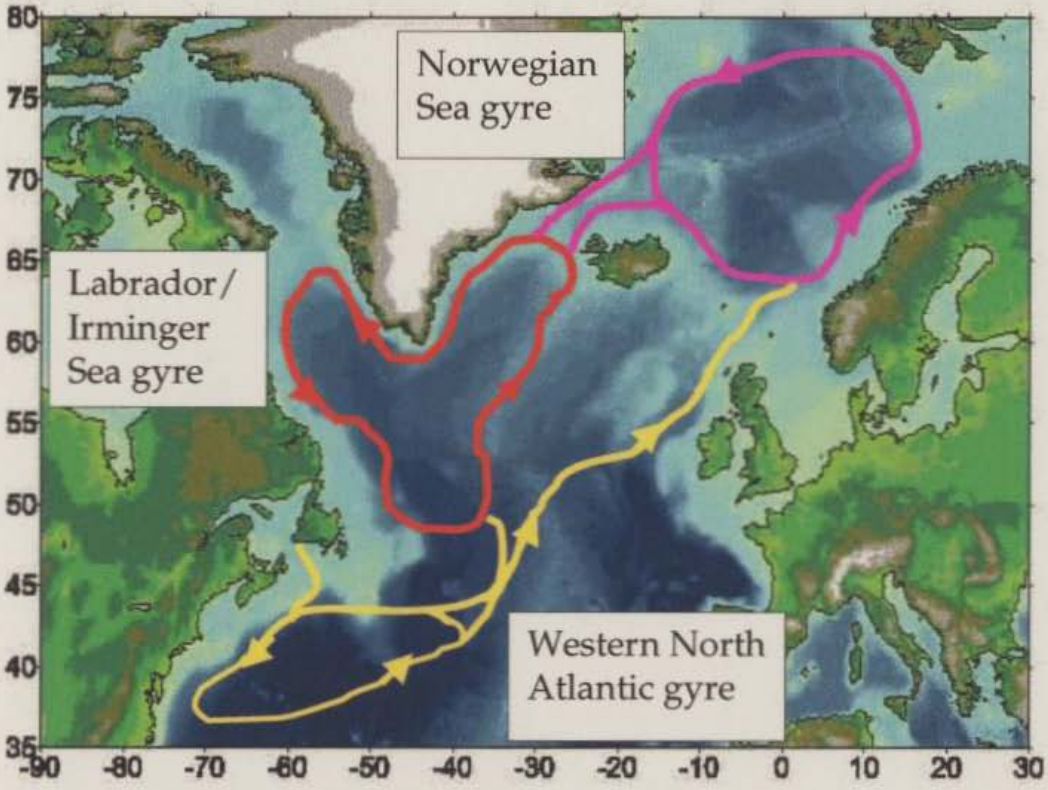

Figure 1.4: Schematic of the gyre system in the North Atlantic. Purple represents the Norwegian Sea gyre, yellow the Western North Atlantic gyre, and red the Labrador/Irminger Sea gyre.

This study aims to examine the effect of circulation patterns, biological processes, and seasonal water properties upon the distribution of *Calanus finmarchicus* within the Labrador Sea. To achieve these goals, I have used existing data to parameterise and calibrate a biological model of *Calanus finmarchicus*. This model is then coupled with a three-dimensional physical circulation model that provides velocity and temperature fields. A spatially-explicit, bimonthly chlorophyll data set derived from SeaWiFS satellite observations is used as a proxy for food availability. The modelled system output is then compared with available observations from the Labrador Sea and its environs, in an attempt to reproduce, explore, and understand large-scale features of *Calanus finmarchicus* distributions in the region.

1.2 Objectives of this study

The objectives of this study are threefold:

(i) *Calanus finmarchicus* is an important zooplankton in the Labrador Sea (Kielhorn, 1952; ICNAF, 1968; Huntley *et al.*, 1983), but a complete map of its distribution over the region does not exist. I will attempt to match existing spatial population data, especially Planque (1997), and attempt to predict large-scale population patterns for regions in which there is no data, by utilising a coupled biological and physical model system.

(ii) I will examine the impact of the model parameterisations and sensitivities in order to gain an understanding of these functions on model behaviour. I will attempt to replicate existing features of data sets and the literature. I will pay especial attention to the timing of emergence from diapause in the region, and how this affects the fit of the model to data. Diapause is a key behavioural component of the *Calanus finmarchicus* life-cycle, and can play an important role in determining population sustainability (Hirche, 1996).

(iii) I will look to assess whether a population in the Labrador Sea can be self-sustaining, and examine the effect of advection of individuals from outside the region upon population viability.

To achieve these objectives, I have endeavored to remove much of the natural stochastic fluctuation that is inherently present in both the biological and physical systems, and focus upon the mean state of the coupled model. The physical model therefore represents averaged seasonal circulation states, the phytoplankton data from the SeaWiFS satellite is compiled from a three-year period into a bimonthly format, and the biological model operates within the framework of a set of parameterisations and sensitivity tests, in order to reduce result uncertainty. The models and data structures are briefly described in sections 1.5 & 1.6, with more detail provided in chapters 2 & 3.

1.3 Regional Physical Processes

It has been determined from observational evidence (Lazier 1973) and modelling studies (Oberhuber 1993) that the circulation in the northern Labrador Sea is cyclonic. The East Greenland current flows southwards along the eastern coast of Greenland, joins with the Irminger Current, and passes the island's southernmost tip, at which point it becomes the West Greenland Current (WGC), flowing northwards along the western coast of Greenland (Cuny *et al.*, 2002). The WGC divides at around 60°N, one part flowing northwards as described, the other heading on a more westerly trajectory towards the continental slope off Labrador, where it makes up some 80% of the Labrador Current (Lazier, 1982). The Baffin Island Current, flowing southwards from Baffin Bay, forms the other 20% of the Labrador Current, which then flows along the continental shelf and slope towards Flemish Cap. At Flemish Cap, it splits, with one branch heading eastwards, and the other southwards and then south-eastwards past Nova Scotia. The North Atlantic Current (NAC), which is formed at the turning point of the Gulf Stream in the Newfoundland Basin, heads north then north-west past the Flemish Cap to around 52°N, at which point it turns sharply towards the east in a 140km diameter curve (Lazier, 1992) then leaves the Labrador Sea. The main regional circulation features are shown in Figure 1.5.

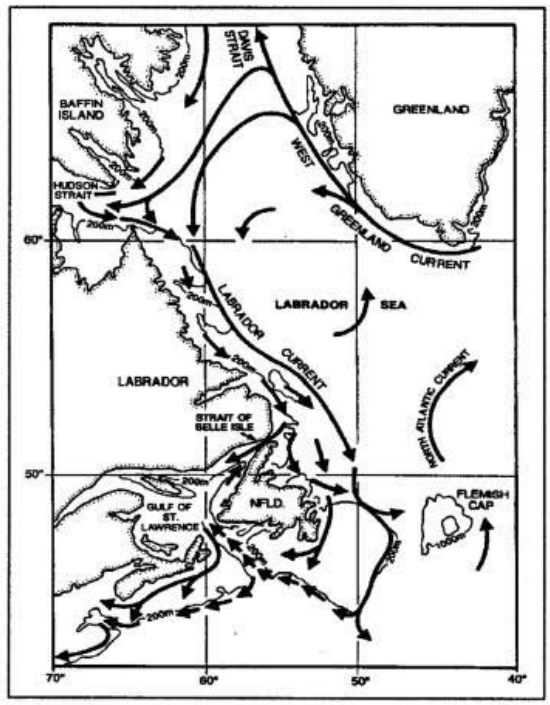

Figure 1.5: Circulation patterns within the Labrador Sea. Modified from Chapman & Beardsley (1989).

The Labrador Sea spans a region of greater than 1,000,000 km^2, with a maximum depth of 3000m. The circulation is driven by wind forcing over the Labrador Sea, regional freshwater inputs, and convection associated with winter cooling (Lazier & Wright, 1993). Sea ice formation and melting also plays a significant role (Yao *et al.*, 2000). The Labrador Sea is of major interest oceanographically for its deep convection processes (Clarke & Gascard, 1983; Marshall *et al.*, 1998); it is one of the few places in the world where winter mixing may reach down to 1000 metres or more. This mixing

plays an important role in regulating seasonal phytoplankton productivity; if a large proportion of their time is spent below the critical photosynthetic depth (Mann & Lazier, 1996) production will be limited.

Extensive hydrographic and transport data for the Labrador Current and Labrador Sea are available: among others, observations of annual velocity variations (Lazier & Wright, 1993), transport along a transect from Cape Farewell to Flemish Cap (Clarke, 1984), hydrographic and current-meter data (Clarke & Gascard, 1983), modelling studies (Tang *et al.*, 1999 ; Yao *et al.*, 2000) and seasonal temperature and salinity variations (Lazier, 1982). Ocean Weather Station Bravo (OWS-B), located at 56°30'N, 51°00'W (approximately the centre of the region of interest) has an extensive time-series of temperature and salinity data, analysed by Lazier (1980). Loder *et al.* (1998) consider surface heat fluxes and sea ice melting to be extremely important factors in influencing the Labrador Current. Another feature in the region is possible decadal variability in salinity (Clarke, 1984).

From observation of the "Great Salinity Anomaly" in the North Atlantic (Dickson *et al.*, 1988), it is possible to calculate the apparent time-scale for the circulation of water within the Labrador Sea (Dickson *et al.*, 1988; Belkin *et al.*, 1998). Following the course of a large salinity anomaly in both the 1970's (Dickson *et al.*, 1988) and 1980's (Belkin *et al.*, 1998) would seem to indicate a period of 2 to 3 years for the transport of water from the west coast of Greenland cyclonically down to Newfoundland and onwards (out

of the modelled region). When considering *Calanus finmarchicus* that are advected from the Irminger Sea into the Labrador Sea, multiple generations produced from these individuals would likely become resident in the Labrador Sea before exiting the region.

1.4 Regional Biological Features

Calanus finmarchicus is the dominant zooplankter over much of the North Atlantic (Planque, 1997), and the literature seems to indicate that this also holds true for the Labrador Sea (Kielhorn, 1952; Huntley *et al.*, 1983). *Calanus finmarchicus* is a zooplankter with a complex life-history, consisting of thirteen differentiated stages; an egg stage, six nauplii (juvenile) stages, five copepodite stages and an adult stage. Late stage copepodites, mainly stage five (CV), also overwinter at depth (Hirche, 1996). The life history is shown diagramatically in Figure 1.6.

Diapausing individuals migrate from depth (around 500-1500m in the open ocean and continental slope; Hirche, 1996) during the spring (the timing varies regionally), and upon reaching the surface layer they moult to adulthood and begin to reproduce. The overwintering generation is labelled G0 and the new generation G1 (terminology due to McLaren). Individuals of the new generation moult successively through nauplii and copepodite stages, and upon reaching CV, either enter diapause (to become next years G0 generation) or moult to an adult to produce a second (G2) generation. The production of a second generation appears to be latitudinally and regionally dependent (Head *et al.*, 2000). The growth of *Calanus finmarchicus* changes with both food availability and temperature (Mauchline, 1998). In a food-saturated environment at 5°C Corkett *et al.* (1986) estimate growth from egg to adult would take around 62.6 days; at 10°C it would be around 35.4 days.

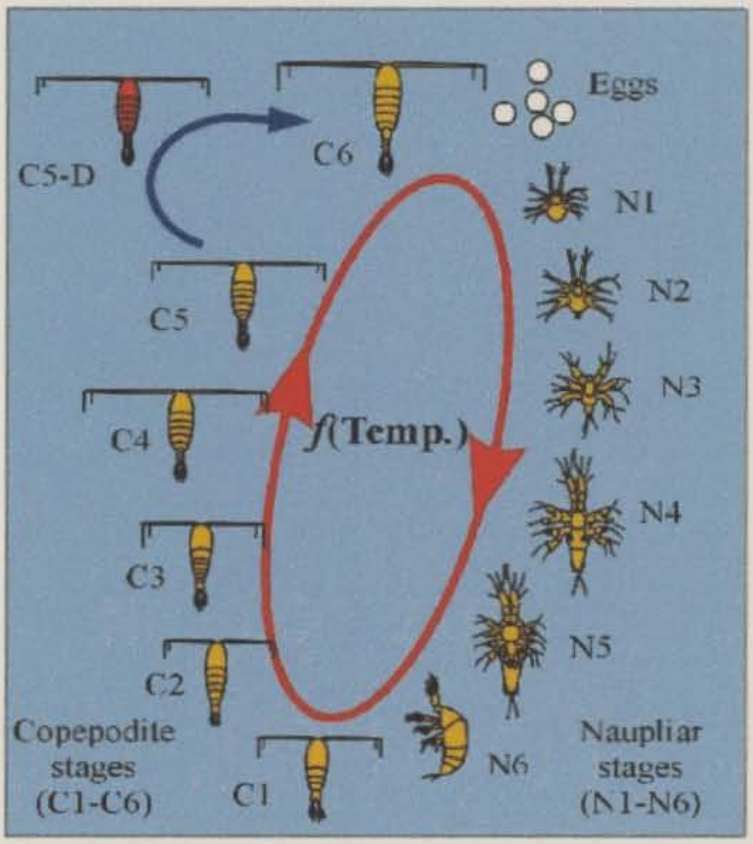

Figure 1.6: *Calanus finmarchicus* life history.

Planque (1997) undertook statistical analysis of Continuous Plankton Recorder (CPR) data that revealed a region of high population density in the waters of the southern Labrador Sea. The central and northern parts of the Labrador Sea have not, however, been included in the CPR surveys since they do not lie on shipping routes. Myers *et al.* (1994) provide an analysis of CPR data in the northwest Atlantic, for which both phytoplankton and *Calanus spp.* data are provided.

Kielhorn (1952) assessed the biology at OWS-B over the course of a year. *Calanus finmarchicus* is a major component of the population during the year surveyed (1950/1951). Transects across the Labrador Sea include those of Head *et al.* (2000), Stuart *et al.* (2000) and the International Commission for the Northwest Atlantic Fisheries (ICNAF, 1968). These surveys provide data for model calibration, though they are all short-term (< 2 month) cruises. Data for the northern part of the Labrador Sea is very sparse, though Huntley *et al.* (1983) examined the community structure of zooplankton in the Davis Strait region. Buchanan & Brown (1981) studied the zooplankton of the Labrador coast and shelf in 1979, and found that calanoid copepods dominated in both density and biomass. The region contained a mixture of both arctic and Atlantic species.

Ecological studies of *Calanus* spp. in the Labrador Sea have been undertaken (Head *et al.* 2000), pointing to the relationship between the spring phytoplankton bloom and *Calanus finmarchicus* development. In particular, it has been suggested that the timing of the spring bloom is critical for the development of *C. finmarchicus*, in such a way that a late bloom will not provide enough food for the development of the G1 generation (Head *et al.*, 2000), though Huntley & Boyd (1984) contend that food limitation may be less significant for herbivorous zooplankton in coastal seas than in the open ocean. Campbell & Head (2000) estimate egg production rates in the Labrador Sea to be significantly higher than previously considered for *C. finmarchicus*.

1.5 The Models

1.5.1 The physical model

Yao *et al.*'s (2000) three-dimensional, seasonally-averaged diagnostic model, a coupled multicategory ice model and Princeton Ocean Model (Blumberg & Mellor, 1987; Mellor, 1996) is used to provide topography, seasonally averaged circulation patterns, and temperature fields for the Labrador Sea region. Use of a diagnostic model allows for reproduction of essential features in current velocity while eliminating temporal forcing, thereby reducing the complexity of analysis, a useful feature in a coupled model system. The time-step for advective processes to move *Calanus finmarchicus* in the coupled model system is one-quarter of a day. The model is further described in Chapter 2.

1.5.2 The *Calanus finmarchicus* model

Many different methods exist for modelling zooplankton population dynamics (Harris *et al.*, 2000), a large proportion of which have been applied to the life-history of *Calanus finmarchicus*, including weight structured models (Heath *et al.*, 1997; Trela *et al.*, 2001), stage structured models (Zakardjian *et al.*, 2001), stage and age structured models (Miller & Tande, 1993), Lagrangian ensemble models (Carlotti & Wolf, 1998) and individual-based models (Miller *et al.*, 1998). For this study, the model is based on that of Trela *et al.* (2001), a linearly-distributed weight-based model which provides a

reasonable balance between minimising computational demands (important for insertion within a three-dimensional system) and provision of an accurate representation of population dynamics. Life history features such as diapause, non-feeding stages, and stage-specific moulting weights have been added to the model. The extensive literature on modelling *Calanus finmarchicus* provides a benchmark with which to validate accuracy. The model is described in more detail in Chapter 2.

1.6 Integrating the models & data sets

Additional data are required to complete the coupled-model system; more specifically, phytoplankton concentration plays an important role in *Calanus finmarchicus* growth. *Calanus finmarchicus* is predominantly herbivorous (Mauchline, 1998), though when diatoms are rare and protists abundant then they can also be consumed (Ohman & Runge, 1994). Phytoplankton density is derived from SeaWiFS images (Hooker *et al.*, 1992), within the box locations described by Petrie & Mason (2000) and used as a food source proxy. This food source is intended to be representative of food availability, and, along with tuned food uptake parameters, provide a reasonable rate of *Calanus finmarchicus* growth and stage progression. These, and further data boxes, have been processed and provided by P. Pepin and G. Harrison (Department of Fisheries and Oceans, herein DFO). The analysis of this data and its extension to cover the whole of the Labrador Sea is described in Chapter 3.

The spatial domain of the coupled-model region covers an area ranging from 44°N to 66°N, 40°W to 66°W. The physical model flow-fields advect *Calanus finmarchicus* populations every one-quarter of a day, and the biological model is run with a time-step of one day. *Calanus finmarchicus* is advected by the modelled velocity fields, grows in relation to temperature and phytoplankton density, and follows an annual cycle that includes regionally dependent diapause entrance and emergence. For more details of the biological-physical model coupling and data integration, see Chapter 3.

1.7 Thesis outline

Chapter 2 provides the details of both the biological and physical models. Chapter 3 presents information on the integration of SeaWiFS chlorophyll data, and model coupling. The results of sensitivity tests of the model running in a one-dimensional (vertical) context are presented in Chapter 4. Chapter 5 contains an overview of existing literature on *Calanus finmarchicus* in the Labrador Sea, and presents two hypotheses on the timing of diapause emergence in the region. The full three-dimensional model system and model runs that have been undertaken in order to assess population distributions are then described and discussed. In Chapter 6, I provide a summary and conclusions. Chapter 7 lists the references that have been cited in this work.

Chapter 2

Biological & Physical Models

2.1 The Calanus finmarchicus model

2.1.1 A brief survey of *Calanus finmarchicus* models

Population models have been extensively utilised as a tool to analyse zooplankton population dynamics, with modelling approaches being divided into several categories, including: stage and weight structured models, matrix models, cohort models, individual based models (IBM's) and Lagrangian ensemble models (LEM's). These are all life history models that include information on weight/stage, and are more structurally complex than undifferentiated ecosystem models such as that of Fasham *et al.* (1990). Zooplankton models may further be integrated within community and ecosystem models. More recently, spatially explicit models have been created to examine regional population dynamics (Heath *et al.*, 1997; Lynch *et al.*, 1998; Miller *et al.*, 1998). Carlotti *et al.* (2000) provide an exhaustive reference of zooplankton modelling techniques.

Calanus finmarchicus models follow many of the above paradigms, with the model selection being dependent upon the situational requirements of the particular

system under study. Carlotti & Nival (1992) proposed an age-within-stage copepod model that has its basis in Carlotti & Sciandra (1989). The model was used to test the hypothesis of Carlotti *et al.* (1993) - that critical (temperature dependent) moulting weights for each stage of *Calanus finmarchicus* exist. Carlotti & Radach (1996) then coupled a LEM with a one-dimensional physical and biological model of the upper oceanic layer to examine *Calanus finmarchicus* populations within the North Sea, and concluded that *C. finmarchicus* was not the main limiting factor for the phytoplankton bloom in the northern North Sea. Another age-within-stage model is that of Miller & Tande (1993), which was fitted to data from the Malangen fjord system in Norway and used to study stage durations.

Weight-based models of *Calanus* include those of Bryant *et al.* (1997), a weight structured model of *Calanus finmarchicus* within the northern North Sea, and Heath *et al.* (1998), an explicit age and weight structured model of *Calanus* sp. in the Fair Isle current to the north of Scotland. Bryant *et al.* (1997) concluded that the spatially resolved model failed to reproduce major features of the observed distribution in the northern North Sea, and that improved forcing data was necessary, along with a greater understanding of *Calanus finmarchicus* physiology and mortality rates. Trela *et al.* (2001) created a weight-class population model that contained a linear weight distribution within each class in order to more accurately simulate weight-dependant processes. The model also has the dual advantages of being computationally efficient and reducing numerical diffusion.

The only LEM, to date, that has been utilised to study *Calanus finmarchicus* is that of Carlotti & Wolf (1998). In this case, the model is strongly (i.e. two-way) coupled with a phytoplankton population in a one-dimensional ecosystem model, and then examined within the context of data from OWS-India (about 400km south of Iceland). The model compared reasonably well with both existing data sets and Eulerian based models.

Miller *et al.* (1998) coupled a vector-based IBM of *Calanus finmarchicus* to a circulation-based model of the Gulf of Maine – Georges Bank region to facilitate understanding of resting stock locations. Another study within the Gulf of Maine was performed by Lynch *et al.* (1998), who utilised a stage-based model within a three-dimensional circulation model to examine the effect of the circulation field on *Calanus finmarchicus* distributions. Zakardjian *et al.* (2001) also coupled a *Calanus finmarchicus* and three-dimensional hydrodynamic model to examine a region that includes the Gulf of St. Lawrence, Scotian Shelf and the Gulf of Maine. The model fitted reasonably well to existing data, but tended to underestimate observed abundances.

Of the models listed above, three (Miller & Tande, 1993; Miller *et al.*, 1998; Zakardjian *et al.*, 2001) assume that growth is not food-limited and depends purely upon temperature, modelled in all cases with a Belehrádek function (Corkett *et al.*, 1986). The model of Lynch *et al.* (1998) utilises a temperature based growth rate which linearly decreases below a fixed non-limiting food concentration. The other five *Calanus*

finmarchicus models (Carlotti & Radach, 1996; Bryant *et al.*, 1997; Heath *et al.*, 1998; Carlotti & Wolf, 1998; Trela *et al.*, 2001) all factor both temperature and weight-dependant food ingestion into growth.

2.1.2 *Calanus finmarchicus* model selection

Two requirements that are often in opposition for any biological model are the ability to match to data, and computational efficiency. Complex models lead to increased numerical requirements and difficulty in interpreting results, yet may fit to data with more accuracy than simpler, numerically more efficient models. This tug-of-war between complexity and simplicity may be partially responsible for the many varieties of zooplankton models, and could be considered the main reason for the selection of the *Calanus finmarchicus* model used within the present study, which is based upon that of Trela *et al.* (2000) (herein TdeYE).

The model of TdeYE differs from the other models considered in the section above in that it is at heart a weight-based model, yet represents individuals within each class by a linear distribution rather than a single variable. This provides a reasonable balance between simplicity and accuracy, and has the useful properties of reducing numerical diffusion, weight dependent growth within each class, and an accurate representation of periods of starvation (TdeYE). The distribution within a weight class changes in relation to individual growth (which itself changes relative to the ambient

temperature and food availability), and should the new distribution broach either the upper or lower class boundary, transfer to the next class or starvation occurs respectively. Figure 2.1 shows the transfer from one class to the next in conceptual form. For a complete overview of this model, see TdeYE.

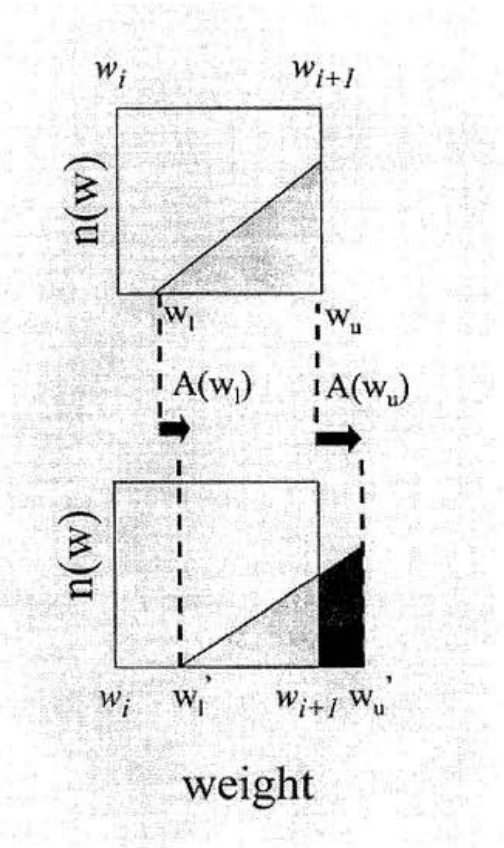

Figure 2.1: Transfer of individuals between classes (from TdeYE). w_i represents the lower weight boundary of the class, w_{i+1} the upper boundary, w_u and w_l the upper and lower boundaries of the weight distribution within the class, $n(w)$ the number of individuals at weight w, and A net assimilation. From TdeYE.

The model of TdeYE has been modified for this study to include features such as diapause, a female maturation period, and the integration of SeaWiFS phytoplankton data.

2.1.3 Model description

Eight classes are present within the model, each of which represents one or more stages in the life history of *Calanus finmarchicus*. This was considered to be the minimum number necessary to represent the important behavioural and physical differences between stages. The inclusion of separate classes for immature females and diapausing individuals allows for more accurate representation of sexual development and seasonal behaviour (Lynch *et al.*, 1998; Zakardjian *et al.*, 2001). The classes are described in Table 2.1

The class structure derives its validity from physiological similarities between stages within each class (Mauchline, 1998). Only stages that have similar metabolic processes are grouped together; thus the non-feeding egg and nauplii stages (Carlotti & Radach, 1996; Carlotti & Wolf, 1998) are contained within one class. In addition, the model encompasses differing growth rates for individuals of different weights due to the functional representation of bio-energetics; thus combining N3-N6 and CI-CIV is logical since their metabolic processes are similar within the envelope of weight dependent growth (Mauchline, 1998).

Table 2.1: Classes within the *Calanus finmarchicus* model.

Class Number	*Stage(s)*
1	Egg, N1, N2
2	N3-N6
3	CI-CIV
4	CV
5	CV (diapause)
6	Immature Female
7	Mature Female
8	Male

Each class is enclosed by a lower weight boundary, w_i, and an upper weight boundary, w_{i+1}. The weights are structural only, and do not include lipid stores. These boundaries represent moulting weights to and from class respectively, i.e. the weights at which an individual ceases to be a member of one class and progresses onward to the next. Carlotti *et al.* (1993) suggested that no overlapping takes place between the ranges of structural weights for successive copepodite stages at a given temperature. However, moulting weights for each stage are difficult to determine, since there is significant variation both regionally (Carlotti *et al.,* 1993), between individuals (McLaren, 1986), and as a function of temperature. McLaren *et al.* (1988) noted that it was

'disappointing to find a paucity of published information on such classical matters as lengths and weights of subadult stages, so useful for estimating growth rates'.

The model therefore utilises a weight-based structure that aims to provide a reasonable value for each stage, while allowing for differences between individuals. If the relative weights of each class are correct, then the absolute values are less important, since any inaccuracies (which lead to incorrect growth and development rates) can be corrected by tuning food uptake parameters to the available data. Thus the moulting weight parameterisation aims to be a self-consistent data set, with values taken directly from the literature.

The weight of newly laid eggs is set at 0.3 μg *C* (Carlotti *et al.,* 1998). N1 and N2 stages do not eat, and since their growth is purely temperature dependent (Carlotti *et al.* 1996) there is no moulting weight for early nauplii, simply a weight loss from metabolic processes. Progress through class 1 (Egg, N1 & N2) is therefore determined by ambient temperature. The weight at which individuals moult to class 3 (CI-CIV) is derived from the upper-left graph in Figure (2) of Carlotti *et al.* (1993); it is considered to be mid-way between the high-weight value and the low-weight value. A similar process is followed for determining moulting weight to CV, except that the upper-left graph in Figure (3) of Carlotti *et al.* (1993), 'CV values in the NW Atlantic', is used. Moulting weight to adulthood uses the bottom-left graph in Figure (3). Maturation weight for females is

considered to be the adult weight + 20%, a value similar to that in Carlotti & Radach (1996) for moulting at 8°C, and one which ensures that the maximum mature female weight in the model is still contained within the set of combined literature weights (bottom-centre graph, figure (3), Carlotti *et al.*, 1993). The moulting weights are presented in Table 2.2

Table 2.2: Critical moulting weights to class, all in $\mu g\ C$

CI	*CV*	*Immature female / Adult male*	*Mature Female*
3.8	108.0	217.0	260.0

Growth for eggs and individuals in stages N1 and N2 follows the Belehrádrek function (Corkett *et al.*, 1986), with development time for stage *i* in days given as:

$$D(T) = a_i(T - \beta)^{\alpha} \qquad 2.1$$

where T is the ambient temperature, α=-2.05, and β=-9.11°C. The values of the parameter *a* are obtained from Lynch *et al.* (1998), and summarised in Table 2.3.

Table 2.3: Parameters for the Belehradek growth function, Egg – N2.

Stage	*Belehradek* a_I
Egg	595
N1	387
N2	582

Since they do not feed, eggs, N1 and N2 individuals lose body weight equivalent to their metabolic costs (equation 2.12) at every time step.

Diapausing individuals are assumed not to feed or grow (Lynch *et al.*, 1998) and energy expenditure from metabolic costs is assumed to be insignificant, since metabolism is greatly reduced during diapause (Hirche, 1996). Mature females do not grow, but do feed and are considered to invest all of their net assimilation into egg production. Adult males are considered to feed and grow, with an upper weight cap equal to that of mature females; though they play no further part in the model after reaching adulthood, they are tracked simply to retain an accurate measure of *C. finmarchicus* biomass.

It is well known that later copepodite (CIII-CV) and adult individuals may seasonally develop lipid stores irrespective of their structural growth (Kattner & Krause, 1987). The model does not explicitly track lipid stores, but it has been suggested by

McLaren (1986) that structural growth of individuals is exponential between copepodite stages, irrespective of lipid stores, and by Carlotti *et al.* (1993) that structural weights do not overlap. We hope that the model captures this exponential growth by having structural moulting weights to and from each class. The model includes a more accurate representation of weight loss and starvation than in most studies (TdeYE) due to its linear distribution within class, and since mortality rates are tuned to match growth with data, this should provide reasonable results without the complication of differentiating zooplankton chemical make-up.

The sex ratio for individuals maturing to adulthood is set to 0.5, as in Zakardjian *et al.* (2001). Little more can be done in the absence of field data defining the sex ratio.

Individuals within class i are weight-distributed following the linear functions of TdeYE; the details are outlined here for convenience. There are three possible distributions for individuals between w_i and w_{i+1}:

Case 1:	$n(w) = 0$	for $w(i) < w < z(i)$	2.2
	$n(w) = x + y * w$	for $z(i) <= w <= w(i+1)$	
Case 2:	$n(w) = x + y * w$	for $w(i) <= w <= w(i+1)$	
Case 3:	$n(w) = x + y * w$	for $w(i) <= w <= z(i)$	
	$n(w) = 0$	for $z(i) <= w <= w(i+1)$	

where x, y, and $z(i)$ are parameters of the linear distribution (TdeYE) and $n(w)$ is the number of individuals of weight w. The three possible distributions are shown in Figure 2.2.

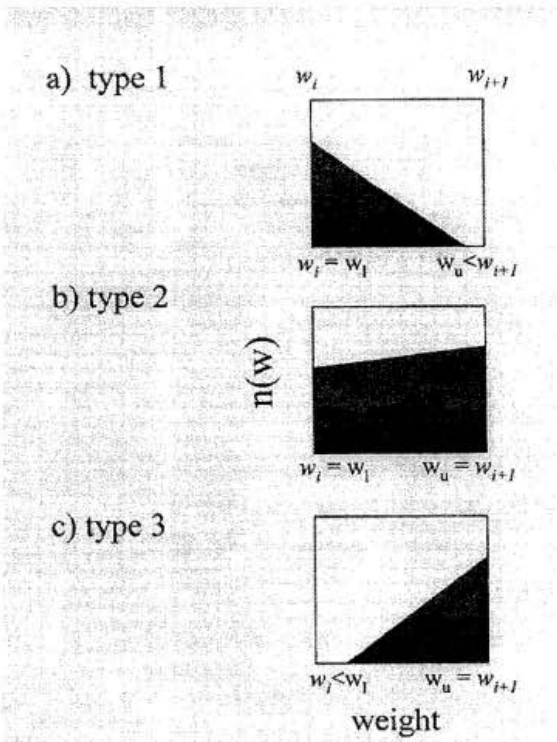

Figure 2.2: Linear class weight distributions. Parameters as above. From TdeYE.

The number of individuals in class i is labelled N_i, and the summed weight of individuals W_i. The time rate-of-change of individuals in class i can be represented in differential equation form as follows:

$$\frac{dN_i}{dt} = T_{i-1}^N - T_i^N - \delta N_i \qquad 2.3$$

$$T_i^N = [A(w_{i+1})]^+ n(w_{i+1}) \qquad 2.4$$

where T_{i-1} represents transfer to class i from the class below, T_i transfer to class $i+1$ from class i, δ_i mortality, $A(w_{i+1})$ net assimilation of individuals at weight w_{i+1}, and $n(w_{i+1})$ the number of individuals at weight w_{i+1}. Within this manuscript, $[x]^+$ denotes the function $f(x)$ where $f(x) = max[x,0]$; thus transfer of individuals to the next class occurs only when the net assimilation within the class is positive. The representation for weight in class i is similar:

$$\frac{dW_i}{dt} = T_{i-1}^W - T_i^W + [G_i]^+ - \delta W_i \qquad 2.5$$

$$G(i) = \int_{w_l}^{w_u} A(w)n(w)dw \qquad 2.6$$

where $[G_i]$ is the net assimilation within class i.

Mature females do not grow, and are assumed to invest all net assimilation into egg production. Thus

$$T_0^N = \beta N_7 \qquad 2.7$$

$$T_0^W = T_0^N w_1 \qquad 2.8$$

where N_7 is the number of mature adult females, and β [d^{-1}] is the per capita fecundity of adult females:

$$\beta = [A_q]^+ / w_1 \qquad 2.9$$

For both mature adult females and adult males

$$T_i^N = T_i^W = 0 \qquad 2.10$$

i.e. individuals do not progress to a new class once they reach mature adulthood.

The individual food uptake rate U and basal metabolic cost M are:

$$U = aw^b \frac{F}{c+F} Q_{10}^{\frac{(T-T_{ref})}{10^\circ C}} \qquad 2.11$$

$$M = kw^g Q_{10}^{\frac{(T-T_{ref})}{10^\circ C}} \qquad 2.12$$

where a is the maximum uptake rate coefficient, b is the maximum uptake rate exponent, c is the food half saturation coefficient, F the food concentration, Q_{10} the temperature quotient, T the temperature, T_{ref} the reference temperature of Q_{10}, k the basal costs coefficient, and g the basal costs coefficient. The net assimilation rate A is calculated by subtracting the basal metabolic cost M from the assimilated uptake ϵU; growth is thus

dependent upon both ambient temperature and food availability. Though no 'low food concentration threshold' beneath which *Calanus finmarchicus* do not feed (Frost, 1975) has not been directly included, in practice, as food concentrations tend towards zero, the Michaelis-Mentin function $F/(c+F)$ will also tend towards zero. Food uptake will therefore be small relative to metabolic costs, and a similar starvation effect will occur. Including a low threshold value within the model would likely increase the rate of starvation of individuals at very low concentrations, and cause a decrease in the final population.

There are a considerable number of species that may predate upon *Calanus finmarchicus*, and these species can have very different vertical distributions. Surveys on Georges Bank have shown that Chaetognaths, Cnidaria, gamarid amphipods and euphasiids were the most abundant invertebrate predators of zooplankton between 1977-1987 (Sullivan & Meise, 1996). In general, predators were more numerous in shallow waters (0-60m), less common in mid-depth waters (60-100m), and at their lowest concentrations in deep waters (>100m). The most abundant invertebrate predator was the Chaetognath *Sagitta elegans* (Sullivan & Meise, 1996). A preliminary analysis of the overwintering of *Calanus finmarchicus* in Norwegian fjords (Kaartvedt, 1996) suggests that the vertical distribution during diapause may reduce predation by the mesopelagic fish *Maurolicus muelleri* (generally 100-150m) and *Benthosema glaciale* (generally below 200m by day). *Benthosema glaciale* is also present in the Davis Strait, generally between 300 and 900 metres (Sameoto, 1989); it has also been observed feeding on

Calanus finmarchicus in the upper 50 metres of the water column on the Nova Scotian slope during the night (Sameoto, 1988). *Meganyctiphanes norvegica* was shown to be an important predator on copepods in the Northeast Atlantic (Bamstedt & Karlson, 1998).

Diapausing behaviour in *Calanus finmarchicus* may thus reduce predation (Kaardvedt, 1996; Mauchline, 1998) through vertical positioning. Alternatively, or perhaps concurrently, it may provide enhanced survival for individuals due to their arrested development and reduced metabolism, and may provide a mechanism for the synchronisation of reproductive pulses (Hirche, 1996). We do not explicitly model for predation, except through the fixed natural mortality that is higher for copepods near the surface than those at diapausing depth.

Values for mortality parameters in the literature vary widely, in part due to the considerable difficulty of measuring mortality accurately in the field, and for the vast range of regimes and locations in which *Calanus finmarchicus* resides. Indeed, mortality parameterisations for a single class may vary by a factor of five (Carlotti & Radach, 1993; Zakardjian *et al.*, 2002) between models. The selection of appropriate values for mortality is often a case of tuning the parameters to match to existing data sets (Lynch *et al.*, 1998). Some models have a stage-specific mortality (Zakardjian *et al.*, 2002) that generally decreases with class progression, while others (Lynch *et al.*, 1998; Carlotti & Wolf, 1998) have similar values for most nauplii or copepodite stages. Detailed mortality estimates for the Labrador Sea are not available, so for this study background mortality

has been set to a fixed value of of 5 % d^{-1} for all classes except diapausing individuals, which have a value ten times smaller at 0.5 % d^{-1}. These values are well within both the upper and lower limits that exist in the modelling literature, for all stages. Mortality has been tuned to provide a reasonable representation of class biomass progression at two key locations in the Labrador Sea (Chpater 4). Should net assimilation be negative, then the weight of organisms within a class is reduced proportionally, until the mean weight of individuals approaches the lower boundary of the class, at which point starvation mortality (a separate quantity from background mortality) occurs:

$$\delta_s = -\gamma_i / w_i \qquad 2.13$$

where δ_s represents starvation mortality, and γ_i per capita net assimilation within class i.

Diapausing individuals are considered to be CV's (Hirche, 1996). The diapause function is as follows:

(i) for $t < dt$ 2.14

$$diap\_out(t) = 0$$

(ii) for $dt < t <= dt + 30$

$$diap\_out(t) = (t - dt)/30$$

(iii) for $t > dt + 30$

$$diap\_out(t) = 0$$

(iv) for all values of t

$$diap\_in(t) = 1 - \sigma$$
$$0 \leq \sigma \leq 1$$

where t is time in days, dt is a latitudinally-varying parameter which allows for regional variation in timing of entrance and exit, and σ is a maximum diapause entry factor. *diap_in* represents the fraction of CV's entering diapause each timestep. If the value of σ is high, then most CV individuals of each new generation will remain at the surface and moult to adult; if it is low, individuals have a greater chance of entering diapause. Since individuals that moult to CV in the same timestep may not enter diapause simultaneously, individuals of different weights enter diapause. Given that most of the Labrador Sea region appears only to have one generation or, if a second generation does appear, it is insignificant in terms of regional production (Kielhorn, 1952; Head *et al.*, 2000), the value of σ is set to 0.5. This ensures there is a chance for a second generation, but it is unlikely and very much dependent upon development rates. Unless individuals develop extremely fast (due to high temperatures and/or food availability) a second generation would be small, if indeed it appears at all. This fits well with available data on *Calanus finmarchicus* in the region (Kielhorn, 1952; Huntley *et al.*, 1983). *diap_out* represents the fraction of individuals exiting diapause each timestep. All individuals exit diapause within a thirty-day span, with most individuals exiting in the early part of this period. This short time-span for ascent of the population from diapause matches Kielhorn's (1952) Bravo data. CV's from the G0 generation do not re-enter diapause.

Figure 2.3 shows the *diap_in* and *diap_out* function for individuals at the centre of the Bravo SeaWiFS box (for location details see Chapter 3).

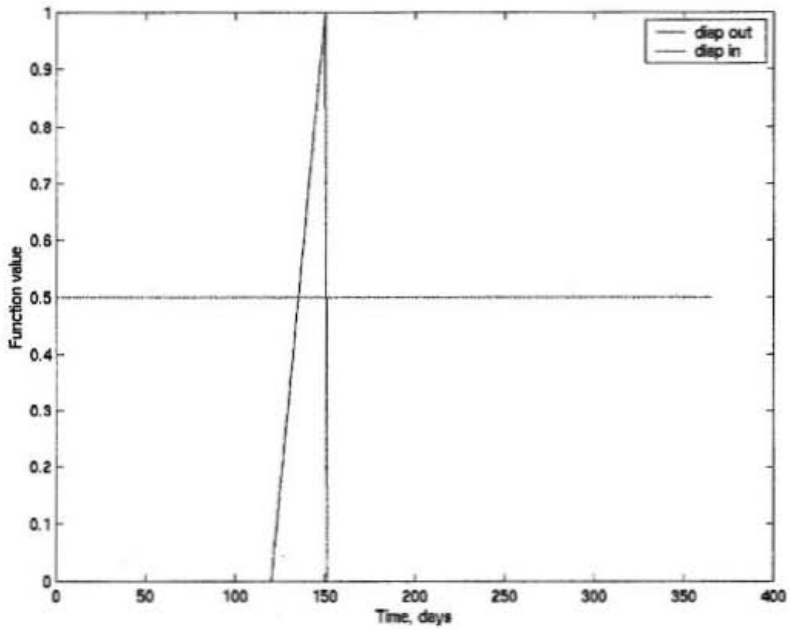

Figure 2.3: Diapause functions for individuals at Bravo (57.42°N, 51.50°W). $dt = 120$.

Table 2.4 lists the various parameters that are used within the *Calanus finmarchicus* model.

Table 2.4: Parameters used within the *Calanus finmarchicus* model.

Parameter	*Symbol*	*Units*	*Value*	*Source*
Maximum uptake rate coefficient	a	$mgC^{(1-b)}d^{-1}$	0.0828 - 0.13	Tuned
Maximum uptake rate exponent	b	-	0.7	Carlotti *et al.* (1996)
Food half saturation concentration	c	$mgCm^{-3}$	25	TdeYE
Basal costs coefficient	k	$mgC^{(1-g)}d^{-1}$	0.0116	TdeYE
Maximum diapause entry factor	σ	-	0.5	Fixed
Diapause exit timing	dt	*d*	varies	Tuned
Basal costs exponent	g	-	0.65	TdeYE
Temperature quotient	Q_{10}	-	2.0	TdeYE
Reference temperature of Q_{10}	T_{ref}	℃	10	TdeYE
Absorption efficiency minus SDA	Є	-	0.6	TdeYE
Mortality, non-diapausing classes	δ	d^{-1}	0.05	Fixed
Mortality, diapausing class	δ_d	d^{-1}	0.005	Fixed
Number of classes	q	-	8	Fixed

2.2 The Physical Model

2.2.1 Model Description

In order to acquire a description of *Calanus finmarchicus* distributions within the Labrador Sea, a knowledge of the physical transport within the region is necessary; plankton are, by definition, passive drifters in the horizontal plane, and thus flow patterns play a significant role in the distribution of individuals and communities. Indeed, it has been hypothesised that the interaction of regional flows and the timing of ascent from diapause may be a critical factor in population dynamics (Backhaus, 1994).

Output from the model of Yao *et al.* (2000) (provided by C. Tang, DFO) is integrated with the *Calanus finmarchicus* model and provides seasonally averaged flow fields for the Labrador Sea, as well as seasonal temperature. This is the sigma coordinate Princeton Ocean Model (Mellor, 1986; Blumberg and Mellor, 1987), with an embedded second-order turbulence closure submodel, and a coupled multicategory ice model. The model has a free surface and uses time splitting for the external mode. Horizontal diffusion follows sigma surfaces and uses a Smagorinsky diffusivity. The above references contain all model equations in full detail; a select few are presented here.

The momentum equations underpin the model (Blumberg & Mellor, 1987):

$$\frac{\partial V}{\partial t}+\mathbf{V}\cdot\nabla V+W\frac{\partial V}{\partial z}+fU=-\frac{1}{\rho_0}\frac{\partial P}{\partial y}+\frac{\partial}{\partial z}(K_M\frac{\partial V}{\partial z})+F_y \qquad 2.15$$

$$\frac{\partial U}{\partial t}+\mathbf{V}\cdot\nabla U+W\frac{\partial U}{\partial z}-fV=-\frac{1}{\rho_0}\frac{\partial P}{\partial x}+\frac{\partial}{\partial z}(K_M\frac{\partial U}{\partial z})+F_x \qquad 2.16$$

where $\mathbf{V}$=(U,V) is the horizontal velocity vector, ρ_0 the reference density, ρ the in situ density, g the gravitational acceleration, P the pressure, and K_M the vertical eddy diffusivity of turbulent momentum mixing. The Coriolis parameter, f, varies latitudinally using the β plane approximation. F_x and F_y represent sub-grid scale processes. The continuity equation is

$$\nabla\cdot\mathbf{V}+\frac{\partial \mathrm{W}}{\partial z}=0 \qquad 2.17$$

The heat and salt balances are as follows:

$$\frac{\partial T}{\partial t}+\mathbf{V}\cdot\nabla T+W\frac{\partial T}{\partial z}=\frac{\partial}{\partial z}\left(K_M\frac{\partial T}{\partial z}\right)-\frac{(1-A)}{\rho c_p}\frac{\partial I}{\partial z}+\Im_T \qquad 2.18$$

$$\frac{\partial S}{\partial t}+\mathbf{V}\cdot\nabla S+W\frac{\partial}{\partial z}S=\frac{\partial}{\partial z}\left(K_M\frac{\partial S}{\partial z}\right)+\Im_s \qquad 2.19$$

where $\Im_T$ and $\Im_S$ represent horizontal diffusion, W is the vertical component of velocity, A the ice-covered fraction, c_p the specific heat of seawater, and I represents shortwave radiation absorption in the water column.

Though the model of Yao *et al* (2000) included diffusive mixing, the coupled model system in this study uses only the output fields of the physical model (as vectors), and so this process is not present, nor vertical mixing. Vertical mixing interacts with *Calanus finamrchicus* behaviour to affect its distribution; within the coupled-model system it is assumed that any *Calanus finmarchicus* in the upper ocean are homogenously spread throughout the mixed layer. In addition, the seasonally averaged circulation does not capture high-frequency forcing variability, and inter-annual fluctuations such as the North Atlantic Oscillation (NAO). While bound by the constraints of these limitations, the model operates within the framework of using an averaged, deterministic physical regime as a point of departure for oceanic forcing.

2.2.2 Model Initialisation and forcing

Monthly climatological data from the National Centers for Environmental Prediction (NCEP)/National Center for Atmospheric Research (NCAR) reanalysis (Kalnay *et al.*, 1996), obtained from the National Oceanic and Atmospheric Administration (NOAA) Climate Diagnostics Center as monthly averages are used for atmospheric forcing. Air temperature at 2m, specific humidity at 2m, precipitation and cloudiness are averaged over the period from 1974-1996 to produce a monthly climatology. Wind at 10m and 6 hour intervals, also from the NCEP/NCAR reanalysis, is used to derive wind stress and the values are then used in the calculation of heat flux. The drag coefficient is calculated as a function of wind speed and air-sea temperature differences (Smith, 1988). Initial ocean temperature and salinity are obtained from an objective analysis of data (Tang & Wang, 1996).

Atmospheric data is bilinearly interpolated to fit the model grid of 1/5° latitude x 1/6° longitude. The model equations are solved using a spherical coordinate system, with a domain ranging from 40°N to 66°N and 40°W to 66°W; note, however, that this is not precisely the same as the region of interest within the coupled model system (see section 3.3 for details). The sixteen vertical sigma levels are as follows: 0, -0.02, -0.04, -0.08, -0.17, -0.25, -0.33, -0.42, -0.50, -0.58, -0.67, -0.75, -0.83, -0.92, -0.96 and –1.00. Prescribed transports occur at open boundaries (see Yao *et al.*, 2000 for details). The

velocity and temperature fields are output matrices that are used in the coupled-model system. For details on model integration, see Chapter 3.

Chapter 3

Model and data set integration, and numerical methods

3.1 The SeaWiFS data set

Calanus finmarchicus is considered to be mainly herbivorous (Mauchline, 1998) - though omnivory is increasingly being studied and quantified (Harris, 1996; Ohman & Runge, 1994). Within the Labrador Sea, the ascent from diapause and coincidence with the initiation of the spring bloom seems to be important for population survival (Head *et al.*, 2000). The modelling of phytoplankton as a major food source therefore takes on considerable importance in the construction of the modelled system.

In the first instance the annual phytoplankton signal was calculated following the approach of Marra & Ho (1993); an NPZ model coupled to the Price-Weller-Pinkel (PWP) model (Price *et al.*, 1986), a one-dimensional (vertical) model of the wind-mixed and buoyancy forced surface layer. Parameters were set to appropriate values for Ocean Weather Station Bravo (OWS-B, located near the centre of the Labrador Sea), to match the annual cycle from Kielhorn (1952). However, this approach was abandoned for a number of reasons: the difficulty in obtaining appropriate parameter values (physical, meteorological and biological) that could be applied or interpolated over the whole of the

Labrador Sea; the difficulty in matching the observed physical and biological cycles over the course of an entire year (for comparison, Marra & Ho (1993) ran their model for 13 days); the difficulty in matching the observed cycles over the entire spatial region; the lack of comprehensive, vertically structured, long term biological and physical data sets from the region; the extra uncertainty and inaccuracy that derives from an additional modelled system within the simulation as a whole; the decoupling from advective processes.

For the reasons listed above, and in order to acquire an accurate picture of phytoplankton density within the model region, data from the SeaWiFS satellite-mounted sensor (Hooker *et al.*, 1992) were utilised. SeaWiFS (Sea-viewing Wide Field-of-view Sensor) is a second-generation remote colour sensor, capable of sensing eight separate bands between 402 and 885 nm. SeaWiFS captures colour images that are calibrated, analysed and processed in order to extract information about chlorophyll-a concentrations and other biogeochemical properties (Hooker *et al.*, 1992; McClain *et al.*, 1992; Aiken *et al.*, 1995). Chlorophyll-a is an important compound in photosynthesis, and within the modelled system can be converted into a proxy for phytoplankton biomass.

The data derived from SeaWiFS is used as a food source for *Calanus finmarchicus*. This is a starting point for the modelling of food limitation; it does not include alternative food sources for the zooplankton, nor subsurface chlorophyll maxima that are not detected by satellite imaging. However, it is intended to provide a more

realistic functional representation of growth than that which is based upon temperature dependency alone. The model is tuned to provide a reasonable population structure and progression within a one-dimensional setting (Chapter 4), and studied for sensitivity to food availability. It is intended that any parameter inaccuracies will be compensated for by this process.

SeaWiFS images captured over the Labrador Sea region have been collated and analysed for a number of locations (Petrie *et al.*, 2000; data provided by P. Pepin & G. Harrison, DFO); additional regions have been compiled for this study (G. Harrison & P. Pepin, DFO). The locations that are used within the coupled-model system are described in Table 3.1, and Figure 3.1 depicts the SeaWiFS data boxes pictorially.

Table 3.1: SeaWIFS data regions included in the coupled-model system. (Petrie & Mason, 2000; P. Pepin, pers. comm., G. Harrison, pers. comm.)

Area	*Latitude (°N)*	*Longitude (°W)*
Avalon Channel	46-48	51.5-53
Bravo	56.63-58.13	50.42-53.17
Green-St. Pierre	45.33-46.33	54-56
Hamilton Bank	53.5-54.5	54-56
Hudson Strait	60.51-61.40	62.72-64.55
Labrador Basin	53.5 – 54.5	42.5 – 43.5
Labrador Shelf	56.91-57.81	59.55-61.20
Southeast Flemish Cap	45-47	42-44
Southeast Shoal	44-46	50-52
St. Anthony Basin	50-52	53-55
West Greenland	61-62	50-52

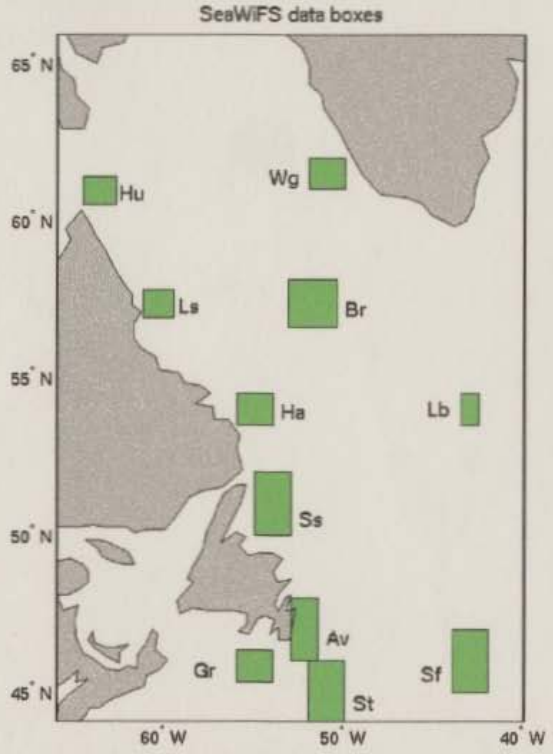

Figure 3.1: SeaWiFS data box locations. Abbreviations as follows: Av – Avalon Channel, Br – Bravo, Gr – Green-St. Pierre, Ha – Hamilton Bank, Hu – Hudson Strait, Lb – Labrador Basin, Ls – Labrador Shelf, Sf – Southeast Flemish Cap, Ss – Southeast Shoal, St – St. Anthony Basin, Wg – West Greenland.

Mean chlorophyll within each 'box' is provided in bimonthly form, and is then further compiled over the period 1998 to 2000 in order to provide a composite annual picture (in two-week intervals) of chlorophyll concentration. If for any two-week period no data exists in any year of the three year span, it is linearly interpolated from the surrounding values. Chlorophyll values are converted to carbon concentration (the units

for food uptake in the biological model) using a *C: Chl* ratio of 50 (Trela, 1996; Head *et al.*, 2000). Phytoplankton are assumed to be homogenous over the entire mixed layer. This is valid if vertical mixing is strong enough to cause a uniform phytoplankton distribution down to the base of the mixed layer (Mann & Lazier, 1996), which is obviously dependent upon the climatology of the region in question (e.g. Smith & Dobson, 1984), but seems reasonable in a mid-to-high latitude region such as the Labrador Sea.

In each of the SeaWiFS data boxes, the spring bloom (for the purposes of the modelled system) is defined to be the largest two consecutive peaks in the annual signal. Within this data set, in a few cases, these peaks occur very late or very early in the year (between October and January), in which case they are disregarded. In one case (SE Flemish Cap), in the year 2000, the peaks are not consecutive. In two instances, there are not enough data for each year to determine the timing of the spring bloom. Both of these problems are resolved when the data is compiled over the three-year period. Figures 3.2 and 3.3 show the timing of the first peak of the spring bloom, and the magnitude of the maximum peak of the spring bloom respectively, relative to latitude, for the uncompiled data.

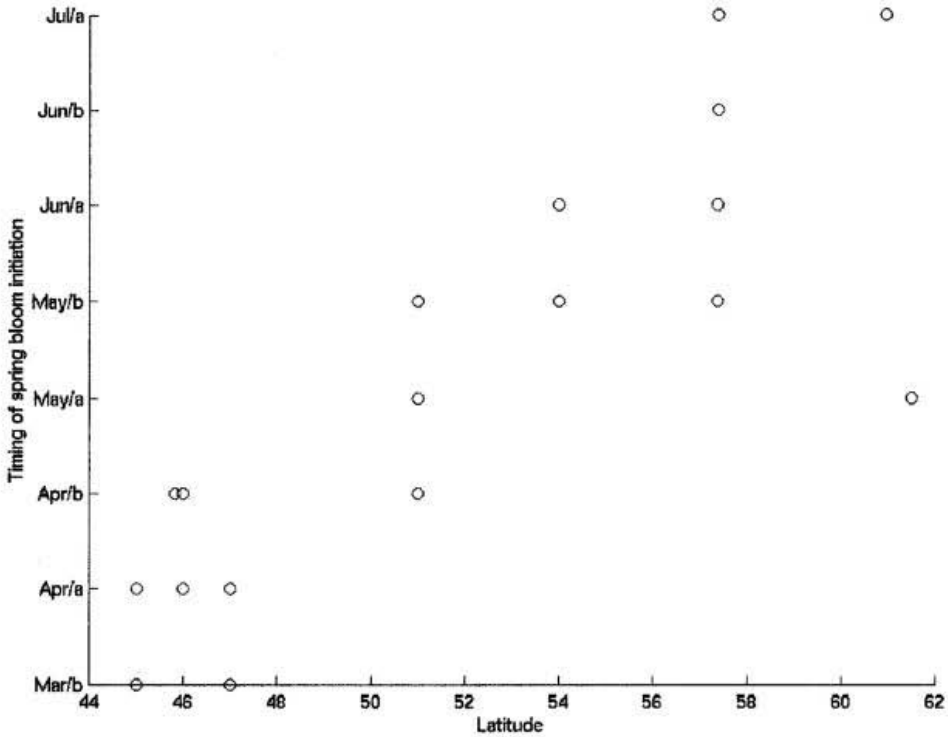

Figure 3.2: Timing of the spring bloom in relation to latitude. Derived from the SeaWiFS data set, 1998-2000. (Month)/a and (Month)/b represent the first and the second half of each month respectively. Latitude in °N. For further details see text.

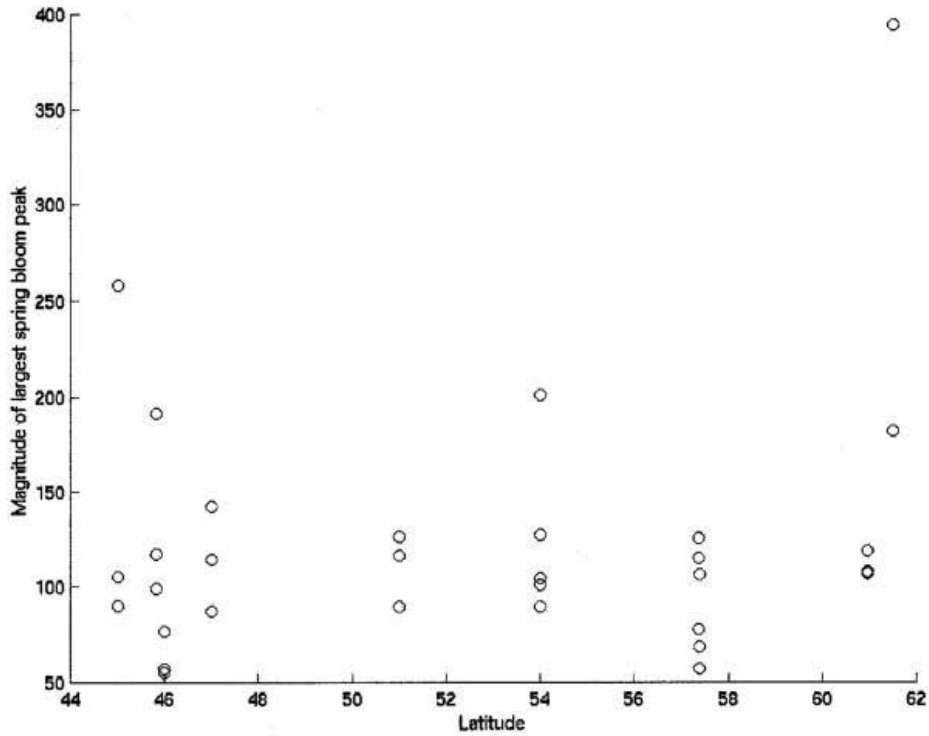

Figure 3.3: Magnitude of the spring bloom in relation to latitude. Derived from the SeaWiFS data, 1998-2000. Magnitude in units of $mg\ C\ m^{-3}$. Latitude in °N. For further details see text.

Though the data covers but a three-year span, it seems that there is a reasonably clear pattern of later bloom development in the north (Figure 3.2); the exception being the West Greenland box (centre 61.5°N), which shows a consistently early bloom relative to its latitude. This may be due to its proximity to the coastal waters off Greenland. It has been suggested that the spring bloom appears earlier in more northerly regions, and progresses anti-clockwise around the Labrador Sea (Matthews, 1968) and southwards (Head *et al.*, 2000). The SeaWiFS data do not bear this out.

The magnitude of the spring bloom bears little relation to latitude. The largest peak comes from West Greenland; it appears that the bloom in this region may well be both early (relative to latitude) and sizeable (Figure 3.3). The spring bloom in all regions is towards the lower end of the chlorophyll concentrations measured by Head *et al.* (2000), but within this range nonetheless. Uncompiled data from the SeaWiFS boxes (no spatial or temporal averaging) shows a considerable variance in values, with a maximum in some cases greater than twice that measured by Head *et al.* (2000). Within the model system (Chapters 4 & 5), the uptake rate parameter a is tuned to adjust for any inaccuracies in the measurement of chlorophyll concentration and provide a growth rate that matches well to literature within the region.

The timing of the spring bloom in relation to latitude is considered when parameterising the diapause emergence function (Chapters 4 and 5). Since the boxes do not cover the entire model region, it is necessary that they be extended to provide a value

at each geographical location within the region. The values derived above are considered to fit in the three-dimensional model system at the surface (x,y) grid-point nearest to the centre of each particular box. Other grid points are then interpolated (after much experimentation) by inversely weighting distance from the two closest box points. Composite, statistically processed data for the entire of the model region was not available for this study, hence necessitating the usage and interpolation of boxes. Figure 3.4 shows the interpolated phytoplankton map in monthly intervals.

Figure 3.4: Interpolated phytoplankton carbon density map for the model region. All values in $mg\ C\ m^{-3}$. White asterisks represent the centre of SeaWiFS derived boxes.

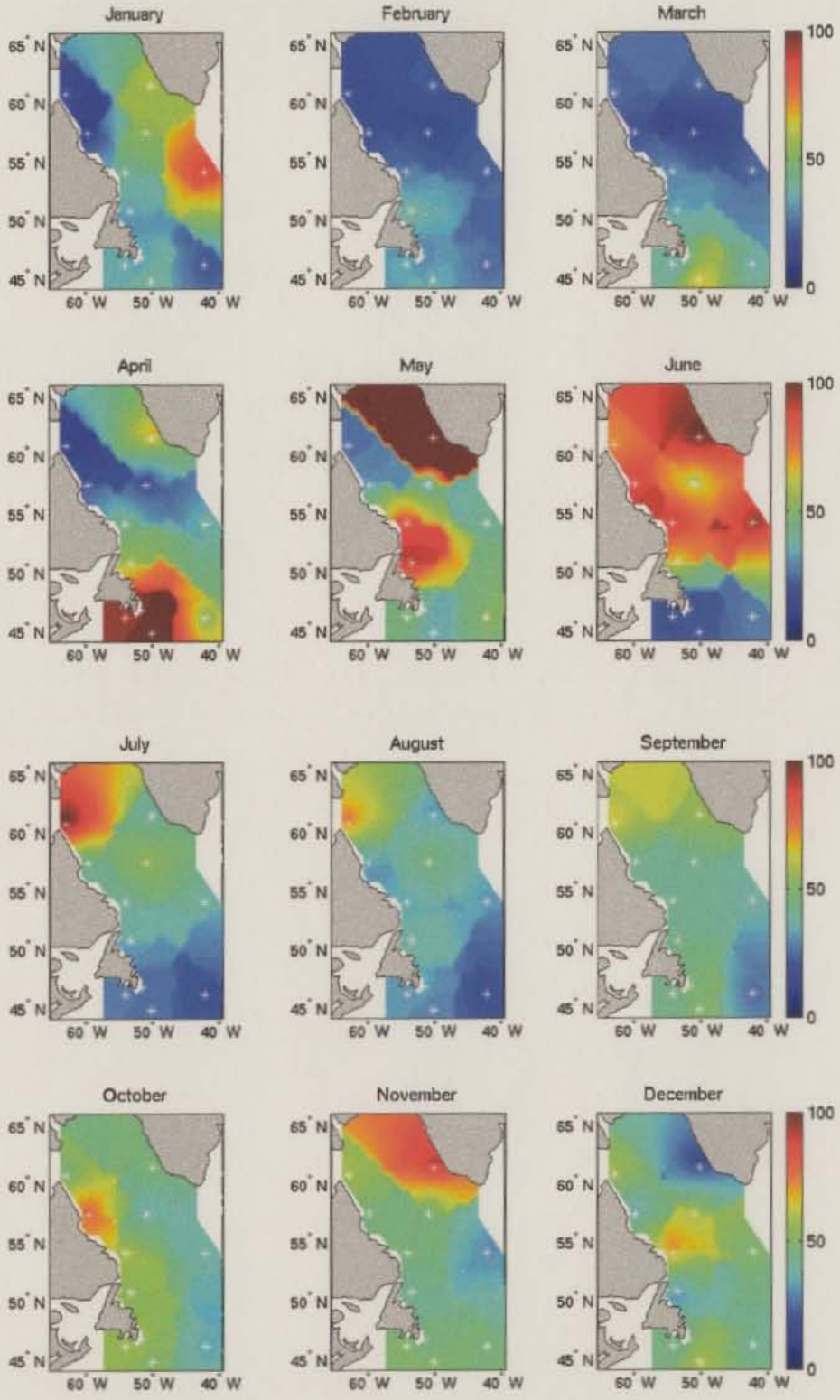
January
February
March
April
May
June
July
August
September
October
November
December
65° N
60° N
55° N
50° N
45° N
60° W
50° W
40° W
100
50
0

3.2 Model Integration

The biological and physical models developed here are coupled through physical oceanographic properties that affect *Calanus finmarchicus* growth and dispersal: transport processes that advect organisms to new locations, and water temperature effects on metabolic rates. Transport processes may advect zooplankton to, or from, patches or regions in which the environment is particularly suited, or unsuitable, for growth, both in terms of physical factors such as temperature, and biological factors such as predation. Surface circulation patterns can differ significantly from those at depth, and thus may combine with *Calanus finmarchicus* behavioural patterns (especially emergence from, and entrance into, diapause) to determine population distributions (Backhaus *et al.*, 1994; Slagstad & Tande, 1996). Many zooplankton metabolic processes are temperature dependent (Harris *et al.*, 2000), including growth rate and developmental rate. *Calanus spp.* geographical distributions may be determined in part by the physical properties of ocean water (Mauchline, 1998), including temperature; species may have adapted to live within specific regimes. Thus regional physical oceanographic features affect *Calanus finmarchicus* survivability, both directly and indirectly.

It can therefore be seen that accurate modelling of advection and temperature within the Labrador Sea is of vital importance in order to provide reasonable insight into *Calanus finmarchicus* distribution and life-history patterns. To this end, the model of Yao *et al.* (2000), described in Chapter 2, provides the velocity and temperature fields for the

system. The original (sigma-coordinate) depth levels are linearly interpolated to nineteen standard depths (0, 20, 40, 60, 80, 100, 120, 140, 160, 180, 200, 300, 400, 500, 600, 700, 800, 900 and 1000 metres) at each grid location. In addition, the grid size of the three-dimensional system (originally 1/5° latitude by 1/6° longitude in the physical model) is reduced by a factor of four. These processes are necessary to reduce the complexity of the coupled model system to a computationally manageable size. Model output is constrained to the region 44°N-66°N and 40°W to 66°W, as shown in Figure 3.5.

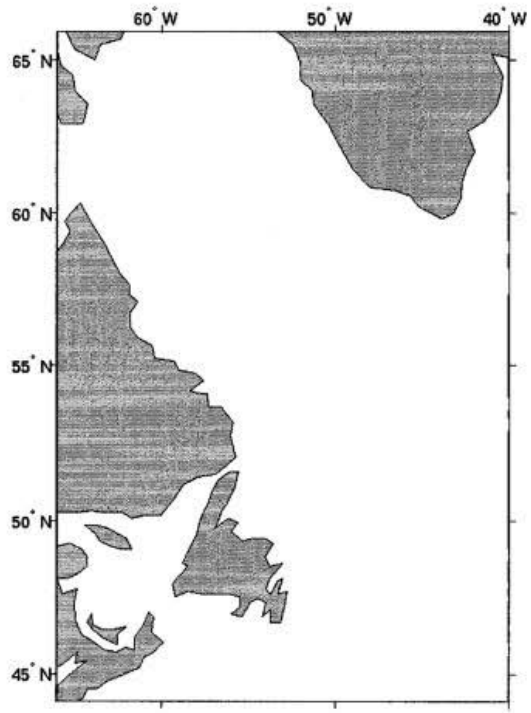

Figure 3.5: The region covered by the physical model.

Individuals from the Gulf of Maine and North Atlantic slope waters appear to overwinter at depths of around 500 metres (Miller *et al.*, 1991). In the Faroe – Shetland Channel, Heath & Jónasdóttir (1999) sampled down to 1000 metres and found the peak concentration of overwintering copepodites at 930 metres depth. Though no studies of diapausing depth in the Labrador Sea have been undertaken, 1000 metres is considered to provide an adequate depth for the model. Diapausing individuals reside at the deepest possible depth in their location. Should they be advected to a new location that is deeper, they will descend, to a maximum of 1000 metres. Upon emergence from diapause, they rise to the mixed-layer. The mixed layer depth is defined to be the depth at which the temperature differs from the surface value by greater than 0.1°C. Individuals are assumed to be spread homogenously within the mixed layer. While *Calanus finmarchcius* is known to undertake diel vertical migration (Mauchline, 1998), the time-step of the model is not fine enough to capture this. We assume that *Calanus finmarchicus* is homogenously distributed within the mixed layer, along with its food source. This seems a reasonable approach given the lack of knowledge of sub-surface chlorophyll values, and the size of the model time-step. Figure 3.6 shows mixed-layer depth in the model region.

Should individuals be advected to a new location in which they encounter sub-surface topography, they rise to the deepest water depth at the new location. Individuals are advected as follows: each (advective) time-step, the distribution of individuals in the horizontal (x,y) plane within each 'grid box' in the model (each of which is centred on a

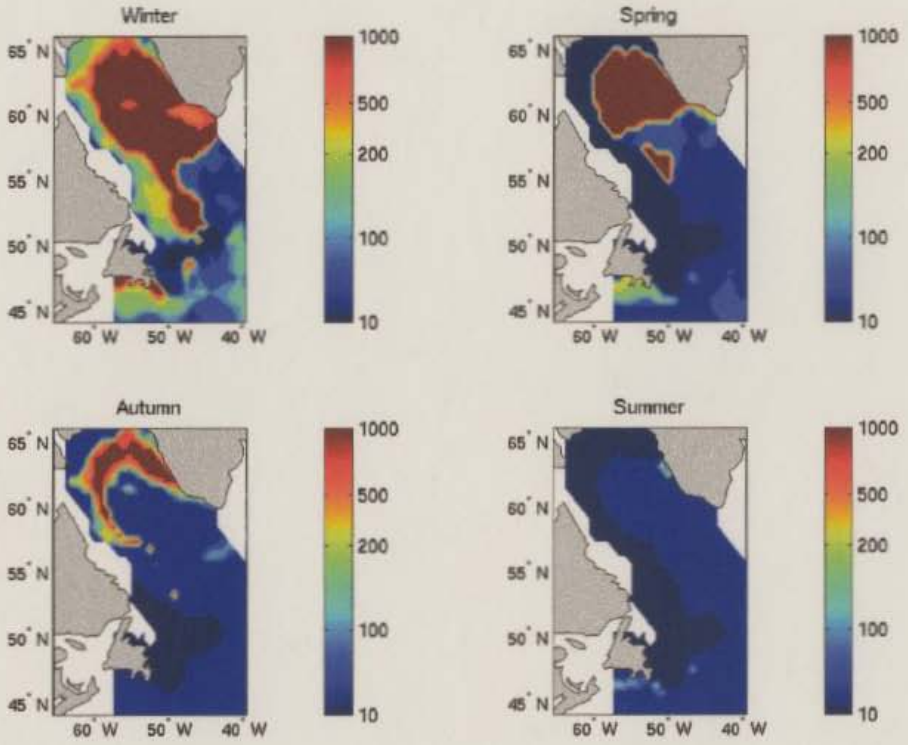

Figure 3.6: Mixed-layer depth in the model region. Clockwise from top left: winter, spring, summer, autumn.

grid point) is assumed to be homogenous. The advection vector is then used to relocate the homogenous distribution, and the number of individuals moved to a new location corresponds to the overlap between the new location of the distribution and the bordering grid boxes. Individuals cannot be moved more than one grid-box per time-step. Indeed, setting the distribution to be homogenous at each time-step will lead to a slight increase in the dispersal of individuals; the time-step has been chosen to minimise this.

The velocity and temperature fields from the physical model are provided in seasonally averaged form: winter (January, February, March), spring (April, May, June), summer (July, August, September) and autumn (October, November, December). Figure 3.7 shows the depth-averaged summer circulation patterns in the physical model.

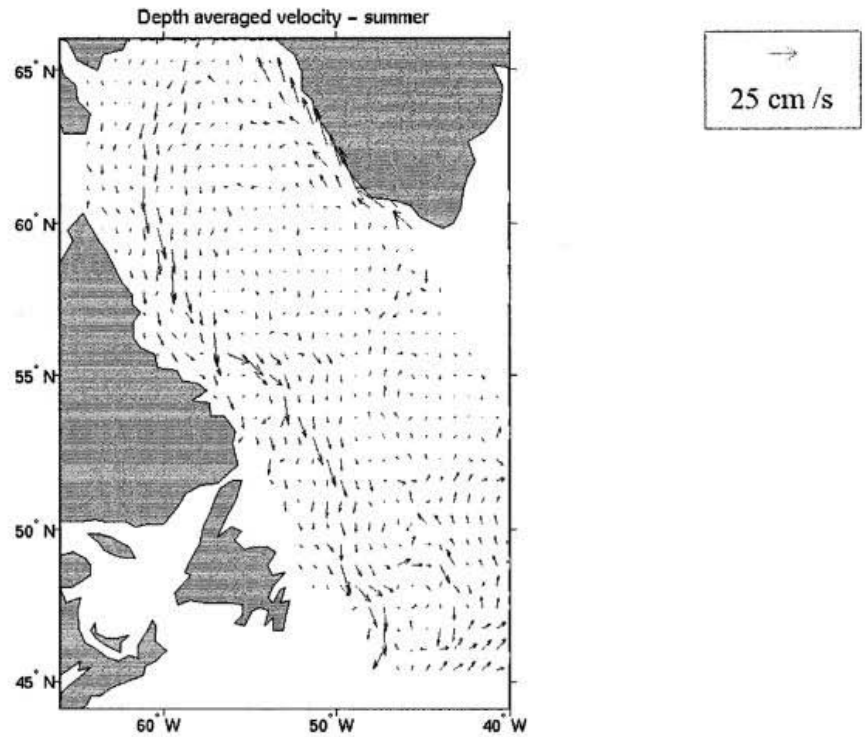

Figure 3.7: Depth averaged circulation, physical model, summer.

3.3 Numerical Methods

The time-step of the biological model is one day. In order to prevent advective instabilities the physical model has a time step of one quarter of a day. The boundary conditions are as follows: outward fluxes at the model boundaries are calculated following transport values derived from the physical model; any individuals that exit the area do not return. Inward flux of individuals at all model boundaries is set to zero, except for model runs which are specifically designated to assess the effect of an inward flux of individuals (further described in Chapter 5). Further details of the numerics of the physical model are presented in Yao *et al.* (2000).

Seasonal change-over for transport, temperature, and mixed-layer depth in the three-dimensional model system occurs on 1 January (Winter), 1 April (Spring), 1 July (Summer), and 1 October (Autumn). A level 4.5 Runge-Kutta scheme is used to solve the system of differential equations in the biological model. This is a variable time-step algorithm that uses a 4^{th} and 5^{th} order formula pair. The model is programmed in Matlab.

Chapter 4

One-dimensional model runs

4.1 Study rationale

In order to understand the behaviour of the biological model in a three-dimensional setting, and to set parameters for the biological model by comparison of simulations with observations, the model was first run in a one-dimensional (vertical) form, without the obfuscating effect of advective processes being present. The aims of this section are to attain an understanding of the dynamics of the biological model, to parameterise the biological model effectively for integration within the three-dimensional system, to examine the model response at several locations, and to assess model sensitivity to data sampling and parameterisation.

Two locations were selected for study in one dimension (corresponding to SeaWiFS data locations): Bravo (56.63°-58.13°N, 50.42°-53.17°W), and Southeast Flemish Cap (45°-47°N, 45°-47°W). For the purposes of this study, the one-dimensional model runs are considered to be at the centre of their respective data boxes; the temperature field is taken from physical model grid point (Yao *et al.*, 2000) to which this is closest.

4.2 Forcing data

The setting is considered to be one-dimensional as follows: diapausing individuals reside at 1000m depth, while active individuals reside in the mixed layer. Phytoplankton density values for Bravo and the Southeast Flemish Cap, derived from the SeaWiFS data sets provided by G. Harrison and P. Pepin (pers. comm.), are used as a food source (see Chapter 3). Surface temperature is provided from the physical model on a seasonal basis. Figures 4.1 and 4.2 show phytoplankton concentration (in $mg\ C\ m^{-3}$) and sea surface temperature (SST) respectively at the two locations. The phytoplankton data set has been averaged over the period 1998 to 2000.

Within the modelled system, the spring bloom is defined as being the two largest peaks in the phytoplankton signal each year. At both locations, these peaks are consecutive. The signals are divided into seasons as follows: winter (January – March), spring (April – June), summer (July – September) and autumn (October – December). It can be seen that the spring bloom at Bravo (late June/early July) occurs later than the bloom at Southeast Flemish Cap (late April/early May). The peak chlorophyll value is slightly higher at Bravo (71.5085 $mg\ C\ m^{-3}$). The summer months are relatively low in phytoplankton at Southeast Flemish Cap, while having higher values at Bravo (Figure 4.1).

The temperature is considerably colder at Bravo throughout the year, with the maximum value (5.449°C) occurring in the summer. The SST at Southeast Flemish Cap is always above 10°C, with the maximum occurring in the autumn (14.66°C – Figure 4.2).

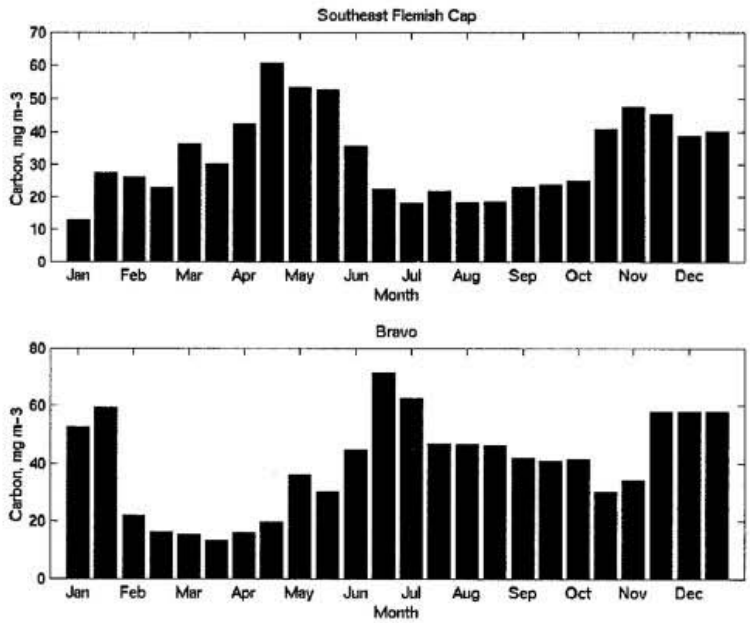

Figure 4.1: Mixed-layer phytoplankton concentration (in $mg\ C\ m^{-3}$) at Southeast Flemish Cap and Bravo. Derived from SeaWiFS data set provided by G. Harrison & P. Pepin, DFO, originally from NASA. Assumes a *C:Chl* ratio of 50.

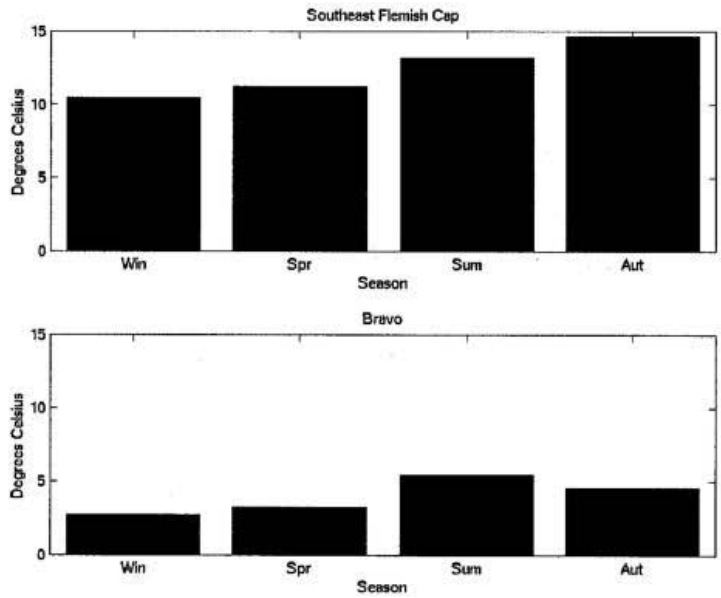

Figure 4.2: Surface temperature at Southeast Flemish Cap and Bravo. Data from the physical model of Yao *et al.* (2000).

4.3 Model Setup – Bravo

Kielhorn's 1950/1951 survey of the plankton at OWS-B forms the main reference when determining population parameterisations at Bravo (Kielhorn, 1952). The diapausing timing factor, *dt*, is set to 120 days, corresponding to the end of April. Most individuals of the G0 generation thus exit diapause during May, as in Kielhorn (1952). Kielhorn states that

> 'when the zooplankton was at its greatest numerical value, on August 1, 1950... the greater part of the zooplankton at this time consisted of the copepodites of *Calanus finmarchicus*'.

The value of *a*, the maximum uptake rate coefficient, is thus tuned until the copepodite maximum occurs in early August; the final value is 0.13. The only model run in which these parameterisations do not hold is the sensitivity test for diapause timing. It has been postulated by Miller *et al.* (1991) that individuals emerge from diapause near-synchronously over much of the region, and that differences in growth and development are due to the timing of the spring bloom. In order to test this, the one-dimensional model is also run with the diapause timing factor, *dt*, set to a value of 75, leading to most CV individuals exiting diapause during the second half of March. A further exploration of the emergence from diapause of *Calanus finmarchicus* in the Labrador Sea is contained in Chapter 5.

Figure 4.3 shows the annual population cycle when initialised with 100 diapausing individuals per m^{-2} on day 1 (January 1). Figure 4.4 compares select model data with Figure (8) from Kielhorn (1952).

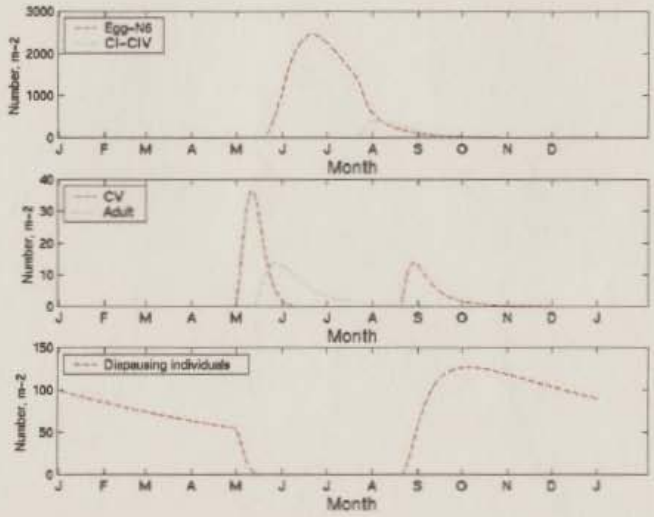

Figure 4.3: Annual population cycle, Bravo, when initialised with 100 diapausing individuals per m^{-2}.

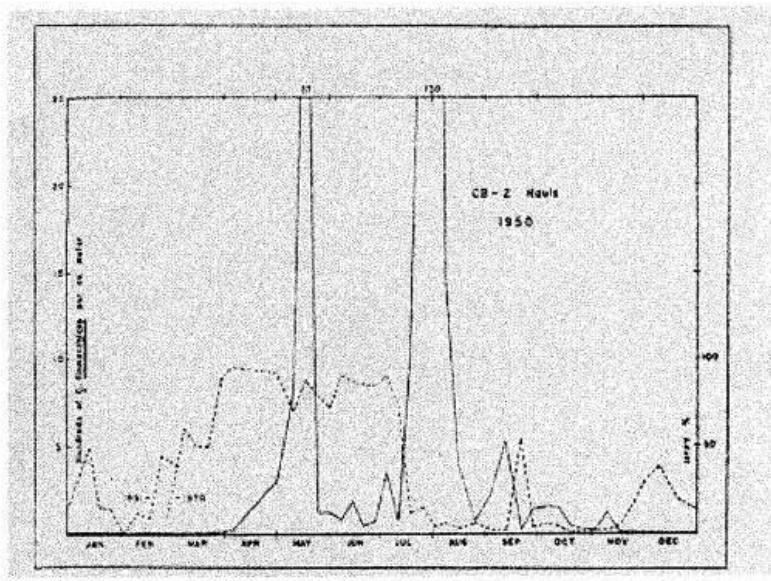

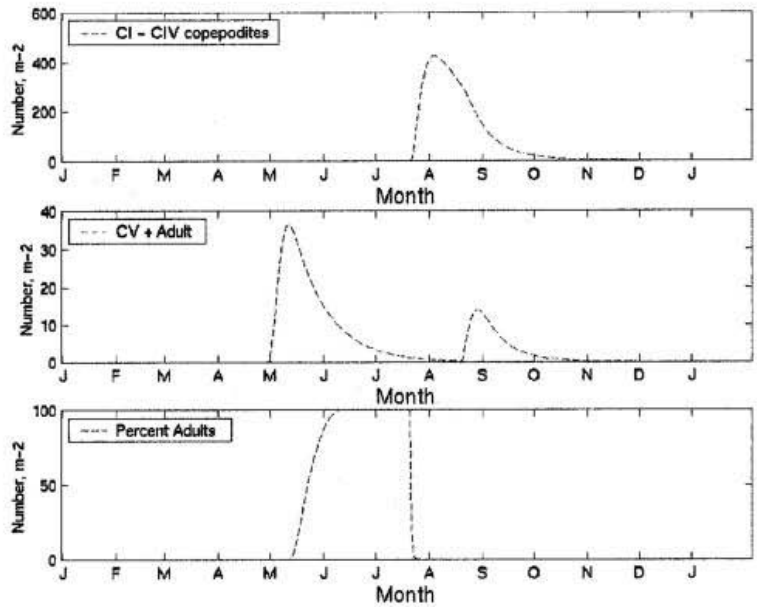

Figure 4.4: Upper: *Calanus finmarchicus* annual cycle, Bravo. From Kielhorn (1952). Solid line represents hundreds of *Calanus finmarchicus* per cubic metre. Dashed line represents percentage adults. Lower: Selected model output, annual cycle, Bravo. Percentage values do not include nauplii. Concentrations in individuals per m^{-2}.

Qualitatively, the timing of the model matches the data reasonably well. In the model, diapause emergence occurs in April, with the peak in surface G0 individuals occurring in May. If we consider, as Kielhorn concluded, that the first peak in his data is the product of emergence of individuals from diapause, then the timing is very similar. The model peak in early August consists mostly of copepodites, in agreement with the observations of Kielhorn (1952). Model peaks are more dispersed than those of the data. Additionally, there is a difference between ratio of the G0 peak and the G1 peak (1 : 11.64) in the model and the same ratio in Kielhorn's data (1 : 3.51). This can perhaps be ascribed to the fact that the sharp decline in surface G0 individuals in the data does not occur in the model, and thus the adults are more productive over a longer time period. Another factor for consideration is that the region does not exist in isolation, such that advective processes could cause transport of individuals through Bravo. If the zooplankton distributions around this area are non-homogeneous, the advective influence would imply strong spatial variability in the results of Kielhorn (1952).

The model and data show qualitatively similar features in the winter: minimal surface activity, with no G2 generation in the model, though a small percentage of G1 individuals remain at the surface during the winter. Kielhorn noted that the data gave evidence of just one main annual generation of *Calanus finmarchicus*; this is corroborated in Head *et al.* (2000). The modelled population has around 12% fewer diapausing individuals at the end of the year when compared to the start.

4.4 Sensitivity tests

Sensitivity tests were conducted in order to determine the dependence of the model on changes in both internal parameters and external forcing data; the original parameter values are described in Chapter 2. All sensitivity tests show the percentage change in the number of diapausing individuals between the start and end of an annual run. The tests are initialised with 100 diapausing individuals. Each test is composed of eleven separate model runs. Table 4.3 lists the sensitivity tests.

Table 4.1: Sensitivity tests, biological model, Bravo.

Test name	*Change from standard run*
Surface mortality	Mortality changed for non-diapausing individuals.
Diapausing mortality	Mortality changed for diapausing individuals.
Temperature	Mixed layer temperature varied by a constant amount over the annual cycle.
Food	Food is varied by a constant amount over the annual cycle
Diapause timing	Diapause emergence timing modified by up to 25 days.
Early emergence	Emergence from diapause occurs in late March, to bring it in line with Matthews (1968) and Miller *et al.* (1991). The diapause emergence factor, *dt*, is set to a value of 75.

4.5 Results: Bravo

4.5.1 Mortality sensitivity tests, Bravo

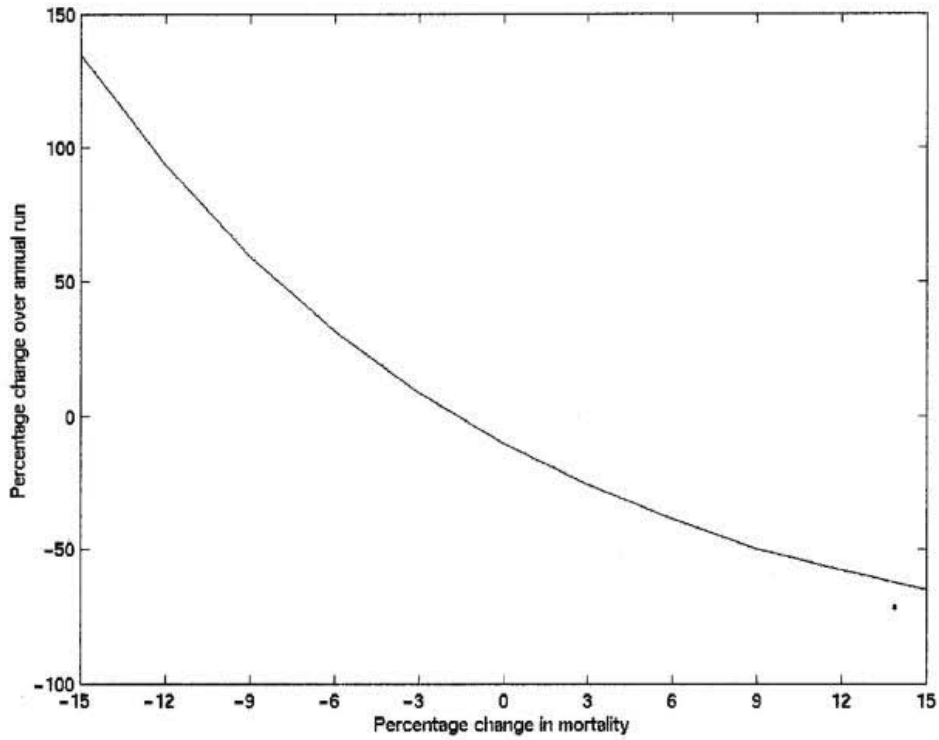

Figure 4.5: Surface mortality sensitivity tests for the biological model, Bravo.

Changing the surface mortality parameter results in a non-linear population response, with percentage response in the model being disproportionately large when compared to the parameter change (Figure 4.5). This is due to a number of factors; particularly that altering mortality influences the number of adult females that live to produce eggs, and hence the size of the G1 generation. Although mortality has no effect

on the growth rate of individuals, it does act at every time step and hence affects the number of individuals that live to moult to the next stage.

A further decrease in mortality produces a response (population growth) that grows near exponentially (not all results shown). The biological realism of this is questionable, since there are processes that are not represented in the model (over-grazing, competition for resources) that would prevent this curve from an exponential increase *ad infinitum*.

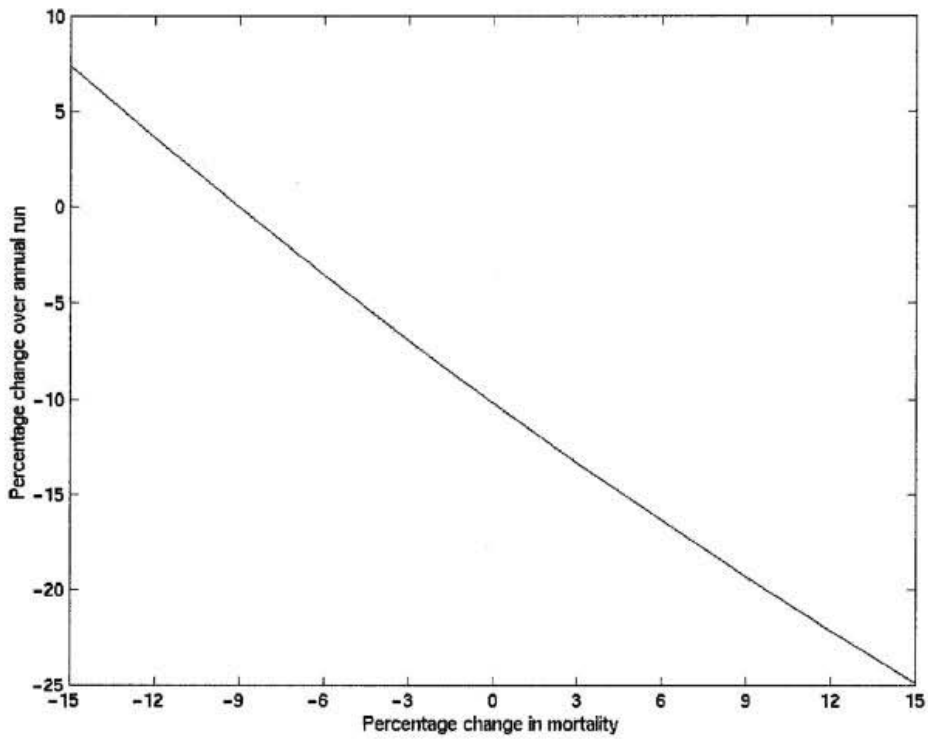

Figure 4.6: Diapausing mortality sensitivity tests for the biological model, Bravo.

The diapausing mortality response is much closer to linearity than that of the surface mortality; it also has a significantly decreased proportional response on the population size. If it is taken into consideration that the diapausing mortality is smaller by a factor of ten than the surface mortality then this is perhaps not surprising. The percentage effect on population size of both an equal increase or decrease in mortality is essentially similar (Figure 4.6)

4.5.2 Temperature sensitivity tests, Bravo

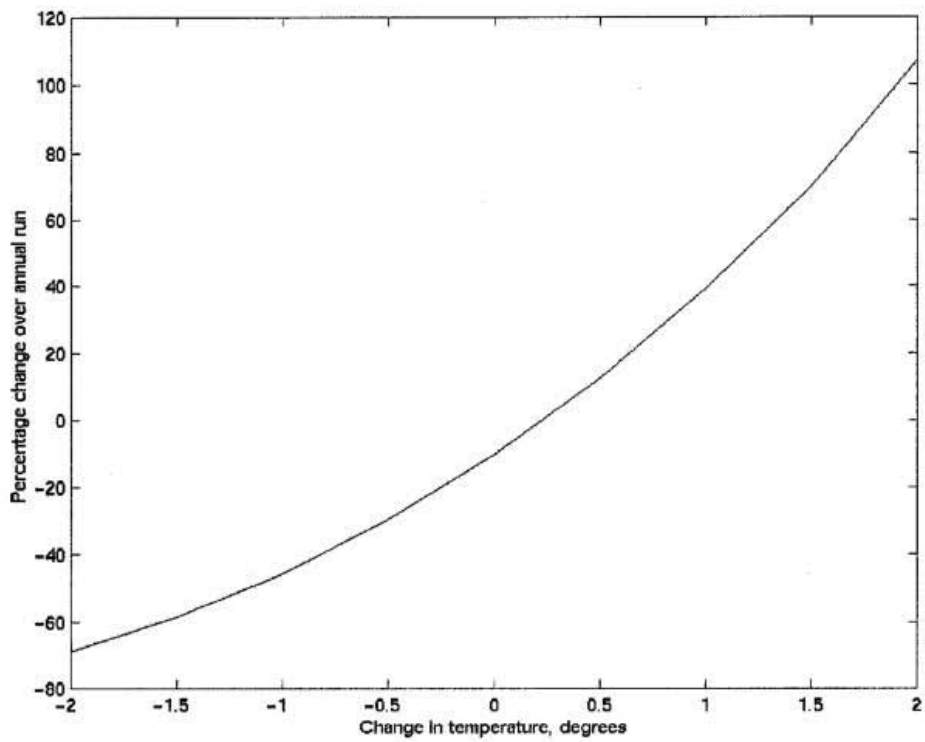

Figure 4.7: Temperature sensitivity tests for the biological model, Bravo. The temperature is changed by a fixed amount at every time step.

Changing the temperature results in a response that, as expected, decreases the population size if the temperature is reduced (since metabolic processes, and therefore growth, are slower), and increases the population size if the temperature is increased. The model shows more sensitivity to an increase in temperature than a decrease (Figure 4.7).

4.5.3 Food sensitivity tests, Bravo

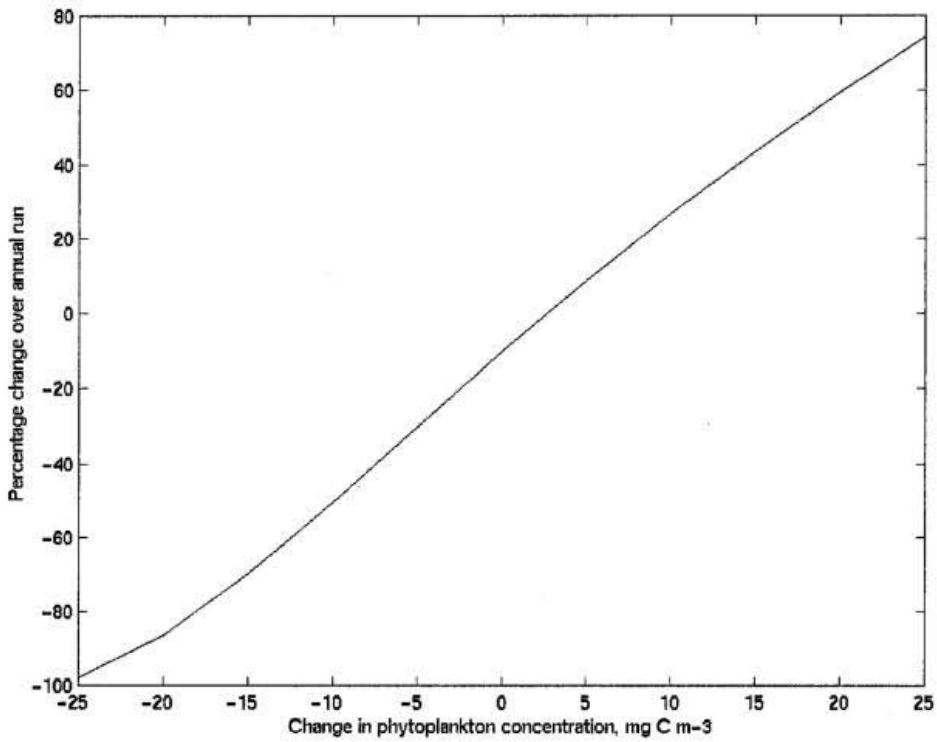

Figure 4.8: Phytoplankton concentration sensitivity tests for the biological model. The phytoplankton concentration is modified by a fixed amount for each time step.

Since phytoplankton are a major source of food for *Calanus finmarchicus* (Mauchline, 1998), sensitivity to food availability is unsurprisingly high. Given that the half-saturation concentration of phytoplankton is 25 $mg\ C\ m^{-3}$, and that in the summer months (when the zooplankton are most active at the surface) the phytoplankton concentration varies between 40.89 and 62.78 $mg\ C\ m^{-3}$, it is not surprising that reducing the food availability by 25 $mg\ C\ m^{-3}$ results in a population collapse to near zero in one year. An increase in food availability leads to more rapid growth, and hence an increased population size at the end of the year (Figure 4.8).

This sensitivity test could also be useful when considering the validity of the SeaWiFS data set, and the *C:Chl* ratio parameter, as both of these have an effect on the food availability data.

4.5.4 Diapause timing sensitivity tests, Bravo

The results of the diapause timing sensitivity tests are shown in Figure 4.9. At Bravo, earlier emergence leads to an reduced final population, while later emergence causes a population increase. This is because individuals that emerge earlier are have a greater mismatch with the time of the spring bloom (Figures 4.1 and 4.3) in addition to spending more time in the cooler spring waters (Figure 4.2). The converse holds true for later emergence. The percentage change in final population for both early and late emergence is very similar.

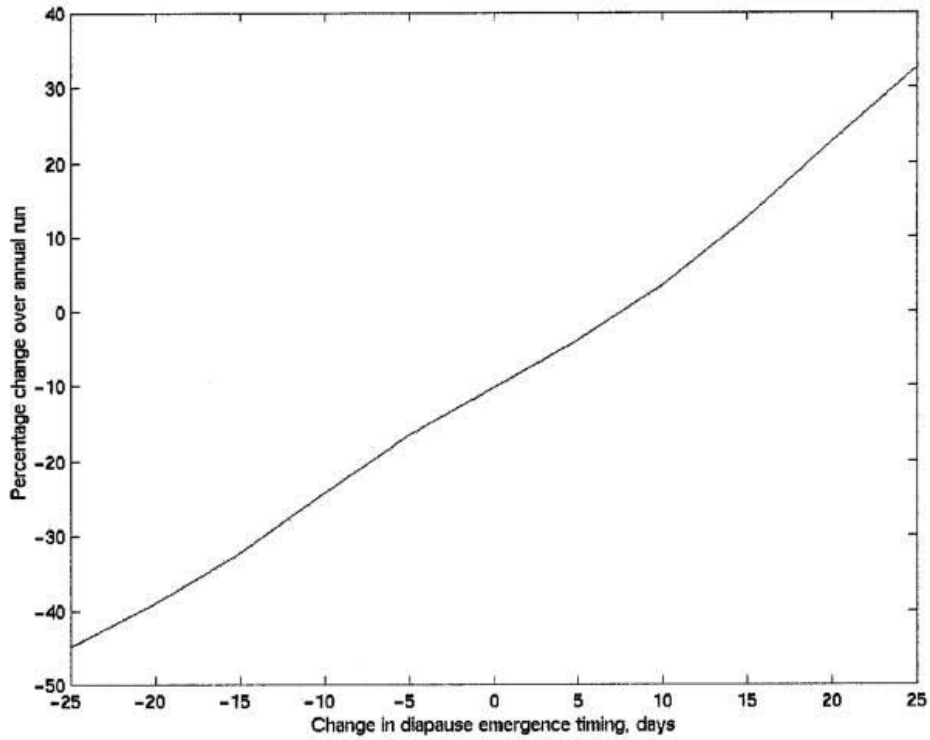

Figure 4.9: Diapause timing sensitivity tests, Bravo.

4.5.5 Early emergence sensitivity tests, Bravo

If the diapause timing factor is set to a value of 75, in order to match the data of Matthews (1968) and Miller *et al.* (1991) the diapausing population decreases by 65.25% over the course of a year, a significantly higher number than the 10.20% in the standard one-dimensional Bravo run. This is due to a combination of lower temperatures and reduced food (see Figures 4.1 & 4.2) at the time of emergence and for a few months until the spring bloom. This leads to slower maturation rates from CV to adult, reduced egg production, and reduced growth for early stages of the G1 generation, in a similar fashion to the diapause timing sensitivity tests (section 4.5.4).

4.6 Model setup: Southeast Flemish Cap

The Southeast Flemish Cap box is at a similar latitude, and a little to the east of the data collected by Anderson (1990), who studied zooplankton populations on the Flemish Cap. Anderson considered the timing of spring egg-production to occur approximately one month later on the Flemish Cap than the shelf waters off Nova Scotia (Anderson, 1990). Back calculation from the data indicated that peak reproduction occurred around the middle of April; in order to match to this, *a* was set to the value of 0.09 and the emergence timing modifier, *dt*, to 75. The results are shown below.

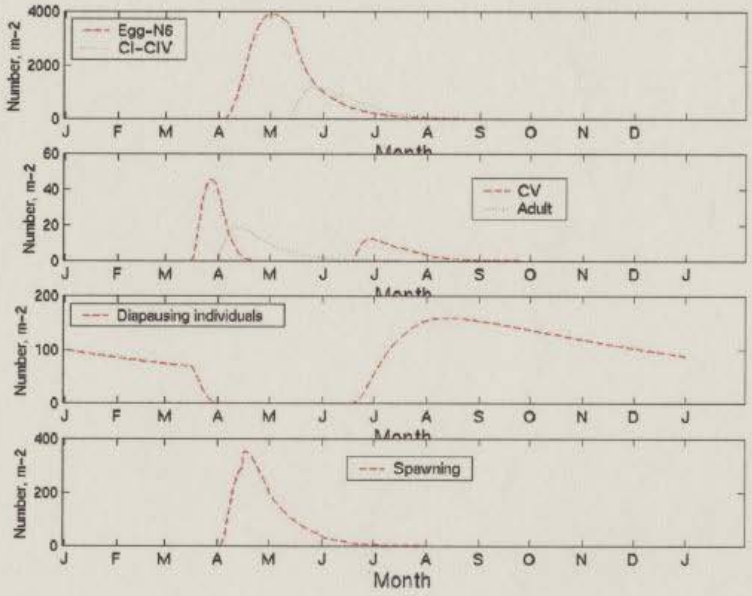

Figure 4.10: Modelled annual cycle, surface individuals, Southeast Flemish Cap, when intialised with 100 individuals per m^{-2}.

Peak spawning in the model occurs in mid-April, which matches well with Anderson (1990). Given that emergence occurs in February off parts of the Scotian Shelf (McLaren & Corkett, 1986), and that the timing of peak spawning is around a month later off the Flemish Cap than in this region (Anderson, 1990), it is reasonable to assume that emergence from diapause also occurs one month later during March, and this is reflected in the model. The modelled diapausing population decreases by around 12 percent over the year. The peak of nauplii individuals is coincident with the spring bloom. No G2 generation appears in the model.

Perhaps the best validation for the model is a comparison with Figure (6) of Anderson (1990). In this diagram, predicted development times are plotted; peak egg-production in April, nauplii developing from April until mid-May, CI-CIV from mid May to early June, and CV's first appearing in early June. The modelled population closely follows this pattern (Figure 4.10). Figure 6 of Anderson (1990) is reproduced in Figure 4.11 below.

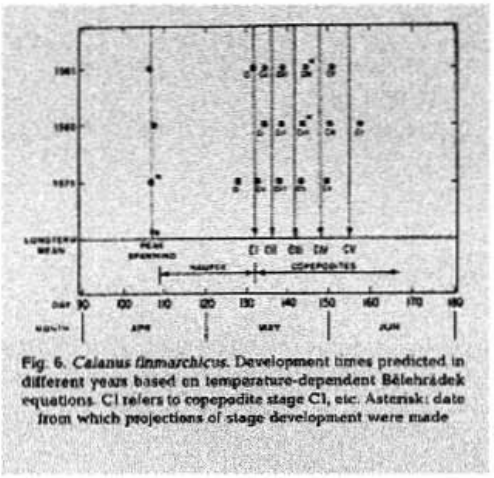

Fig. 6. *Calanus finmarchicus*. Development times predicted in different years based on temperature-dependent Bělehrádek equations. CI refers to copepodite stage CI, etc. Asterisk: date from which projections of stage development were made

Figure 4.11: *Calanus finmarchicus*. Development times predicted in different years based on temperature-dependent Belehradek equations. From Anderson (1990).

The sensitivity tests for this model run are similar to those at Bravo, with the exception that an early emergence test ($dt = 75$) is not included - since the early emergence timing is the same as that of the standard run for SE Flemish Cap. Each test is composed of eleven separate model runs. The tests are initialised with 100 diapausing individuals. The sensitivity tests are listed in Table 4.4:

Table 4.2: Sensitivity tests, biological model, SE Flemish Cap.

Test name	*Change from standard run*
Surface mortality	Mortality changed for non-diapausing individuals.
Diapausing mortality	Mortality changed for diapausing individuals.
Temperature	Mixed layer temperature varied by a constant amount over the annual cycle
Food	Food is varied by a constant amount over the annual cycle
Diapause timing	Diapause emergence timing modified by up to 25 days.

4.7 Results: Southeast Flemish Cap

4.7.1 Mortality sensitivity tests, SE Flemish Cap

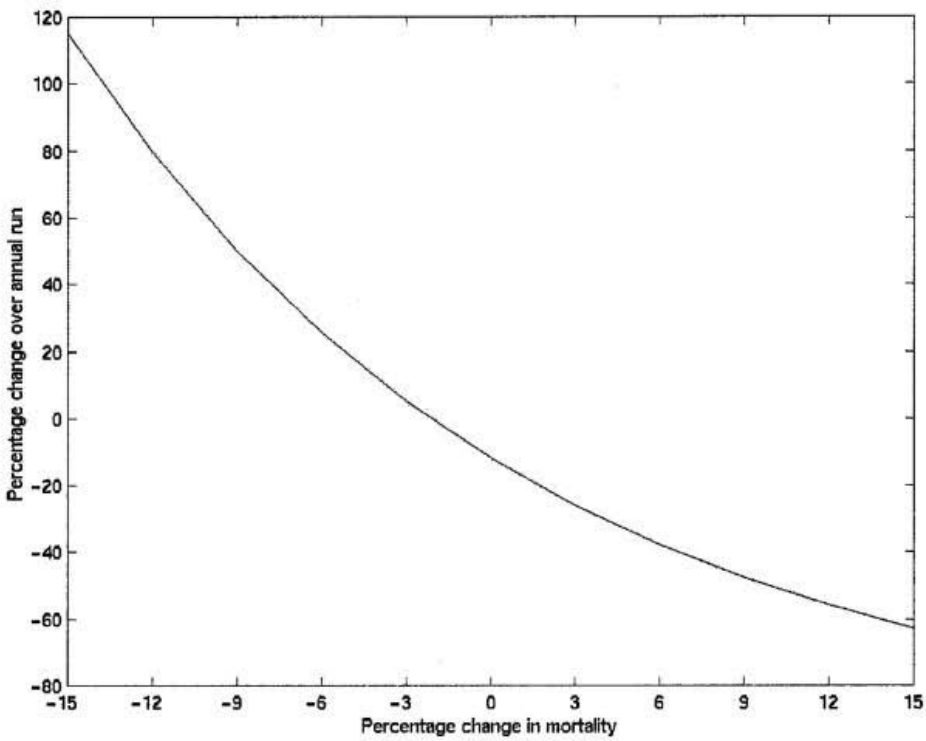

Figure 4.12: Results, surface mortality sensitivity test for biological model, Southeast Flemish Cap.

The annual cycle at Southeast Flemish Cap is very sensitive to mortality parameterisation, especially to a decrease in mortality, which leads to a relatively much

larger increase in population size (Figure 4.12). The results are very similar to those at Bravo.

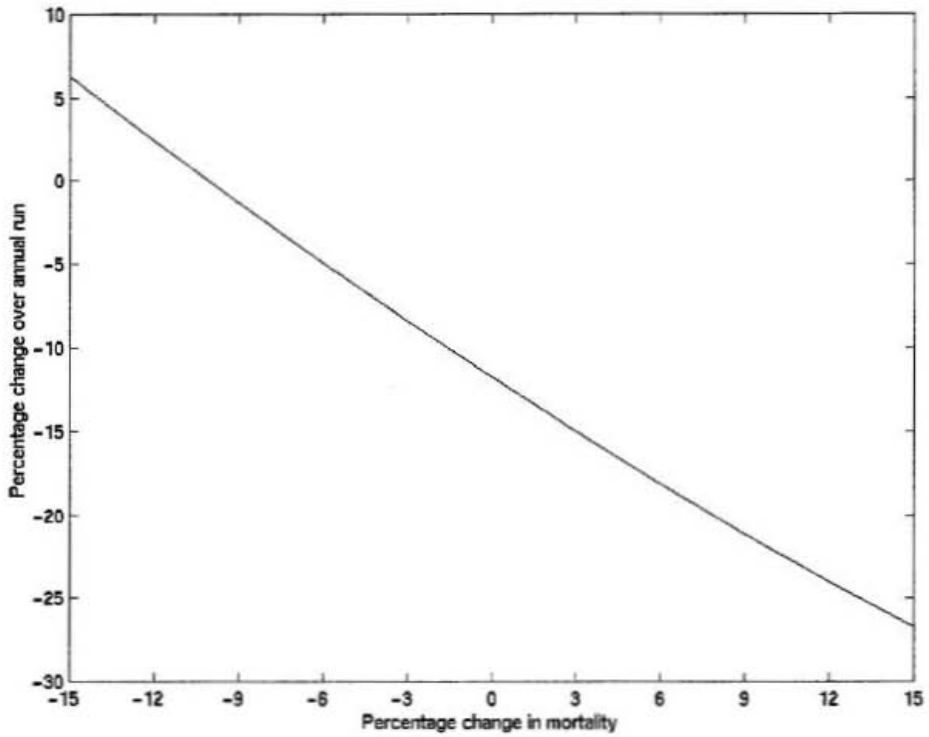

Figure 4.13: Results, diapausing mortality sensitivity tests for biological model, Southeast Flemish Cap

The sensitivity to diapausing mortality at Southeast Flemish Cap shows a near-linear response, with a much smaller disparity between change in mortality and change in final population numbers than for surface individuals (Figure 4.13). It can be postulated that this is due to diapausing mortality having a numerical value that is ten times smaller

than surface mortality, and hence a percentage change in diapausing mortality being of smaller magnitude than a percentage change in surface mortality.

4.7.2 Temperature sensitivity tests, SE Flemish Cap

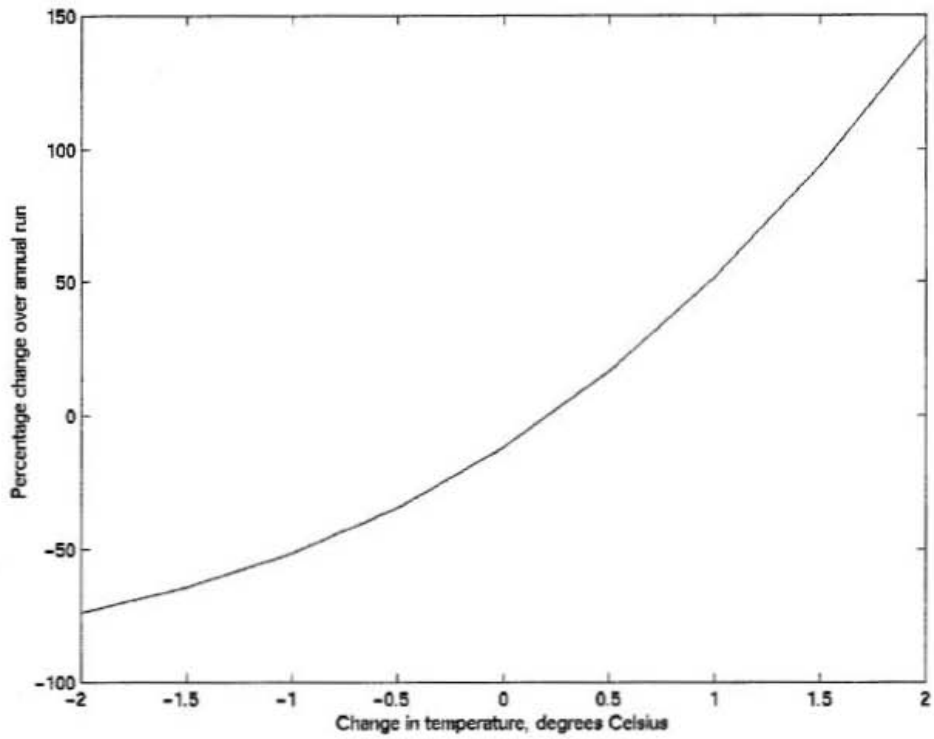

Figure 4.14: Results, temperature sensitivity tests for the biological model, Southeast Flemish Cap.

The model shows a non-linear response to modification of the temperature data values, with an increase in temperature providing a more rapid change than a decrease (Figure 4.14). The result is very similar to that of the sensitivity test at Bravo.

4.7.3 Food sensitivity tests, SE Flemish Cap

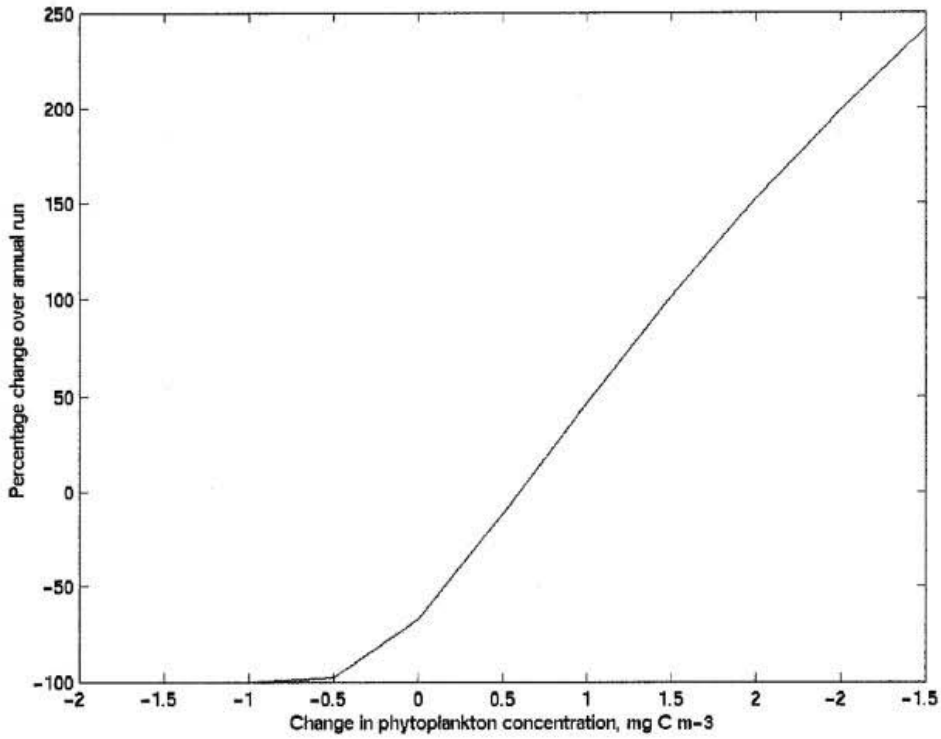

Figure 4.15: Results, phytoplankton concentration sensitivity tests for the biological model, Southeast Flemish Cap.

Interestingly, the model shows a rapid population collapse when food is decreased by 10 $mg\ C\ m^{-3}$ – a much more rapid collapse than at Bravo (Figure 4.8). This can easily

be explained by examining the unmodified phytoplankton concentration values for Southeast Flemish Cap; in the summer months, a decrease of this magnitude reduces the food by around one-half, and a reduction of 20 $mg\ C\ m^{-3}$ reduces the food to zero for half of July and all of August. With this in mind, it is not difficult to understand the population collapse that occurs upon food reduction. Increasing food, however, produces a large increase in final diapausing population (Figure 4.15).

4.7.4 Diapause timing sensitivity tests, SE Flemish Cap.

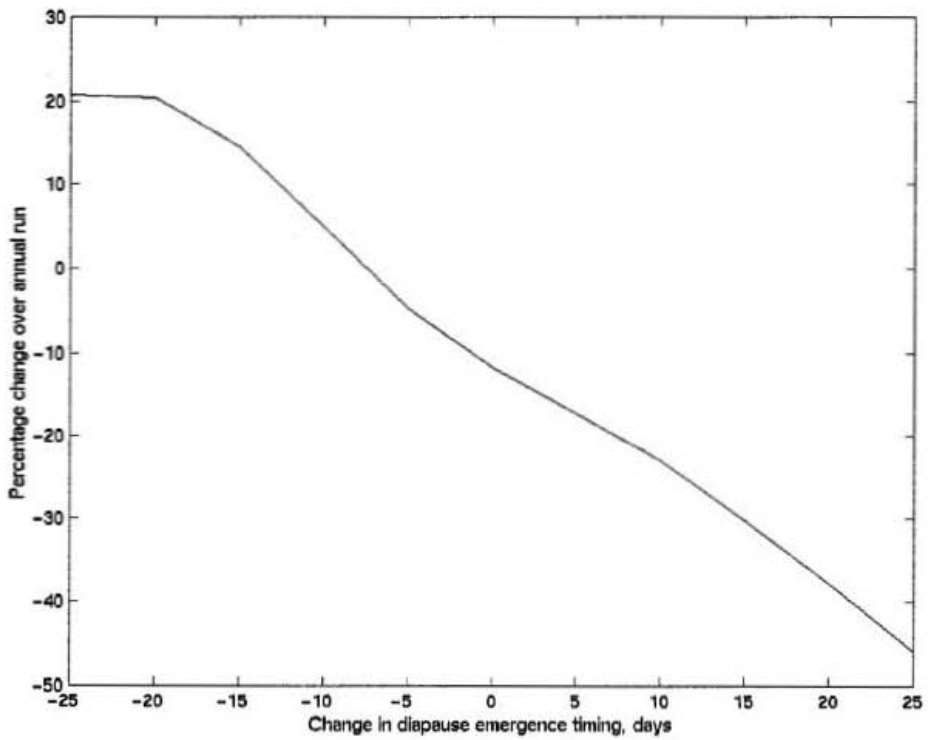

Figure 4.16: Results, diapause timing sensitivity tests, SE Flemish Cap.

The diapause timing sensitivity tests at SE Flemish Cap are interesting because they display the opposite behaviour to the tests at Bravo, with earlier emergence leading to a population increase and vice versa (Figure 4.16). Since the winter and spring temperatures are very similar, this is likely to due to food availability. Whereas Bravo has a relatively high level of food even after the spring bloom, at SE Flemish Cap there is a very low concentration of phytoplankton during the summer months (Figure 4.1), but a higher level prior to the spring bloom. Thus early emergence may lead a greater proportion of the G1 generation's development time being spent in the pre-spring bloom (relatively) food–rich environment. This effect does appear to tail off when diapause emergence is 25 days early (day 50, late February), due to a low level of food at this time relative to the succeeding months.

4.8 Discussion

It is worth noting that the physical and biological oceanographic features of Bravo and Southeast Flemish Cap are very different. Bravo is near the centre of the Labrador Sea and has a late spring bloom (June/July – see Figure 4.1). The SST temperature at Bravo is considerably cooler than that at Southeast Flemish Cap. The Southeast Flemish Cap box, however, has an earlier spring bloom (April/May – see Figure 4.1). Emergence of *Calanus finmarchicus* individuals from diapause occurs later at Bravo (Kielhorn, 1952) than at Southeast Flemish Cap (Anderson, 1990). These differences lead to observably different properties in the dynamics of the populations at each location.

Most sensitivity tests gave fairly similar results at each location, with the most noticeable difference being in the food sensitivity results. Comparison of the annual chlorophyll values (derived from the SeaWiFS data) shows a considerably lower range of values at Southeast Flemish Cap during the months immediately following the spring bloom (20.48-27.52 $mg\ C\ m^{-3}$ in June/July) than at Bravo (40.90 – 46.66 $mg\ C\ m^{-3}$ in Aug/Sep). Though the magnitude of the spring bloom is essentially similar (though a little lower at Southeast Flemish Cap), food availability after this period is much less at SE Flemish Cap. Higher summer temperatures may offset this in the standard run (leading to an almost identical final diapausing population value as at Bravo), but it can be seen from the sensitivity tests that a reduction in food availability down to near-zero causes negative growth in the G1 generation, and thus leads to starvation. However, at

Bravo, a similar reduction still leaves a proportionally greater amount of food, and thus the effects are not so drastic, though still fairly severe. This increased sensitivity to phytoplankton concentration at SE Flemish Cap is also observed when food availability is increased; the final diapausing population increases by a much larger value than that at Bravo.

The response to modification of the temperature data, in contrast to food availability, is startlingly similar between the two models, irrespective of the differences in the data between Bravo and SE Flemish Cap (Bravo has a much cooler SST throughout the entire year). Reducing the temperature produces an almost identical result in each model, while increasing the temperature produces a slightly greater effect at SE Flemish Cap. In both cases, there is a non-linear response that seems to be growing at a near exponential rate. In reality, it is possible that there would be a negative impact on growth rate at high temperatures outside of the normal range of this animal; this has been included in some models (Bryant *et al.*, 1997), though in the system presented in this thesis, the temperatures in the Labrador Sea would seem to be within reasonable limits for the organism (Hirche, 1987).

Sensitivity to changes in mortality parameterisation is again near-identical at each location, with surface mortality modifications having a greater impact than those of diapausing mortality. This differential sensitivity to mortality is likely due to the fact that surface mortality is set to a value ten times greater than diapausing mortality; thus a

percentage change in surface mortality has a correspondingly greater effect on population growth.

The mortality parameterisation is, in essence, a control factor that sets the population decay or growth at every location within the three dimensional model. However, it is difficult to know at which locations the population grows, decays, or maintains a constant value, even without the influence of advective processes. Thus the mortality has been given a value which maintains a roughly constant population (to within around ten percent) at each of the key locations studied within the one-dimensional system. However, it is important to remember that in some sense it is the productivity of each location relative to the others that is important, and these should remain similar irrespective of mortality parameterisation; the results can then be scaled for growth or decay with a new value for the mortality.

At both SE Flemish Cap and Bravo, with emergence timing modelled upon existing data (Kielhorn, 1952; Anderson, 1990), the modelled population emerges from diapause immediately prior to the spring bloom (from the SeaWiFS data). Thus the population has a significant food source available, which may be important for growth and egg production (Head *et al.*, 2000). Modifying emergence timing leads to a different response at each location, with early emergence at Bravo placing individuals in a cooler, relatively food-poor environment, increasing the mis-match with the spring bloom and hence reducing the final population. At SE Flemish Cap early emergence is into waters

that have a fairly constant temperature for the development time of the G1 generation, but may have greater food availability, since phytoplankton concentrations are higher prior to the spring bloom than after. The converse applies for later emergence at each location.

It is interesting to note that when individuals emerge from diapause in March at Bravo ($dt = 75$), to match the timing apparent in Matthews (1968) and hypothesised in Miller *et al.* (1991), there is a significant reduction in population size compared to the standard run after one year. This is due to lower temperatures and less food availability upon emergence. However, the key test of this result is when the model is run in three-dimensions, with simultaneous emergence over the entire region (Chapter 5).

There has been some quantitative study of plankton from inshore Newfoundland, primarily in Conception Bay (Davis, 1982) and Placentia Bay (Davis, 1986). Davis (1982, 1986) provided quite complete analysis of the zooplankton found in inshore Newfoundland waters including bimonthly observations of staged *Calanus finmarchicus*. *Calanus finmarchicus* appeared to have three, or possibly four, generations per year in the region, and was present at or near the surface throughout much of the study period.

The present model does not explicitly include growth or developmental differences between open ocean and near-shore regions (such as Conception Bay). In an attempt to model the structure of this region, fortnightly SeaWiFS chlorophyll and sea-surface temperature data from Station 27 (47.553°N, 52.587°W), also on the Avalon

Peninsula, was used as input data for a one-dimensional model run (results not shown). In this model run, the diapause function was switched off, so that after emergence from diapause (beginning on day 50) all CV's of each successive generation remained at the surface. The model did produce three generations within a one year period, although the timing of the generations does not precisely match the observations of Davis (1982). A doubling of the food supply, or a constant increase of 2°C in the temperature did enable faster growth of each generation, and a higher population density, but still yielded three generations per year. Low spring temperatures in the model, using monthly mean surface temperatures, show the modelled first generation grows much more slowly than is observed. These results indicate that further differentiation and explicit modelling for coastal locations may match the observations of Davis (1982, 1986).

An important question when analysing the sensitivity tests is whether they affect the validity of results for the three-dimensional coupled-model system. The three-dimensional model is being used to investigate patterns in *Calanus finmarchicus* distributions, and hence the relative abundance of individuals between location is of more importance in this study than their absolute value. Though the population is indeed sensitive to parameter changes, these should have a similar effect at all locations (apart from the diapause emergence timing parameter) throughout the region and thus maintain inter-regional relative productivity. I would claim that sensitivities are further offset by tuning the parameter a – the maximum uptake rate coefficient – in order to produce a relatively constant population at both one-dimensional locations.

Chapter 5

Three dimensional model runs

5.1 Motivation for three-dimensional run selection

5.1.1 Existing literature regarding *Calanus finmarchicus* in the Labrador Sea

There are three or four primary sources of data for *Calanus finmarchicus* within the Labrador Sea. An early, year-long study was that of Kielhorn (1952), which examined the planktonic ecology at OWS-Bravo during the course of a full year (1950/1951). These data reveal that diapause emergence occurs in April/May, with a G1 copepodite population maximum occurring in July/August. Around ten years later, the International Commission for the Northwest Atlantic Fisheries conducted a number of cruises between April and July 1963, along transects within the Labrador Sea (ICNAF, 1968). The *Calanus finmarchicus* data was summarised by Matthews (1968), with particular detail on the average stage of development at each location during the cruises:

(i) April, 1963. At most locations, adults were the mean stage of development. There were scattered CI-CIII present. Development was near-uniform across the survey region.

(ii) June, 1963. Within all locations, the mean development stage was CI-CIII.

(iii) July, 1963. The mean stage ranged from CI-CIV, with the coast of Greenland being CI-CIII, and the central Labrador Sea CIV-CV. Development therefore appeared to be fastest in the central Labrador Sea.

It appeared that all locations showed near-equivalence in April (suggesting that emergence from diapause had only recently occurred), with developmental differences becoming more pronounced on later cruises. Note that there are substantial differences between Matthew's and Kielhorn's data – emergence is earlier and growth appears to be faster (if it is assumed that the maximum number of G1 copepodites consist of early stages, which is reasonable due to the cumulative effect of mortality on each stage) in the ICNAF survey.

Anderson (1990) examined a region around the Flemish Cap during 1979-1981. In April, the population was to be dominated by adults, but CI-CIV's were present by May. Individuals appeared to have reached CV by late June.

Planque (1997) examined over 30 years of CPR data (1958-1992) for *Calanus finmarchicus* CV and adults, and compiled the data into monthly log-abundance figures. A reproduction of Figure 17 from Planque (1997), Figure 5.1, shows the importance of

the Labrador Sea for *Calanus finmarchicus*. By July, there appears to be a peak of *C. finmarchicus* in the middle of the southern Labrador Sea.

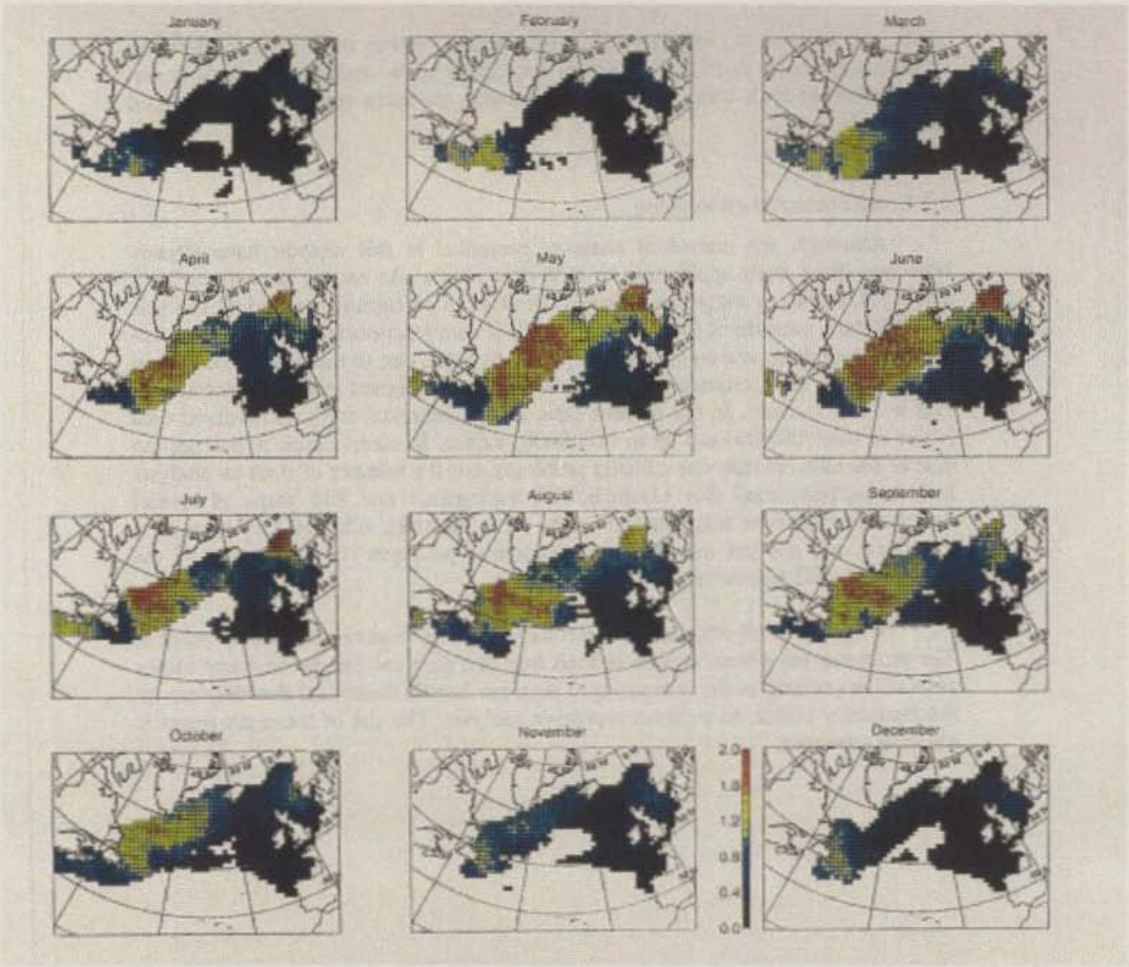

Figure 5.1: Mean monthly distribution of *Calanus finmarchicus* during the period 1958-1992. Log-abundance is indicated by the colour scale. Only pixels with at least 10 years of data are shown on each map. From Planque (1997).

A number of trends are readily observable from these data (considering only the region under study in this thesis). There appears to be a population to the south and east of Newfoundland that emerges from diapause much earlier than the rest of the region, with low numbers of individuals present at the surface from November, and a high concentration appearing in February. For all areas north of Newfoundland, individuals begin to appear at the surface in March or April, with high abundances from April to September.

Planque (1997) also looked at the correlation between the North Atlantic Oscillation (NAO) index (a measure of the pressure difference between Iceland and the Azores) and *Calanus finmarchicus* abundance between 1962 and 1992. A strong negative correlation was discovered.

Head *et al.* (2000) undertook a number of transect surveys in May-June of 1997, from around 42°N to 64°N. CI-CIII individuals were (numerically) dominant in most of the north, with adults more abundant in central and southern regions. Spring bloom conditions were late/post-bloom in the north, bloom conditions at the mid-latitudes, and early bloom in the southeast, and these conditions seemed consistent with those of the ICNAF surveys. Head *et al.* (2000) suggested that early blooms were common in the north and east, perhaps linked to the ice-melt. The hypothesis was put forward that the maturation of G0 females and development of the G1 generation was linked to the spring bloom, such that the G1 generation was more advanced in the north during the period

surveyed due to the earlier spring bloom; differences in water temperature would then tend to speed up development and growth in southern regions.

Miller *et al.* (1991) have suggested that arousal from diapause has a high degree of synchronicity from 40°N to 70°N north, probably taking place in March, or perhaps late February.

5.1.2 Two hypotheses regarding emergence from diapause

When the literature presented in section 5.1.1 is assimilated and combined, I would suggest two hypotheses regarding emergence from diapause in the Labrador Sea and its environs. These hypotheses are presented below:

Hypothesis 1: Kielhorn (1952) indicates that emergence from diapause at Bravo (56°-30'N) occurs in April/May, while Anderson (1990) presents data that would suggest emergence from diapause at Flemish Cap to occur, by back-calculation from peak-spawning data, around the middle of March. From Planque (1997), emergence south of Newfoundland appears to be still earlier. Emergence from diapause is thus latitudinally dependent, being earlier in the south and later in the north.

Hypothesis 2: From Matthews (1968) and Miller (1991), it would seem clear that emergence from diapause occurs at roughly the same time over the entire region (most likely March), except to the south and east of Newfoundland where emergence is earlier. Any differences that arise in population development may be due to different growth rates caused by the timing of the spring bloom and the temperature of the water (Head *et al.* 2000).

The three-dimensional model runs will attempt to explore these two hypotheses, along with relative regional production, advective influences on population distributions, and the effect of an incoming flux of organisms from outside the study area.

5.2 Three dimensional model setup

5.2.1 Model runs

The parameters that were selected for the two one-dimensional model analyses are also used to parameterise the three-dimensional model system, including a linearly interpolated value for the food uptake parameter a derived from the one-dimensional runs that depends upon the latitude of the grid point. The parameter a takes a value of 0.13 at Bravo, and 0.09 at SE Flemish Cap, in order to produce a stage progression that matches to data at these points (see Chapter 4). Between these two locations, the value of a is linearly interpolated by latitude, and this interpolation is continued to the southern boundary of the model. To the north of Bravo, a takes the same value as at Bravo, similarly to the diapause emergence timing parameter.

Runs without advection are carried out in order to assess the relative productivity of each region under different emergence schemes. Following this a number of 'standard' runs utilise different emergence schemes to examine population distributions. Two runs examine the effects of changing the mortality parameterisation. A tracer run at Bravo is conducted in order to examine the model within a pseudo-Lagrangian framework; that is, to follow a population that begins at a single grid point throughout the course of a year. Two model runs look at the effect of an incoming population being carried on the fast-flowing currents to the south of Greenland. One run looks at a population initialised in June. Finally, the standard run is continued for a second year, to assess population

stability. The results of these model runs are described in this chapter. Note: when referring to CV individuals, this excludes those that are in diapause. All model runs are carried out for one year (generally Jan. 1 – Dec. 31). All model results are in individuals per m^{-2}. The model runs are listed in Table 5.1. A further description of each run then follows.

Table 5.1: Three-dimensional model runs

Run Number	*Model Run*	*Diapause emergence timing*	*Comments*
1	No advection	Lat. dependant emergence	No advective processes
2	No advection	Bilatitudinal emergence	No advective processes
3	Standard	Lat. dependant emergence	
4	Standard	Simultaneous emergence	
5	Standard	Bilatitudinal emergence	
6	Standard	Early bilatitudinal emergence	Emergence mid. Feb. for all points north of 50°N
7	Increased mortality	Lat. dependant emergence	Mortality increased by 10% for all classes
8	Decreased mortality	Lat. dependant emergence	Mortality reduced by 10% for all classes
9	Tracer	Lat. dependant emergence	Tracer population at Bravo
10	Depth flux	Lat. dependant emergence	Incoming flux at depth
11	Surface flux	Lat dependant emergence	Incoming flux at surface
12	Mid-year start	Lat. dependant emergence	Starts June 1st
13	Standard, year 2	Lat. dependant emergence	Year 2 of run 3

5.2.2 Non-advective model runs

The non-advective runs (1 & 2) are conducted in order to determine the relative productivity of each region under two different diapause emergence schemes. These runs are initialised with 100 diapausing individuals per m^{-2} at every location. The diapause emergence schemes are described in section 5.2.3.

5.2.3 Standard model runs

Runs 3-6 are the 'standard' runs, being the coupled biological – physical model system with all parameters as standard, and the only difference being the timing of emergence from diapause. These runs determine the influence of advection on population structure, the viability of an isolated population in the Labrador Sea, and the effect of changing the timing of emergence from diapause.

Run 3 utilises latitudinally dependant emergence derived from the one-dimensional model runs as follows: at Bravo, $dt = 120$ (emergence is in early May), at SE Flemish Cap $dt = 75$ (emergence is in mid-March). All grid points south of Bravo are linearly interpolated from the timing at Bravo and SE Flemish Cap. All grid points to the north of Bravo are set with the same emergence timing as at Bravo, justification for which comes from the fact that diapause emergence would be unreasonably late (when matched to any of the data sources) if the interpolation were continued further

northwards. Thus the emergence timing is latitudinally dependent, with a later emergence at higher latitudes. This diapause emergence timing derives from Kielhorn (1952) and Anderson (1990), and fits with hypothesis 1.

Run 4 is a standard run that has simultaneous emergence for all individuals over the entire region, beginning on day 75. This is somewhat similar to the arguments in hypothesis 2, but with emergence being simultaneous over the entire region, rather than having a separate scheme for those individuals to the south of Newfoundland.

Run 5 is set to match hypothesis 2, and the data of Matthews (1968), in that emergence is simultaneous in the Labrador Sea, while being much earlier to the south of Newfoundland. This scheme is referred to as bilatitudinal emergence. All individuals north of 50°N emerge from day 75 (mid March) onwards, while individuals to the south of 50°N emerge from day 16 (mid January).

In run 6 individuals emerge as per bilatitudinal emergence, except that all individual north of 50°N emerge on day 46 (mid February). This is an attempt to assess the effect of changing the emergence timing for the bilatitudinal emergence model run.

All of the standard runs are intialised with the same population structure: 100 diapausing individuals at every location in which the water is of at least 1000 metres in

depth. The effects of advection onto shelf and slope regions can therefore be fully determined.

5.2.4 Mortality runs

Runs seven and eight examine the effect of changing the mortality parameter upon the final population structure. The mortality for every class is increased by 10% or reduced by 10% respectively. The runs are initialised with a population structure as described in section 5.2.3.

5.2.5 Tracer model run

In an attempt to examine the effects of physical transport upon a population beginning at a single location, model run 9 is initialised with 100 diapausing individuals at Bravo only. The population is then followed through the course of a year.

5.2.6 Flux model runs

Runs 10 and 11 examine the effect of a flux at the eastern boundary to the south of Greenland; this is a region which is likely to be of great importance for the flux of individuals into the region, due to fast-flowing incoming currents, its positioning as part

of the North Atlantic gyre structure (Figure 1.4), and the density of *Calanus finmarchicus* individuals contained within the Irminger Sea (Planque, 1997).

The runs do not begin with any *Calanus finmarchicus* present in the modelled region, but have a flux boundary condition set to 100 diapausing or 100 CV individuals respectively, at three grid points to the south of the southern tip of Greenland. Run 10 has the flux condition set (for diapausing individuals) from day 1 to day 120 (the first day of emergence from diapause in the standard run with latitudinally dependent emergence). Run 11 has the flux condition (for surface CV's) from day 121 to day 150 (a period in which CV's are likely to be active in the surface layer, and also a time when there is a high population density to the south of Greenland (Planque, 1997) in the CPR trawls). All other conditions are the same as run 3, the standard run with latitudinally dependent emergence.

5.2.7 Mid-year run

To examine population development from a slightly different approach, run 12 is begun on day 151 (June 1st) instead of day 1 (January 1st). The initial population is based upon a considerably more spatially and structurally coarse representation of the data from Head *et al.* (2000). To the north of 60°N, the concentration of individuals is 1000 m^{-2}; south of this it is 100 m^{-2}. Individuals are only placed in regions that have a depth of at least 1000m. Adults form 50% of total individuals to the south of 60°N, 10% otherwise.

Adults are divided equally between males and females, with females being equally subdivided into mature and immature individuals. CI-CIV copepodites form 40% of individuals to the south of 60°N, 70% otherwise; CV's 10% to the south of 60°N, 20% north of this (based on Figure 8 from Head *et al.*, 2001). Individuals have an initial weight that lies at the mid-point between their current class and the next. No individuals are present in diapause at the start of the run. Diapause entrance follows the latitudinally dependent scheme.

Although this approach is fraught with considerable difficulties (namely the somewhat abstracted initial population, and the lack of comprehensive data – for instance there are no figures for nauplii so these have not been included in the initial population), this run aims to depict population development over the course of an annual cycle beginning in the summer.

5.2.8 Standard run, second year

In order to determine the continued stability of the modelled population, run 3 (the standard run with latitudinally dependent emergence) is continued for another year. Run 13 has the same parameter set as run 3, with the exception that the initial population is equal to the final population for run 3.

5.3 Model run 1 – no advection, latitudinally dependant emergence

The two model runs without advection could be considered to be a set of one-dimensional runs covering the horizontal plane of grid points contained within the three dimensional model. Each point is initialised with one hundred diapausing individuals to produce an initially uniform distribution. Figure 5.2 shows the final distribution of individuals, and Figure 5.3 the monthly average for all individuals

The population of diapausing individuals over the whole of the model region remains within the same order of magnitude at the end of the annual simulation as at the start; an increase of 58.4%, with most growth coming from the productive regions in the south-east. 99.68% of individuals are diapausing at the end of the run. There is no second generation in the region, and surface individuals on day 365 are composed of slow-developing G1 copepodites.

The maximum number of diapausing individuals at the end of the run occurs in the box centred at 45.42°N, 40.3°W (688 individuals). The minimum number of diapausing individuals occurs in the box centred at 44.75°N, 48.3°W (< 2 individuals).

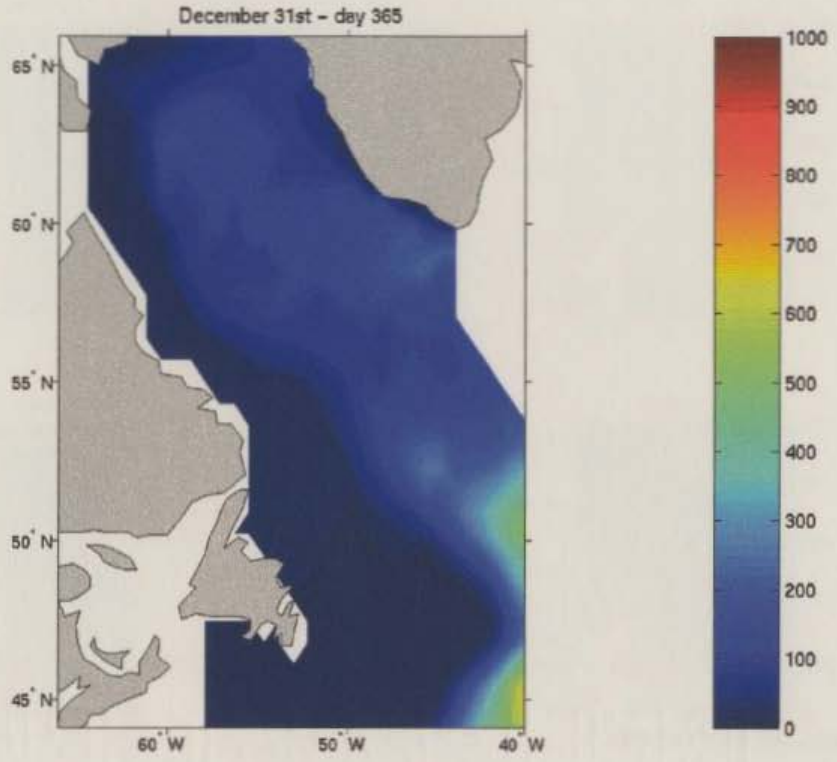

Figure 5.2: Final population, model run 1 – no advection, latitudinally dependent emergence. Number of individuals per m^{-2} on day 365.

The most productive regions are located in the south-east of the model, with a strip along the western boundary of the Labrador Sea being the least productive. Figure 5.3 shows the latitudinally dependent production of the G1 generation very clearly – individuals are produced later in more northerly regions.

Figure 5.3: Results, run 1– no advection, latitudinally dependent emergence. Monthly averages, all individuals.

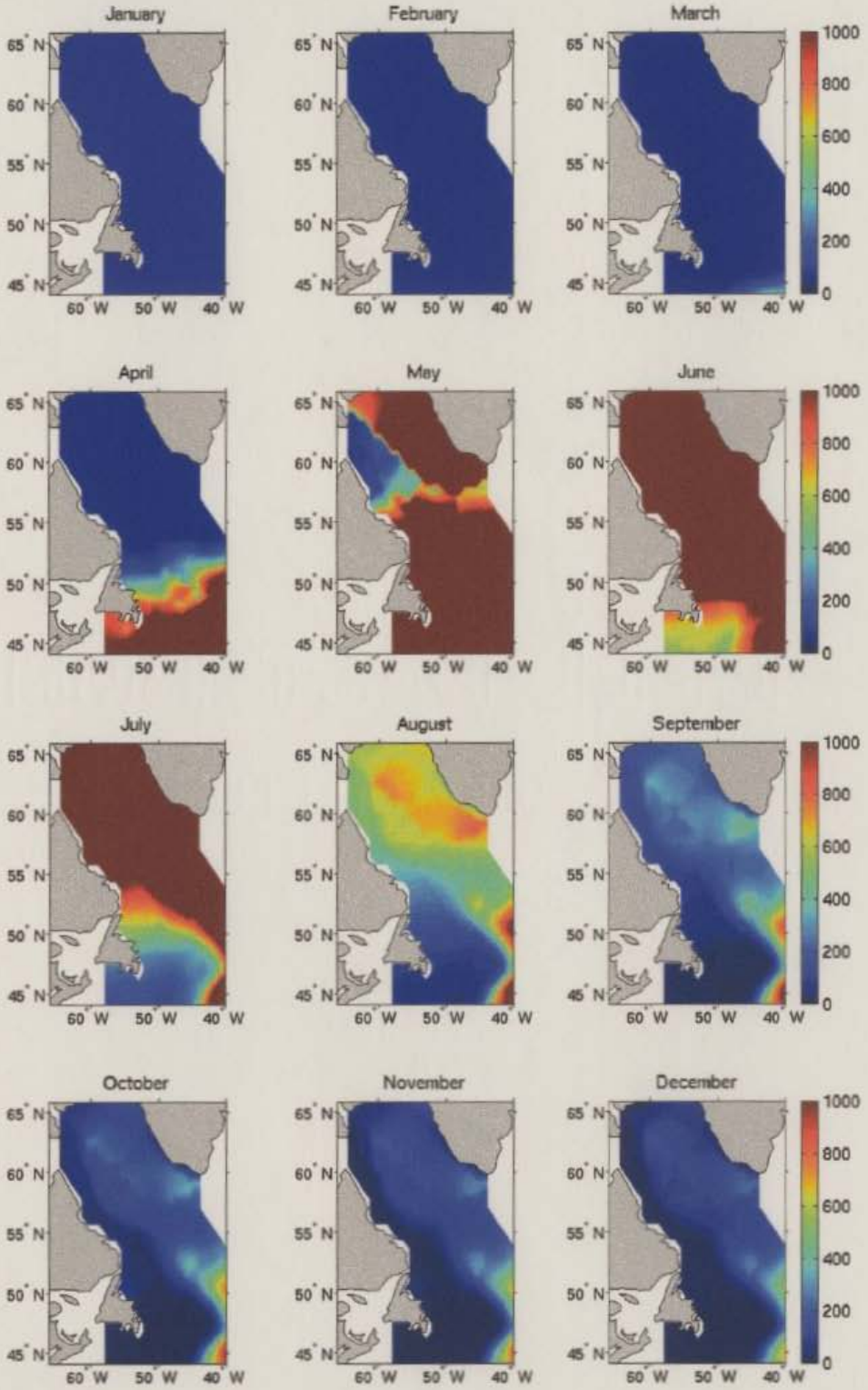
January
February
March
April
May
June
July
August
September
October
November
December
65° N
60° N
55° N
50° N
45° N
60° W
50° W
40° W
1000
800
600
400
200
0

5.4 Model run 2 – no advection, bilatitudinal emergence

Model run 2 is the identical to run 1, except with the bilatitudinal emergence scheme. Figure 5.4 shows the final distribution and Figure 5.5 the monthly averages for all individuals.

Over the whole of the model region, the population decreases by 8.54%. 99.91% of individuals are diapausing at the end of the run, with no second generation produced. The maximum number of diapausing individuals occurs in the box centred at 46.08°N, 40.3 °W (435 individuals). The minimum number of diapausing individuals occurs at 41.42°N, 48.3°W (<1 individual). The most productive regions are once again in the south-eastern area of the model region. Overall the pattern is very similar to run 1, with, in general, lower values for diapausing individuals at each grid point.

The monthly averages (Figure 5.5) clearly show the early emergence south of 50°N, and the near-simultaneous production of the G1 generation to the north of this, with differences in production being due to growth and development rates. The population that emerged early remains very distinct from that to the north, with a clear line break resulting from earlier emergence and descent of these individuals.

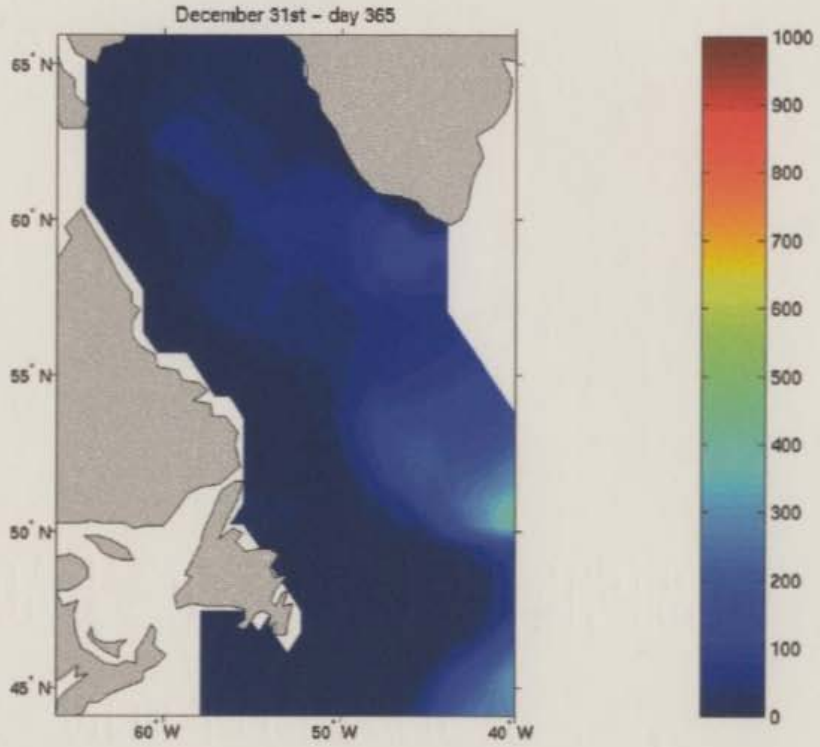

Figure 5.4: Results run 2 – no advection, bilatitudinal emergence. Number of individuals per m^{-2} on day 365.

Figure 5.5: Results, run 2 – no advection, bilatitudinal emergence. Monthly averages, all individuals.

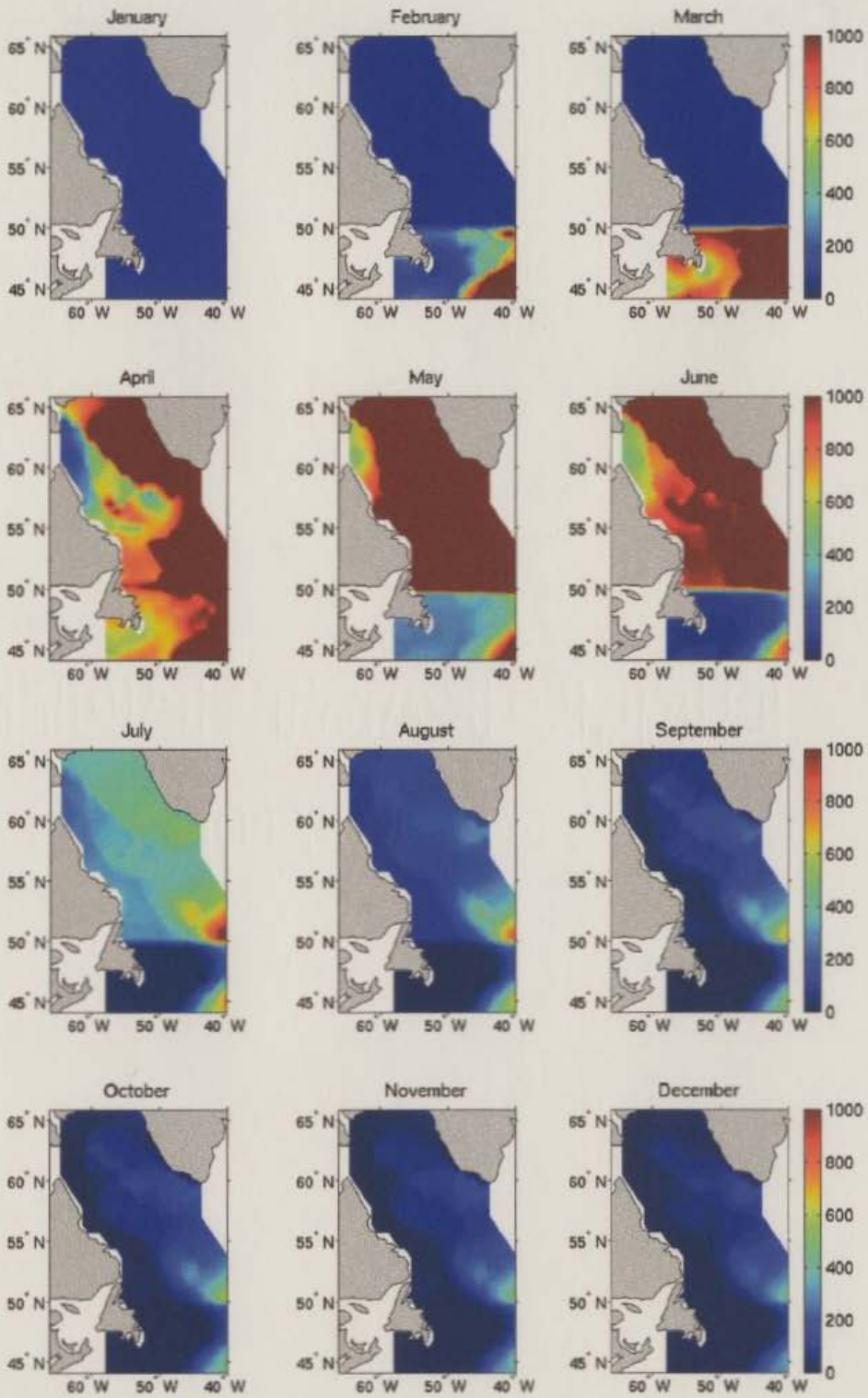
January
February
March
April
May
June
July
August
September
October
November
December
65° N
60° N
55° N
50° N
45° N
60° W
50° W
40° W
1000
800
600
400
200
0

5.5 Model run 3 – standard run, latitudinally dependent emergence

Run 3 is the full three-dimensional system, with parameters derived from the one-dimensional model run, latitudinally dependant emergence, and the advective velocity field in place. Each point of at least 1000 metres in depth is initialised with diapausing individuals – i.e. shelf and slope waters initially contain no individuals. This should enable determination of whether the possibility of individuals being transported onto the continental shelf is valid. Figure 5.6 shows initial and final distributions. Figure 5.7 shows monthly averages of all individuals, and Figure 5.8 monthly Log_{10} averages of surface CV and CVI individuals.

The number of diapausing individuals at the end of the 365 day run is 68.86% of the number of diapausing individuals at the start, with 99.67% of individuals being in diapause. The total number of individuals to leave the area expressed as a percentage of the final number of individuals in the area is 585.79%. The breakdown of exiting individuals is as follows: 11.88% leave from the southern boundary, 87.86% from the eastern boundary, and 0.26% from the northern boundary.

Figure 5.6(d) shows that diapausing individuals reside at the lowest possible depth in their locations; an indication that the model works correctly. Figure 5.7 clearly shows the concentration of diapausing individuals by current patterns (January – March), production of a new generation (beginning in April), a population maximum in the central Labrador Sea region, and a final population of diapausing individuals that is quite

different from the initial. The final diapausing population displays significant heterogeneity, and individuals are located on shelf and slope regions (for the 200m isobath, refer to Figure 1.5).

The 'patchiness' of the modelled population (relative to the model runs without advection) is caused by several interacting properties. The modelled individuals are moved relative to a spatially-static food field (though it changes temporally every two weeks), and thus they may be moved through locations of varying food concentration (and hence growth rate), leading to quite different life-history and population growth than in the non-advective model runs. There is also the mixing of individuals created by the movement of homogeneous populations within each grid box (see Chapter 3). This means a fast moving advective grid point with a velocity vector leading to a grid point with a slower moving vector will lead to an accumulation of individuals in the grid point with the slower velocity, creating some of the spatial patterning seen in the advective model runs.

Figure 5.8 displays the latitudinally dependent emergence of individuals from diapause, and the months with the most CV and adult individuals present at the surface (April – September for the central region).

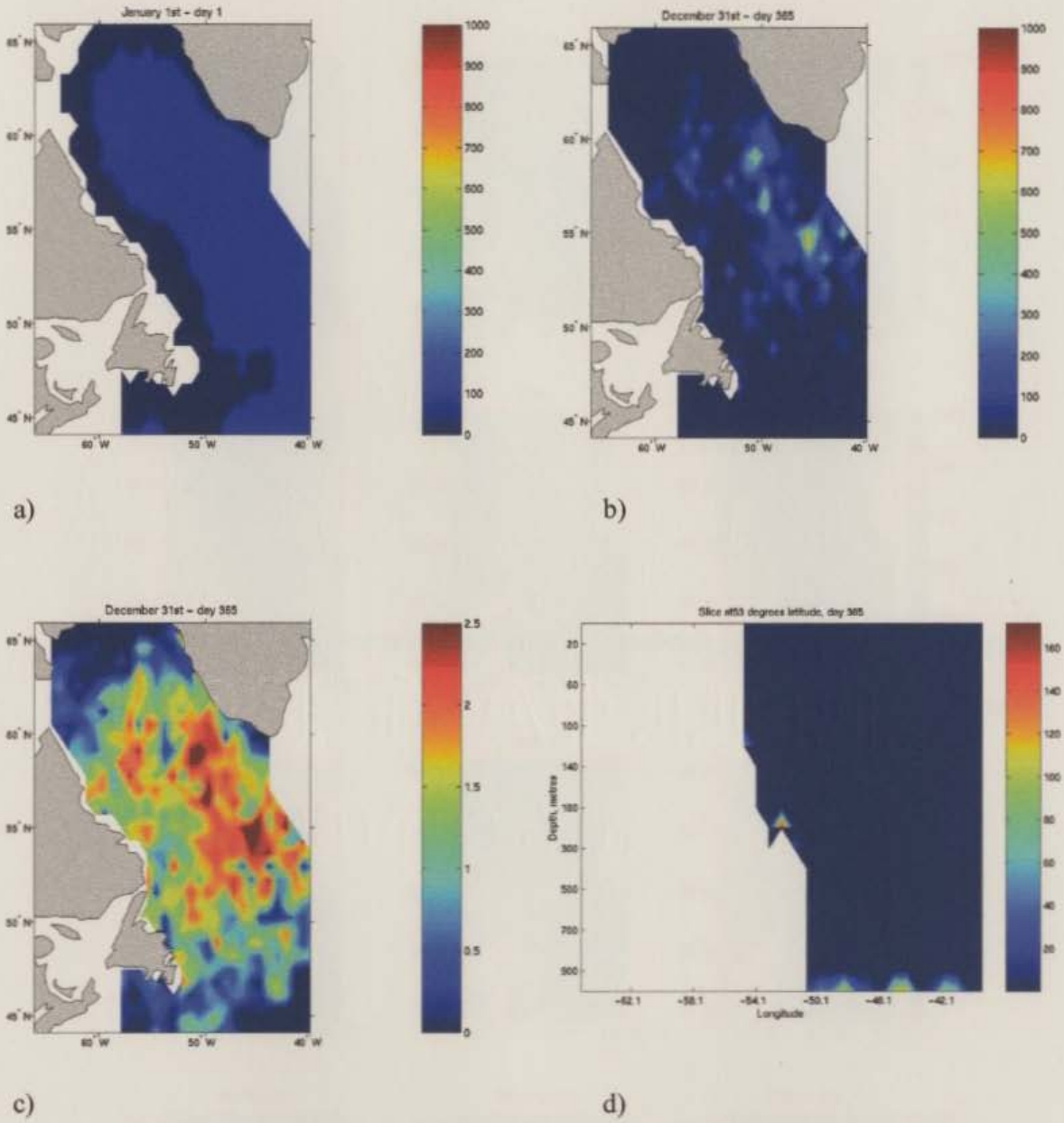

Figure 5.6: Results, run 3 - standard run, latitudinally dependent emergence. The model is initialised with 100 diapausing individuals per m^{-2} at all points of 1000m or greater depth. a) Initial population, day 1. b) Final diapausing individuals, day 365. c) Log_{10} $(x+1)$ where x is final diapausing individuals. d) Latitudinal slice at 53°N, day 365.

Figure 5.7: Results, run 3 – standard run, latitudinally dependent emergence. Monthly averages, all individuals.

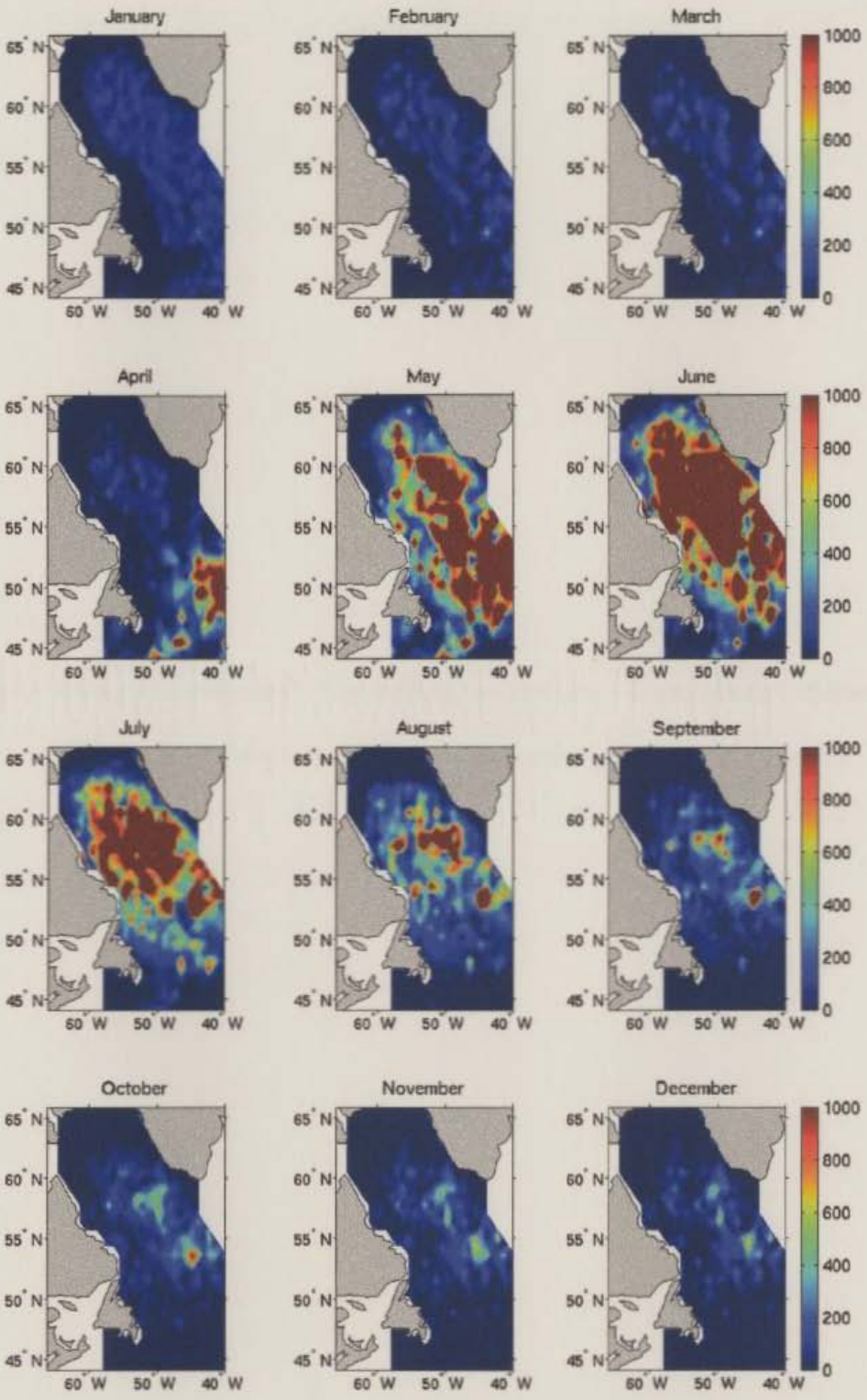
January
February
March
April
May
June
July
August
September
October
November
December
65° N
60° N
55° N
50° N
45° N
60° W
50° W
40° W
1000
800
600
400
200
0

Figure 5.8: Results, run 3 – standard run, latitudinally dependent emergence. Log_{10} $(x+1)$, where x is the monthly average of surface CV and adult individuals.

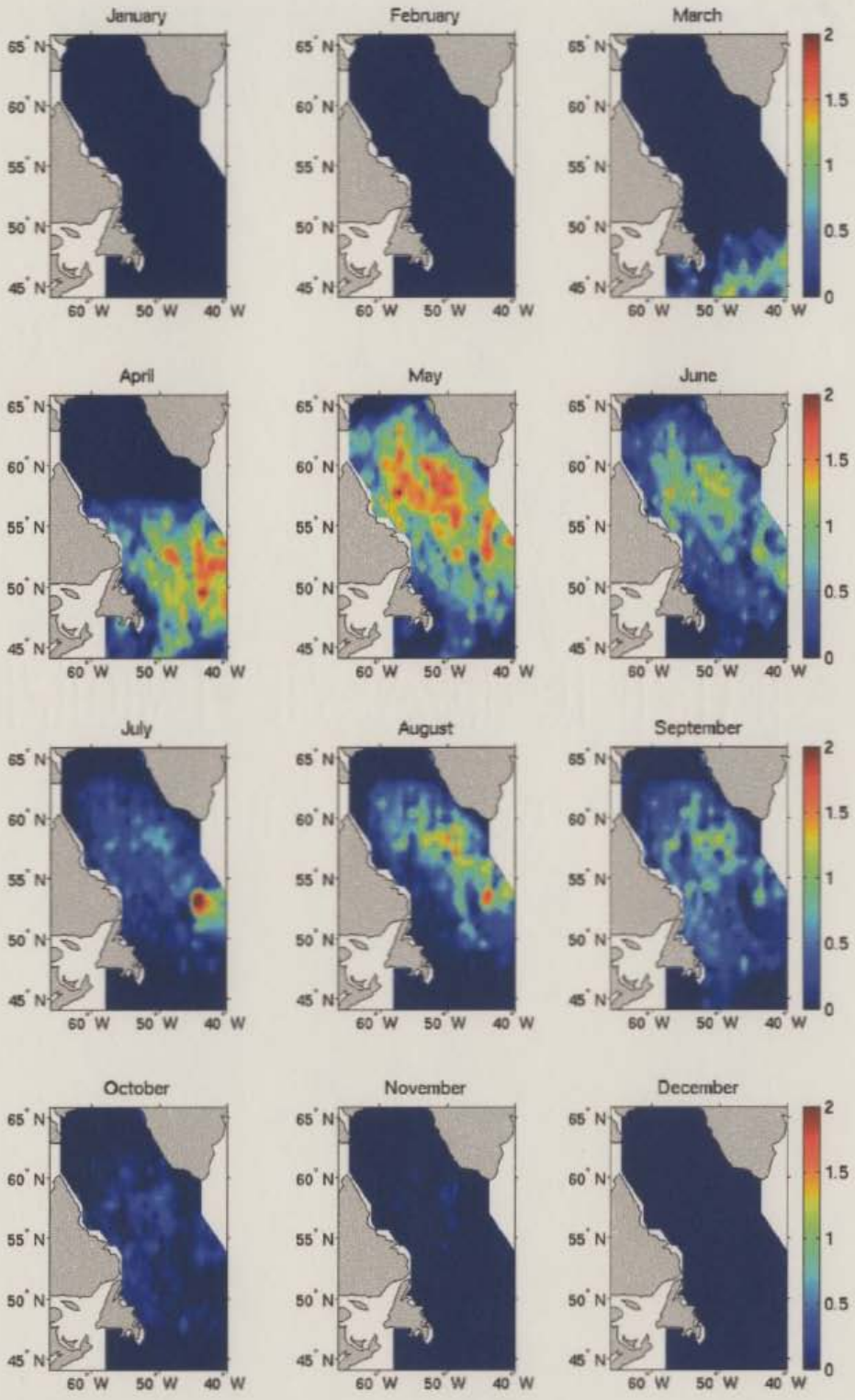
January
February
March
April
May
June
July
August
September
October
November
December
65° N
60° N
55° N
50° N
45° N
60° W
50° W
40° W
2
1.5
1
0.5
0

5.6 Model run 4, standard run, simultaneous emergence

Model run 4 stands as a counterpoint to runs 5 and 6 (which follow hypothesis two; that emergence is simultaneous except for a region south of Newfoundland), and explores the possibility that emergence could be simultaneous over the entire region. Figure 5.9 shows the final population of diapausing individuals, Figure 5.10 monthly averages for all individuals, and Figure 5.11 monthly averages for adult and CV individuals.

The final population of diapausing individuals is 41.40% that of the initial value, with 99.91% of individuals in diapause. Of *Calanus finmarchicus* which leave the region 11.03% of individuals leave by the southern boundary, 0.23% from the northern boundary, and 88.74% from the eastern boundary. Expressed as a percentage of initial individuals, 1055% leave the region over the course of a year.

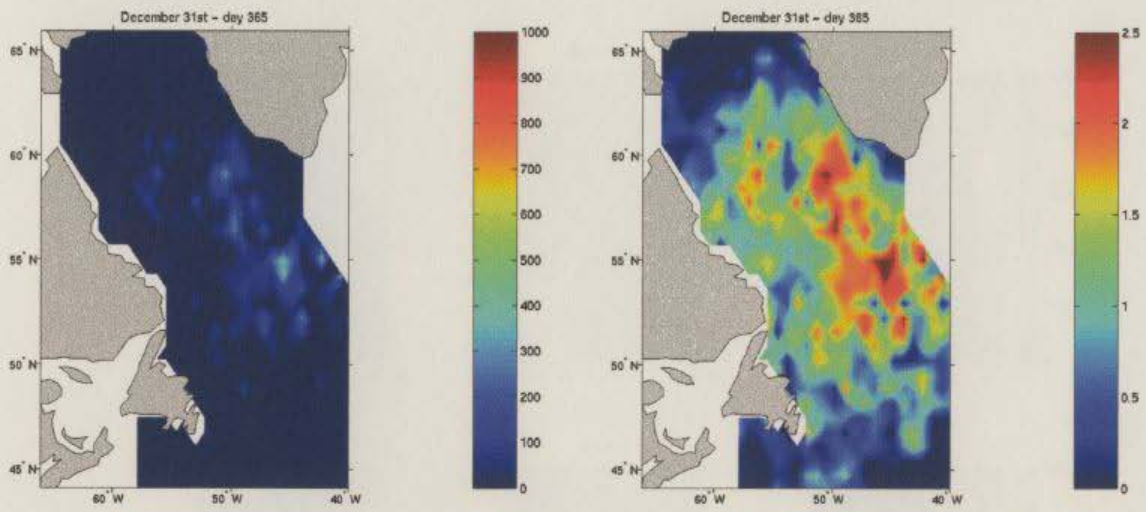

a) b)

Figure 5.9: Results, run 4 – standard run, simultaneous emergence. The model is initialised with 100 diapausing individuals per m^{-2} at all points of 1000m or greater depth. a) Final diapausing individuals, day 365. b) Log_{10} $(x+1)$ where x is final diapausing individuals.

Figure 5.10 shows the near-simultaneous production of a new generation, and Figure 5.11 the simultaneous emergence from diapause of CV individuals.

Figure 5.10: Results, run 4 – standard run, simultaneous emergence. Monthly averages, all individuals.

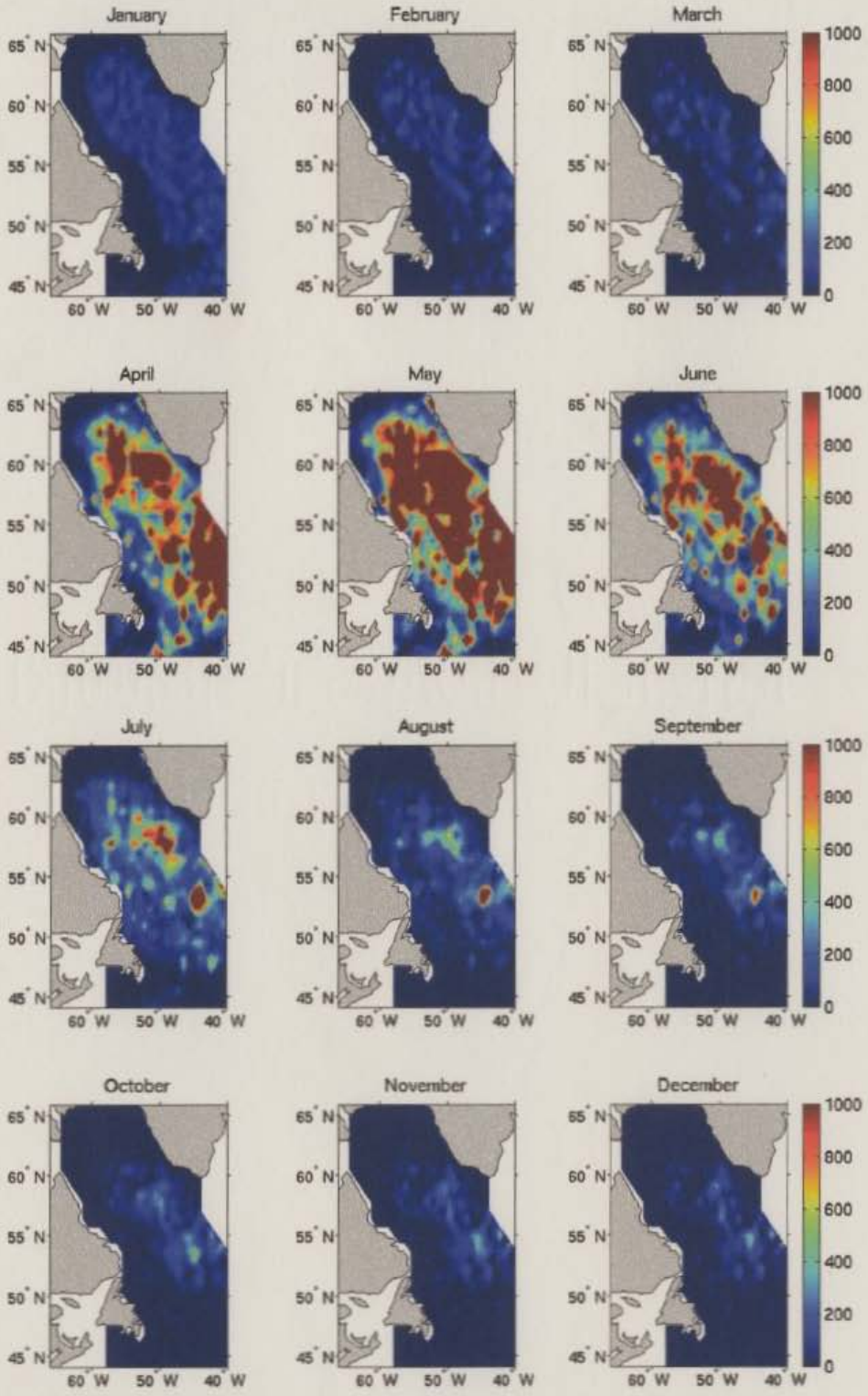
January
February
March
April
May
June
July
August
September
October
November
December
65° N
60° N
55° N
50° N
45° N
60° W
50° W
40° W
1000
800
600
400
200
0

Figure 5.11: Results, run 4 – standard run, simultaneous emergence. $Log_{10}(x+1)$, where x is the monthly average of surface CV and adult individuals.

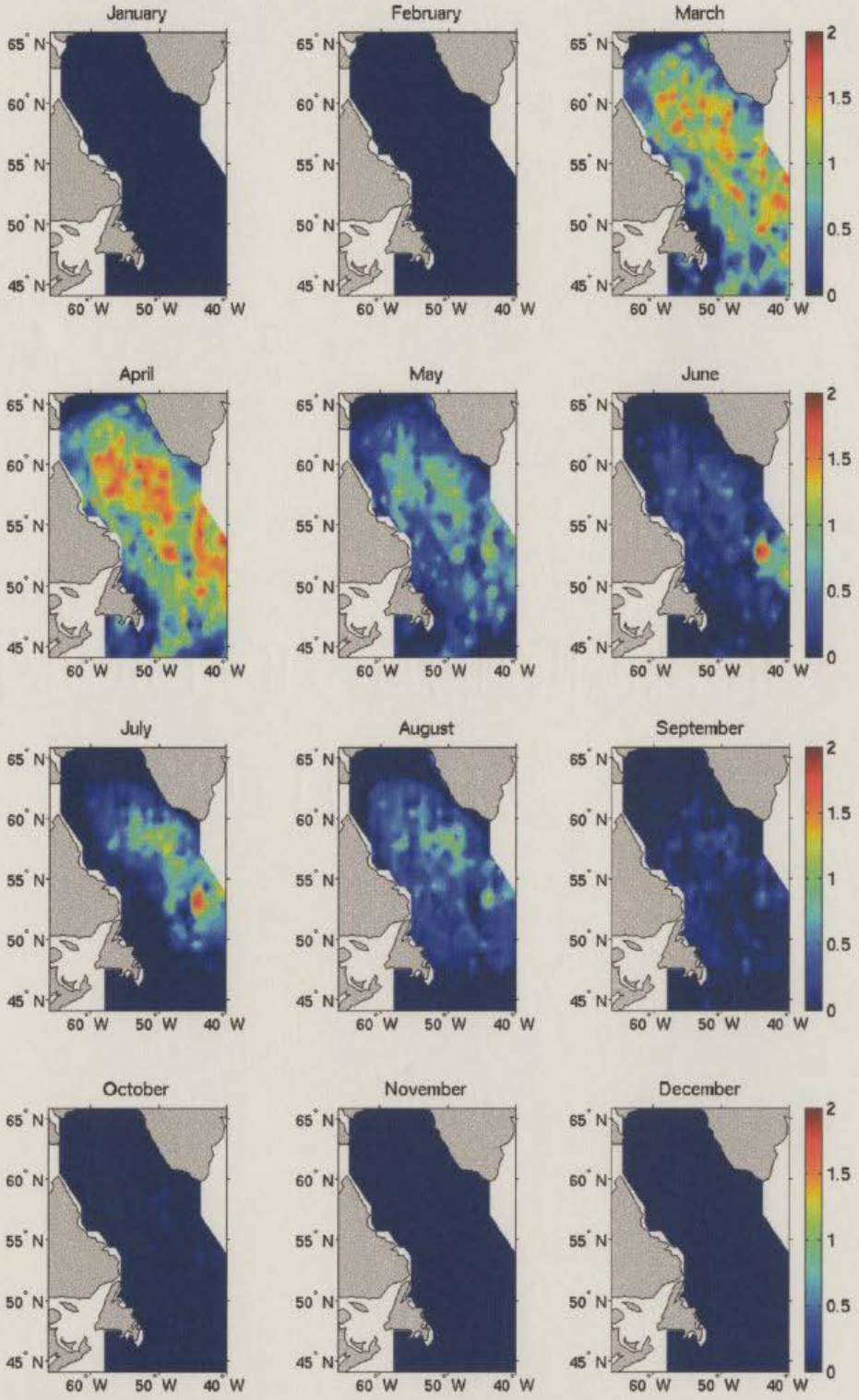
January
February
March
April
May
June
July
August
September
October
November
December
65° N
60° N
55° N
50° N
45° N
60° W
50° W
40° W
2
1.5
1
0.5
0

5.7 Run 5, standard run with bilatitudinal emergence

Run 5 is the same as run 3, except with bilatitudinal emergence (as described in section 5.1).

The final number of diapausing individuals is 38.53% of the initial number, with 99.91% being in diapause. Expressed as a percentage of initial individuals, 923.33% of individuals leave the model region; 8.72% from the southern boundary, 91.01% from the eastern boundary, and 0.28% from the northern boundary.

Figure 5.12 shows the number of diapausing individuals on day 365, Figure 5.13 monthly averages for all individuals, and Figure 5.14 monthly averages for surface CV's and adults.

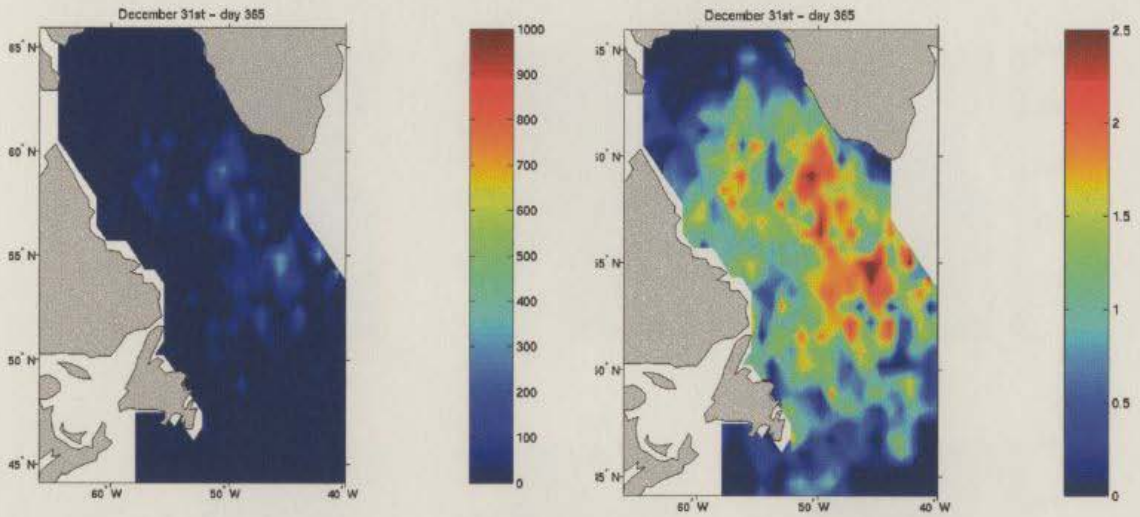

a) b)

Figure 5.12: Results, run 5 – standard run, bilatitudinal emergence. a) Diapausing individuals per m^{-2}, day 365. b) Log_{10} (x+1), where x is the number of diapausing individuals on day 365.

The early emergence from diapause of the regions to the south of Newfoundland can be seen in Figure 5.14, and its effect on the production of a new generation in Figure 5.13.

Figure 5.13: Results, run 5 – standard run, bilatitudinal emergence. Monthly averages, all individuals.

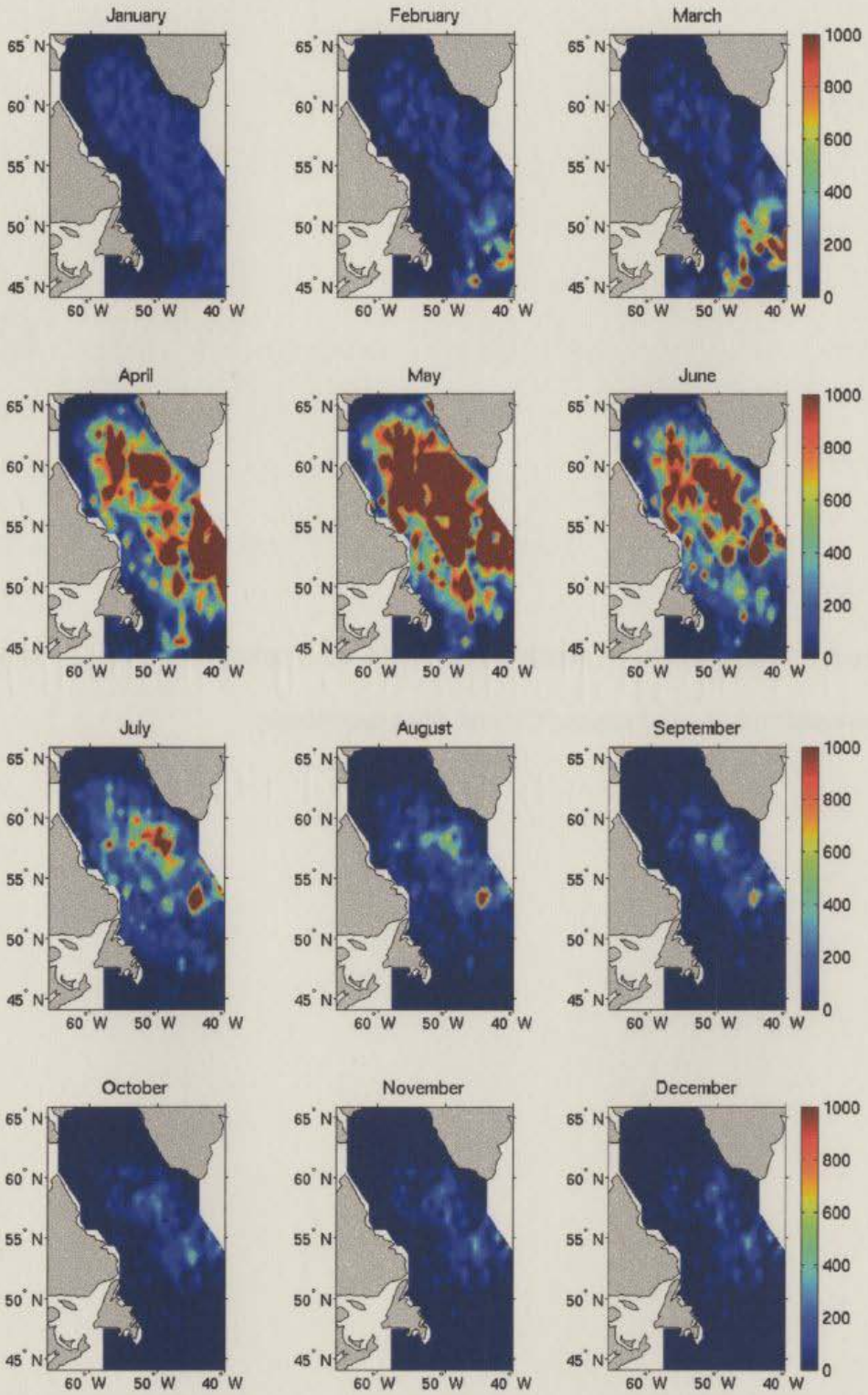
January
February
March
April
May
June
July
August
September
October
November
December
65° N
60° N
55° N
50° N
45° N
60° W
50° W
40° W
1000
800
600
400
200
0

Figure 5.14: Results, run 5 – standard run, bilatitudinal emergence. $Log_{10}(x+1)$, where x is the monthly average of surface CV and adult individuals.

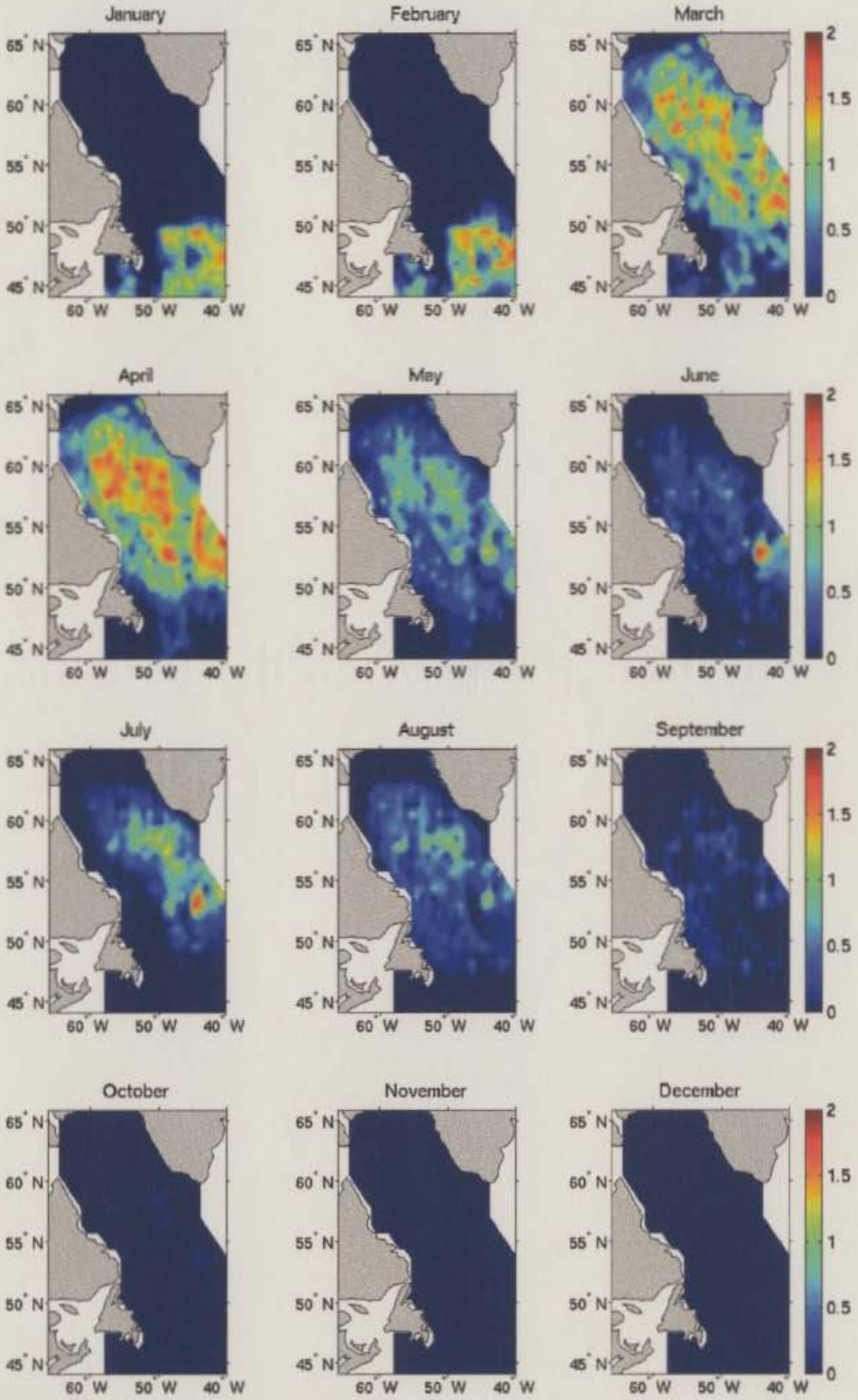
January
February
March
April
May
June
July
August
September
October
November
December
65° N
60° N
55° N
50° N
45° N
60° W
50° W
40° W
2
1.5
1
0.5
0

5.8 Run 6, standard run, early bilatitudinal emergence

Model run 6 is identical to run 5, except that individuals north of 50°N emerge one month earlier, during mid-February, rather than mid-March. Diapausing individuals in run 6 are reduced by 77.64%. 90.44% of individuals that leave the modelled region exit via the eastern boundary, 9.29% from the southern boundary, and 0.26% from the northern boundary. 99.96% of individuals are diapausing at the end of the run, with no second generation.

Figure 5.15 shows diapausing individuals on day 365, Figure 5.16 monthly averages of all individuals, and Figure 5.17 monthly averages of surface CV and CVI individuals.

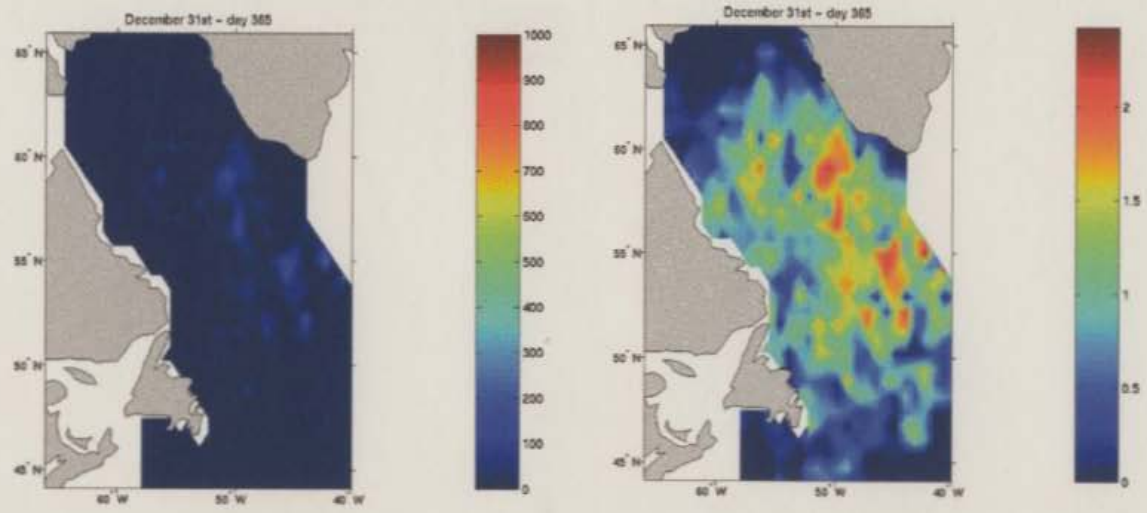

a) b)

Figure 5.15: Results, run 6 – standard run, early bilatitudinal emergence. a) Diapausing individuals per m^{-2}, day 365. b) $\log_{10}(x+1)$, where x is the number of diapausing individuals per m^{-2} on day 365.

Figure 5.16: Results, run 6 – standard run, early bilatitudinal emergence. Monthly averages, all individuals.

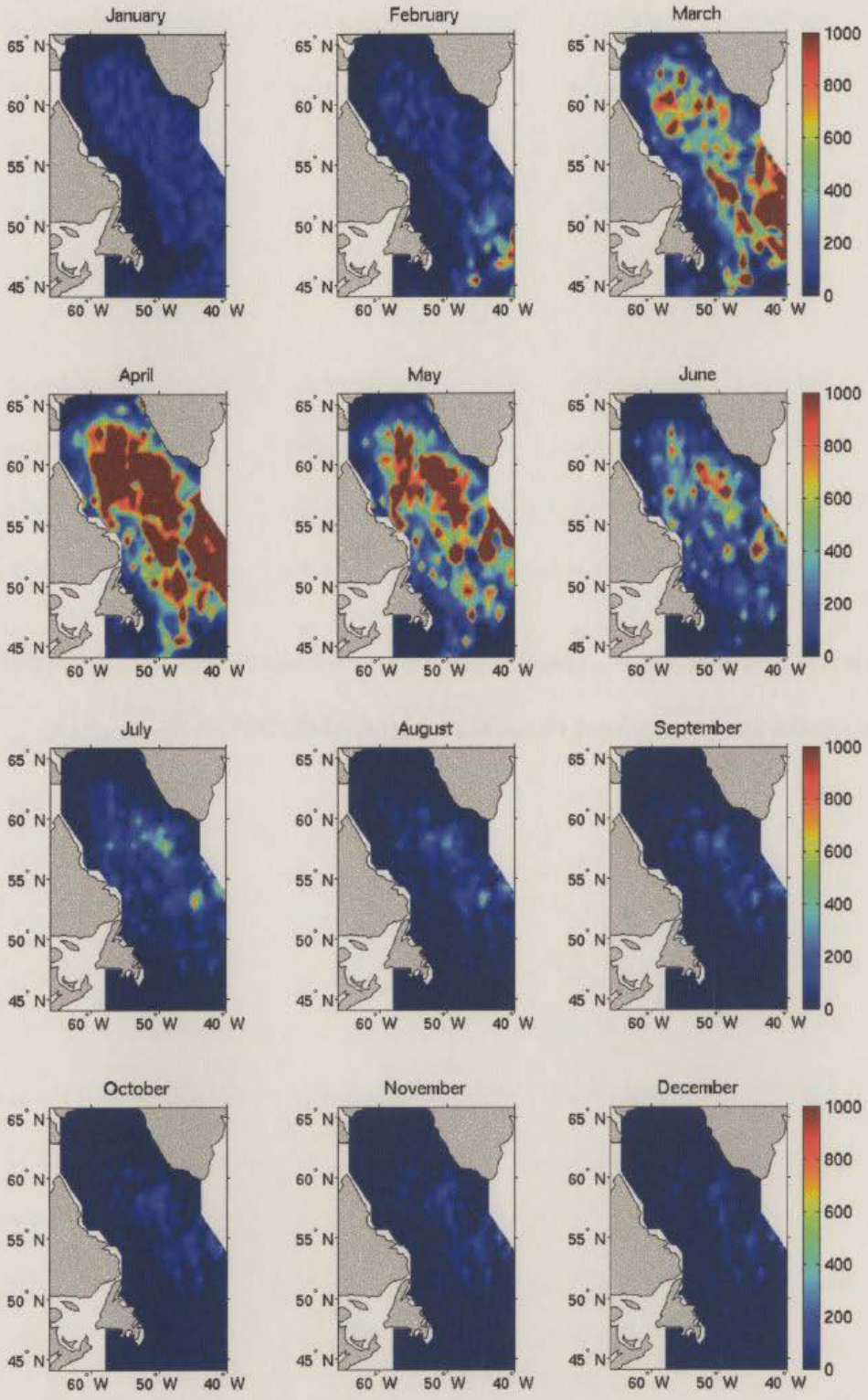
January
February
March
April
May
June
July
August
September
October
November
December
65° N
60° N
55° N
50° N
45° N
60° W
50° W
40° W
1000
800
600
400
200
0

Figure 5.17: Results, run 6 – standard run, early bilatitudinal emergence. $Log_{10}(x+1)$, where x is the monthly average of surface CV and adult individuals.

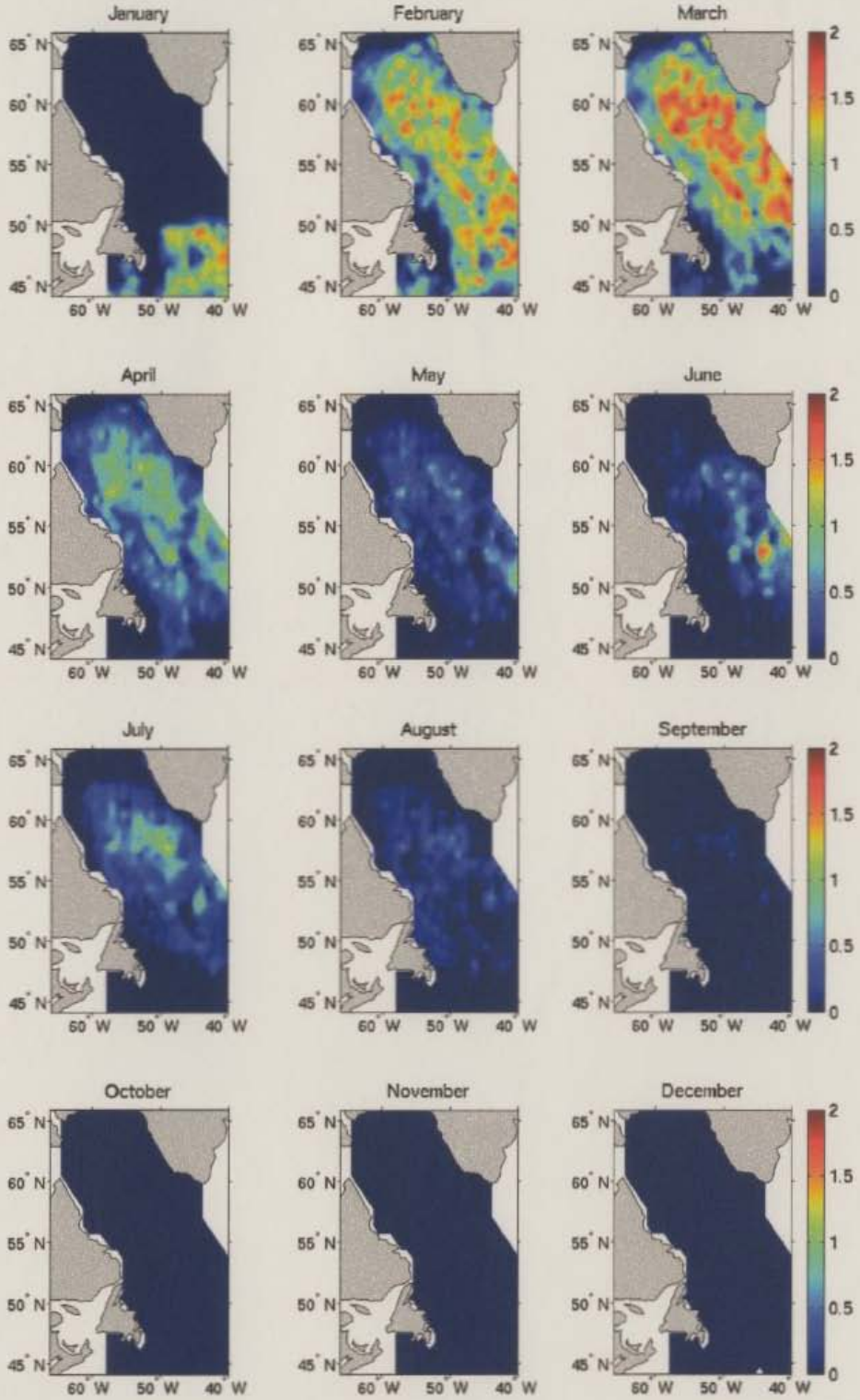
January
February
March
April
May
June
July
August
September
October
November
December
65° N
60° N
55° N
50° N
45° N
60° W
50° W
40° W
2
1.5
1
0.5
0

5.9 Runs with modified mortality parameterisation

Mortality is an important parameter in the construction of zooplankton life history models, and a small change in mortality can cause a population increase to become a population decrease. The range of values for mortality parameters in *Calanus finmarchicus* models is large; for instance, CV mortality parameterisations range from 1%/day (Miller & Tande, 1993) to 5%/day (Lynch *et al.*, 1998). Often, mortality is tuned to give a reasonable value for inter-stage relative abundances, or final population values. Indeed, some models utilise a stage-specific mortality rate (e.g. Miller *et al.*, 1998) (usually concentrated in the egg and early nauplii stages), while others (e.g. Heath *et al.*, 1997) utilise a constant mortality rate for most classes.

In the current model, the mortality rate is the same for all stages except diapause, which has a tenfold lower mortality rate in order to account for the probability of increased survival while in diapause (Mauchline, 1998). The mortality is set to a fixed value which provides a relatively constant population at both the Bravo and SE Flemish Cap locations. Since the model is initialised with an arbitrary number of individuals (100 per m^{-2}), and each location productive in relation to every other location, modifying the mortality value should not invalidate model results unless the relative productivity between locations is changed relative to the previous runs. In order to test this possibility, two model runs were undertaken, initialised as per run 3 (standard run, latitudinally

dependant emergence), but with 10% lesser and 10% greater mortality for all stages respectively. Figure 5.18 shows the results for day 365 of the reduced mortality run, and Figure 5.19 the results for the increased mortality run.

In the case where mortality is reduced by 10%, the final population of diapausing individuals shows an increase of 42.71% over the initial population. When mortality is increased by 10%, the number of diapausing individuals is reduced by 66.46%.

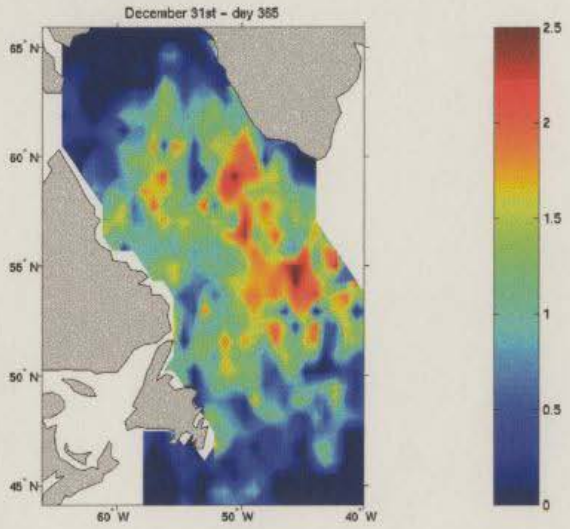

Figure 5.18: Run 7, standard run, mortality for all stages increased by 10%. $Log_{10}(x+1)$, where x is the number of diapausing individuals per m^{-2} on day 365.

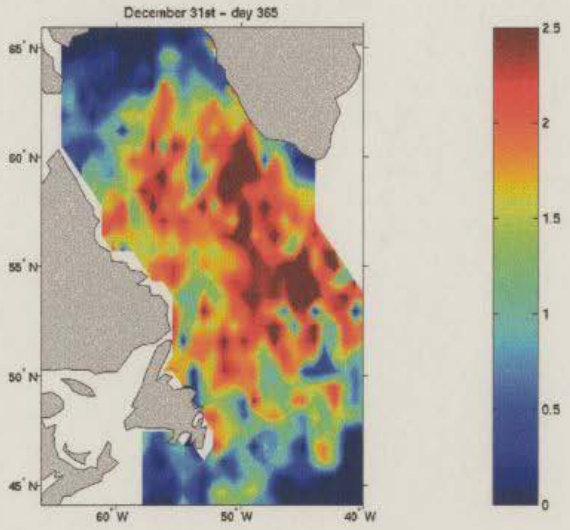

Figure 5.19: Run 8, standard run, mortality for all stages decreased by 10%. $Log_{10}(x+1)$, where x is the number of diapausing individuals per m^{-2} on day 365.

5.10 Tracer model run

Within the three-dimensional model, it is of interest to see how the interaction of advective and biological processes affect the distribution of individuals starting from a single common point. In order to achieve this end, it is necessary to remove much of the noise that comes from the advective movement of individuals, and simply look at a tracer population that is initialised at a single location and then followed over the course of a year. The tracer population that is considered is a group of 100 diapausing individuals beginning on day 365 at Bravo.

The results are shown in Figure 5.20 and 5.21

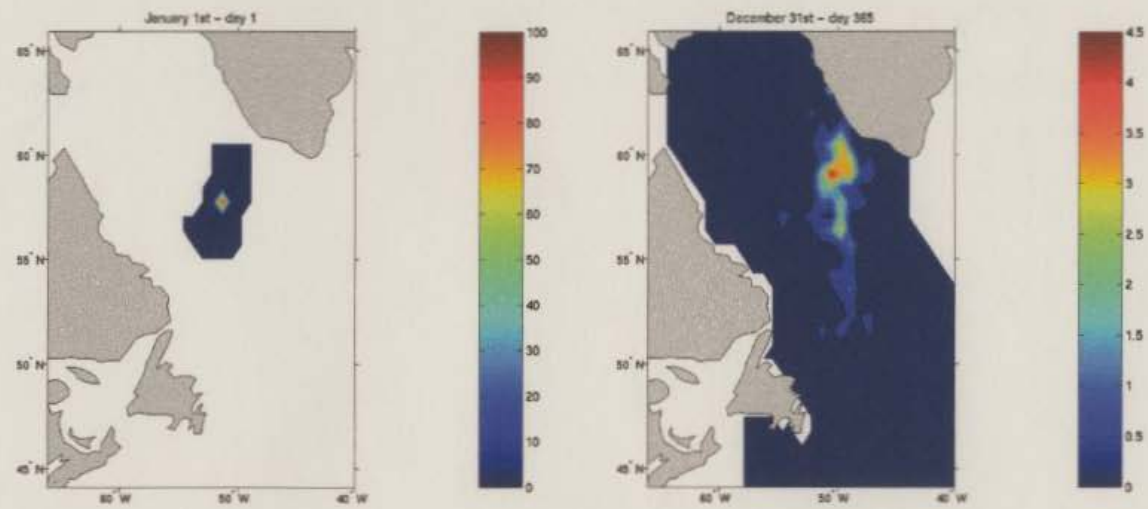

a) b)

Figure 5.20: Results – model run 9, Bravo tracer population. a) Initial population, diapausing individuals per m^{-2}. b) Final population, diapausing individuals per m^{-2}.

After one year, the final dispersal extends over an area from the south-west coast of Greenland down to around 50°N. It can be seen from Figure 5.21 that the zooplankton remain concentrated near to the initial 'seed' position until they emerge from diapause in May, whereupon the distribution disperses rapidly, due to the faster surface currents. When considering the movement of the patch, it is worth noting that a) Bravo is in the centre of the Labrador Sea, and not in a coastal area with high current velocities, and b) that diapausing individuals at this location do not come to the surface until around day 120, and also spend the latter part of the year at depth, where velocities are much lower than at the surface. Both of these factors contribute to the relatively limited movement of the main patch of individuals.

Figure 5.21: Run 9 - tracer run at Bravo (57.41°N, 51.50°W). Monthly averages, all individuals.

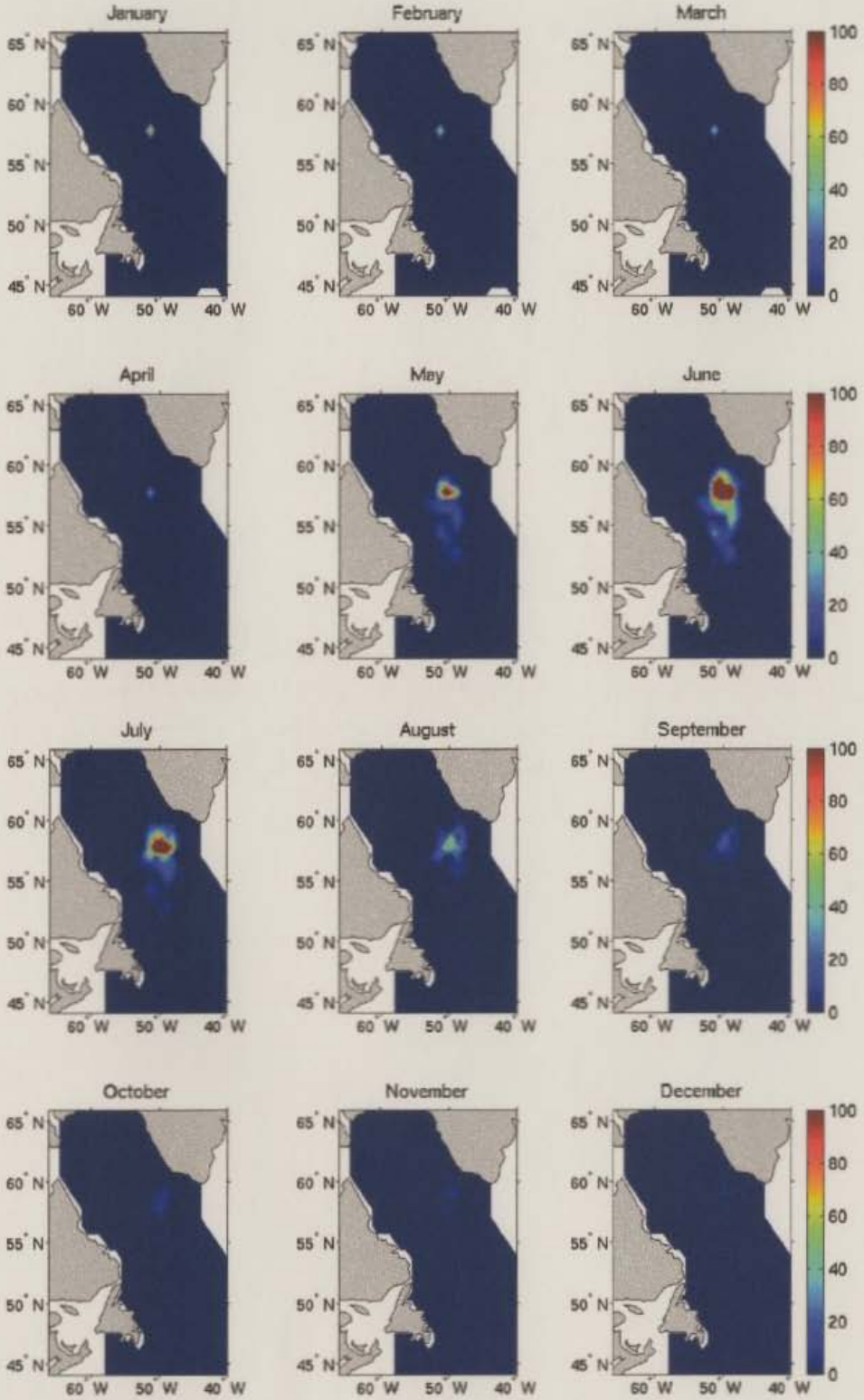
January
February
March
April
May
June
July
August
September
October
November
December
65° N
60° N
55° N
50° N
45° N
60° W
50° W
40° W
100
80
60
40
20
0

5.11 Results, model run 10, depth flux.

In order to assess the effect of an incoming population borne on the East/West Greenland Current, the model was run with a constant incoming flux of individuals immediately to the south of Greenland from 57.42°N, 44.3°W to 58.75°N, 44.3°W. The boundary flux at this point is set to 100 diapausing individuals at 1000m depth, until the emergence from diapause begins (day 120), when a no-flux condition is imposed. Figure 5.22 shows the winter latitudinal currents at the flux boundary, and Figure 5.23 the monthly results of the flux.

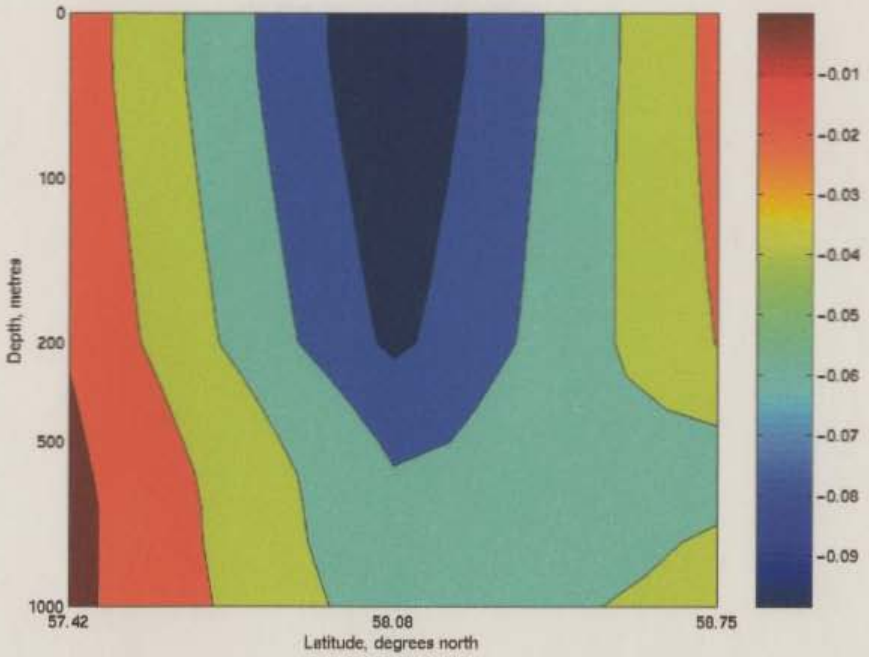

Figure 5.22: Winter longitudinal velocities at flux boundary, in ms^{-1}. Negative indicates westerly flow into the model region.

The flux at depth to the south of Greenland is fairly weak into the model region in the winter (day 1 to 90), with a similar picture for the spring currents. In particular, the surface currents are much stronger. Figure 5.23 shows the results of the run - the number of inflowing individuals is relatively small throughout the entire year.

Figure 5.23: Results, run 10 – flux population at depth. Monthly averages, all individuals.

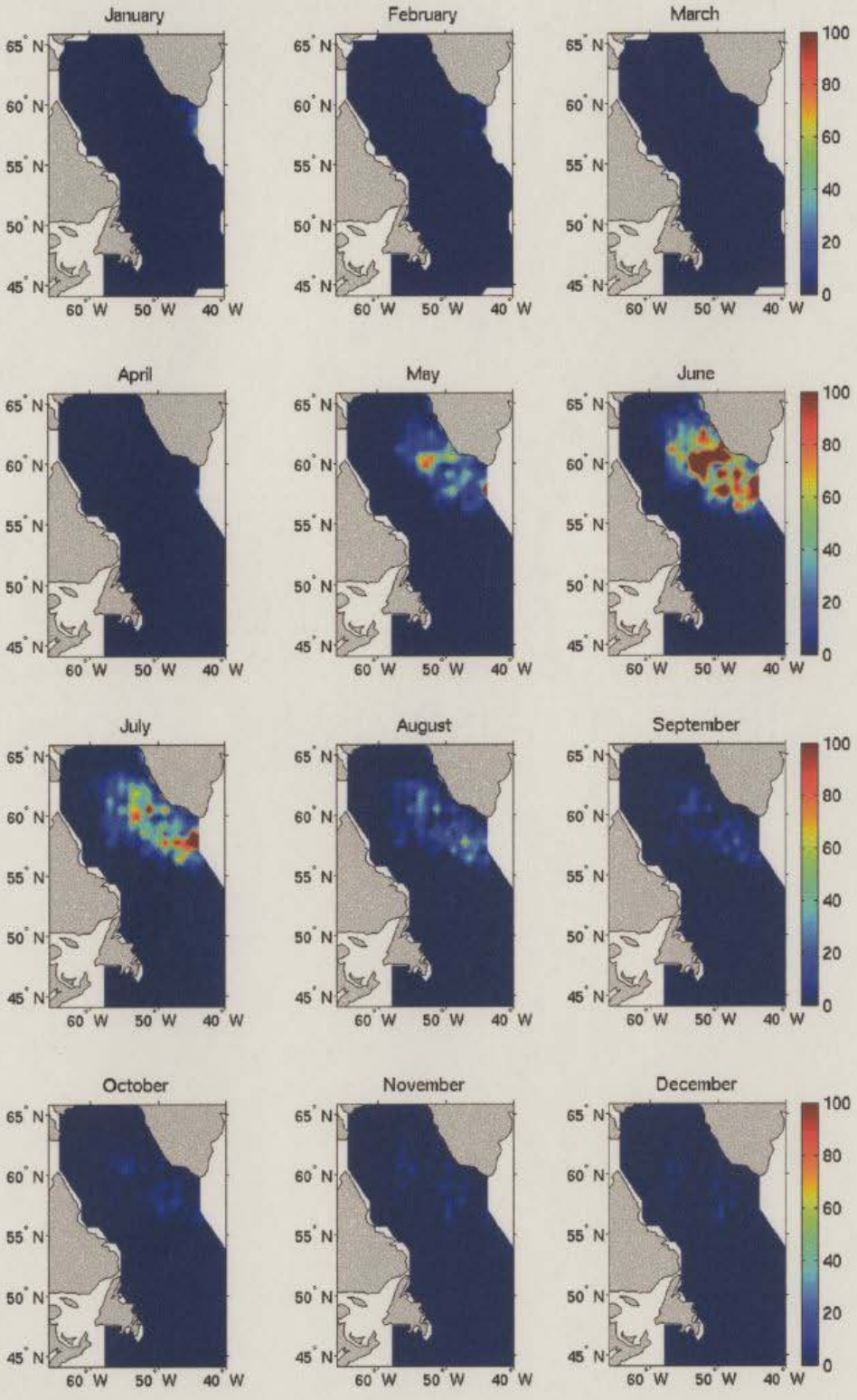
January
February
March
April
May
June
July
August
September
October
November
December
65° N
60° N
55° N
50° N
45° N
60° W
50° W
40° W
100
80
60
40
20
0

5.12 Results, model run 11, surface flux.

Model run 11 is the same as run 10, except that the incoming flux is at the surface. CV's are advected at the same location as run 10 (from 57.42°N, 44.3°W to 58.75°N, 44.3°W) from day 120 to day 195, a period in which individuals are likely to be present at the surface. The boundary flux condition at this point is set to 100 CV's at the surface. In comparison to run 10, the number of days for which the flux condition is set is less (75 as opposed to 120), but the surface currents are much stronger than those at depth. Figure 5.24 shows the latitudinal currents at 1000 metres depth, and Figure 5.25 the monthly results of the flux.

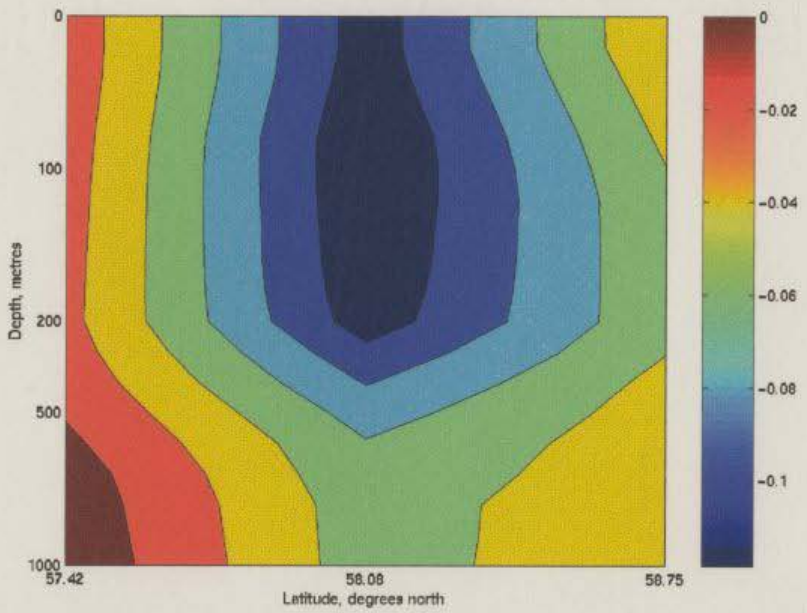

Figure 5.24: Summer velocities at the flux boundary, in ms^{-1}. Negative indicates western flow into the model region.

The summer surface currents are much stronger than those at depth, and also than those during the winter. Many more individuals are advected into the model region than in run 10, even before production of a G1 generation begins (Figure 5.25). Although individuals only begin to flow into the area in May, the final population is around fifty times that of run 10, indicating that surface currents potentially advect individuals much faster than those at depth.

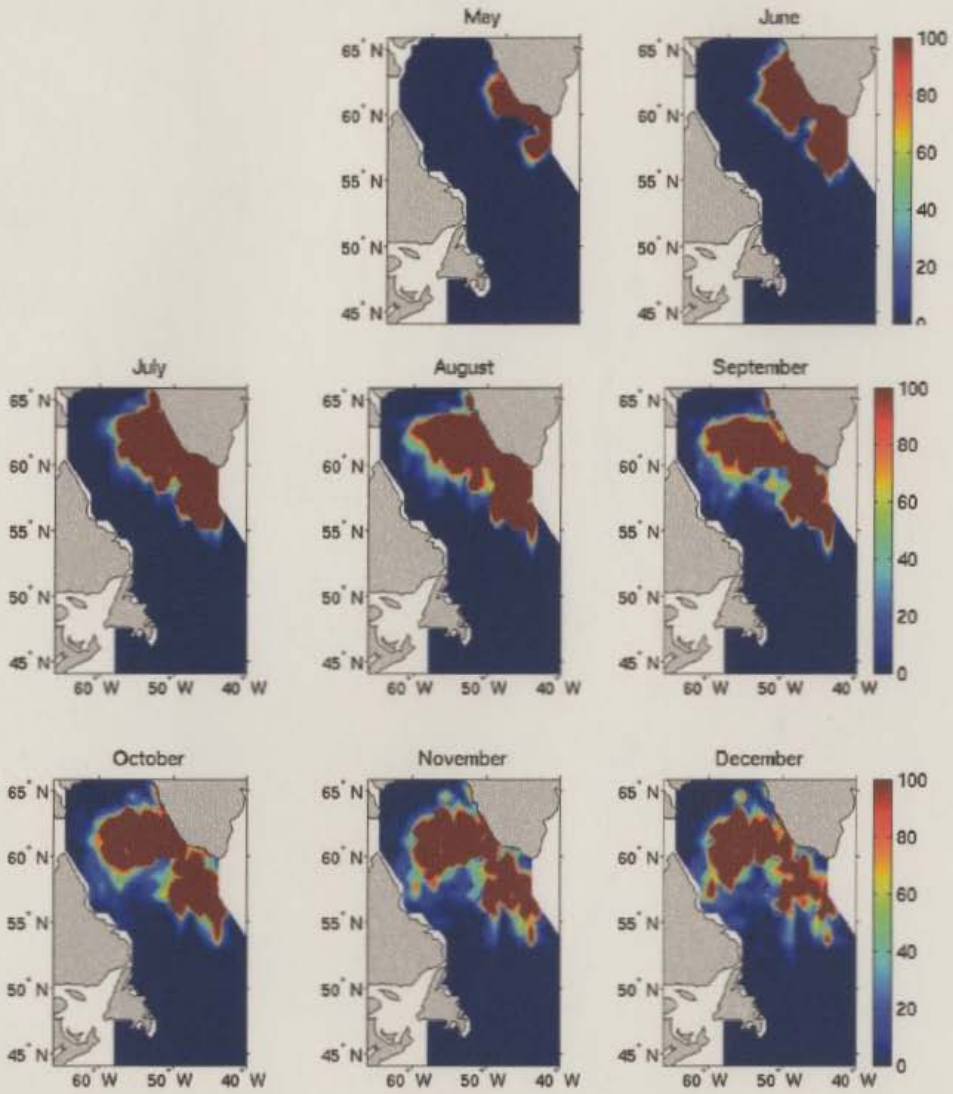

Figure 5.25: Results, run 11 – flux at surface. Monthly averages, all individuals.

5.13 Results, run 12, mid-year start

The mid-year start model run begins on June 1st and continues over the course of an annual cycle to May 31st the following year. The initial population structure is described in section 5.2.7; it is loosely based upon relative abundances from the data of Head *et al.* (2000). The number of individuals in the modelled area at the end of mid-year run expressed as a percentage of the number of individuals at the start of the mid-year run is 336.21%, of which 98.23% are at the surface.

Figure 5.26 shows the initial and final population structure. Figure 5.27 describes population development over the course of a year.

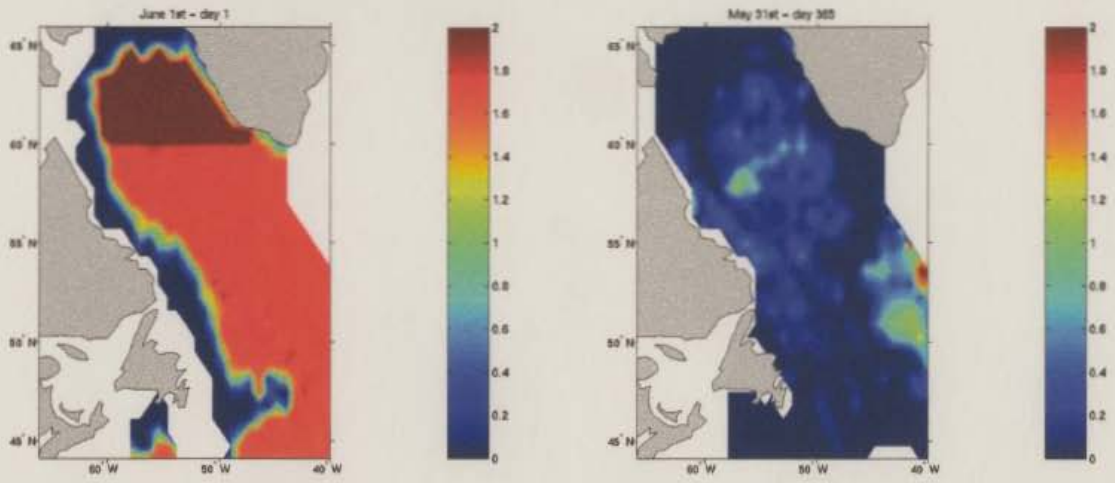

a) b)

Figure 5.26: Results, run 12, mid-year start. a) Log_{10} (x+1), where x is the number of surface CV's and adults per m^{-2} on June 1st (day 1). b) Log_{10} (x+1), where x is the number of surface CV's and adults per m^{-2} on May 31st (day 365).

Figure 5.27: Results, run 12 – mid-year run. $Log_{10}(x+1)$, where x is the monthly average of surface CV and adult individuals.

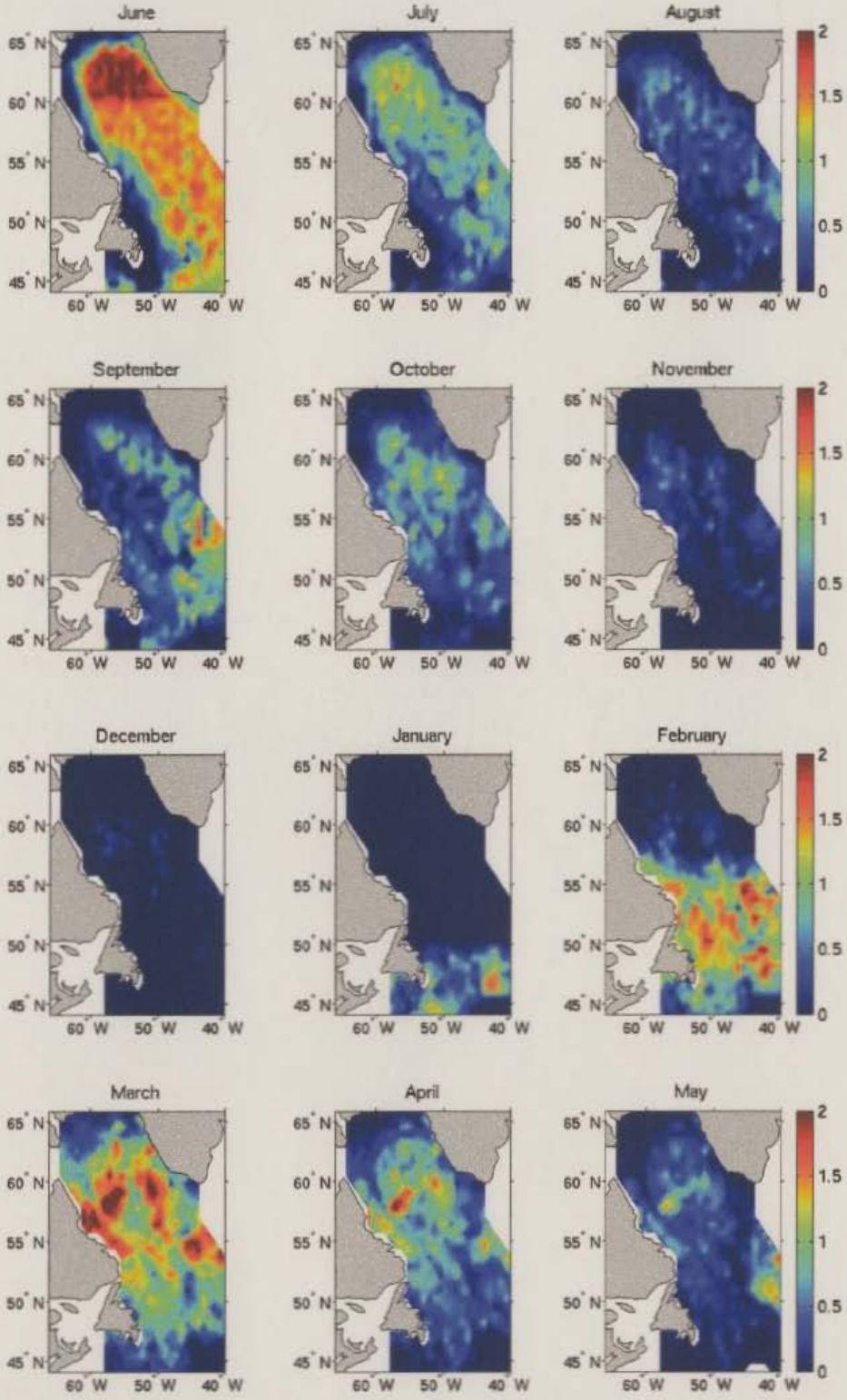
June
July
August
September
October
November
December
January
February
March
April
May
65° N
60° N
55° N
50° N
45° N
60° W
50° W
40° W
2
1.5
1
0.5
0

5.14 Results, Run 13, Standard run, second year

To examine population development over a multi-annual period, the standard model run is allowed to develop for a second year. The initial population on day 1 of year 2 is considered to be the final population on day 365 of year 1; all other aspects of the simulation are the same as model run 3. The results are shown in Figure 5.28, Figure 5.29 and Figure 5.30 below.

The number of diapausing individuals in the modelled area at the end of the year two run expressed as a percentage of the number of diapausing individuals at the start of the year two run is 84.65%.

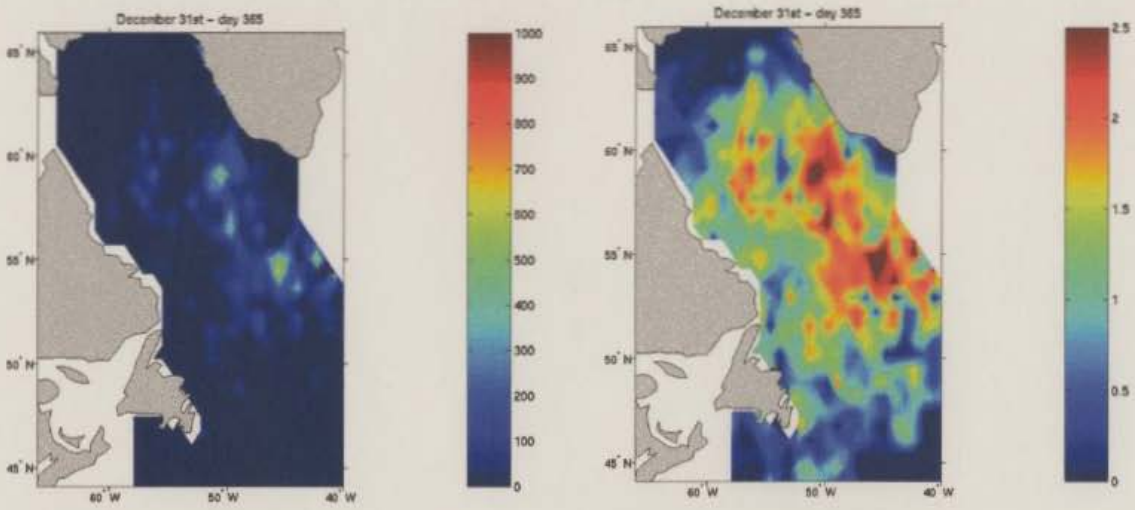

a) b)

Figure 5.28: Results, run 13, year 2 of standard run. a) Diapausing individuals per m^{-2}, day 365. b) Log_{10} $(x+1)$, where x is the number of dipausing individuals on day 365.

Figure 5.29: Results, run 13 – standard run, year 2. Monthly averages, all individuals.

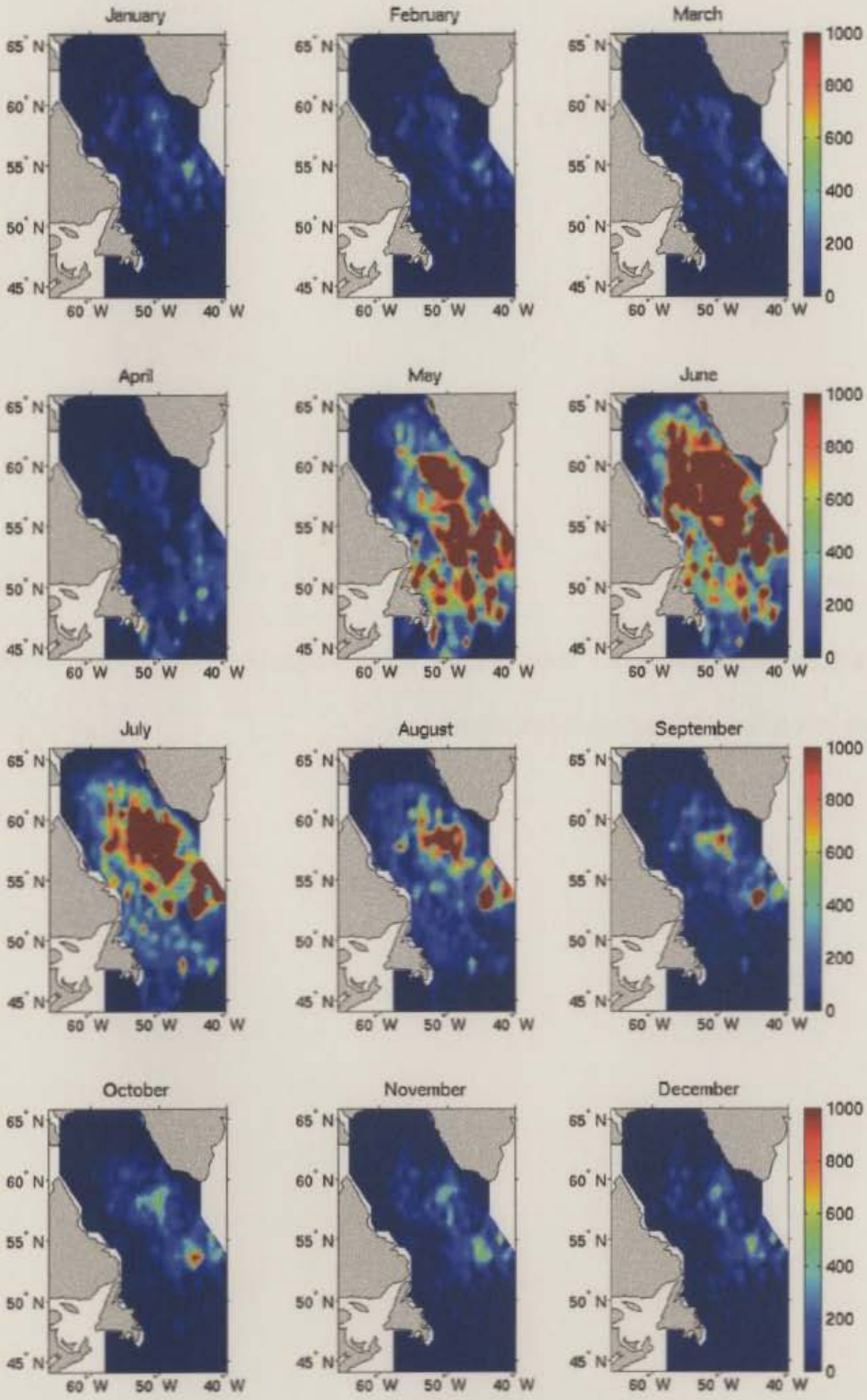
January
February
March
April
May
June
July
August
September
October
November
December
65° N
60° N
55° N
50° N
45° N
60° W
50° W
40° W
1000
800
600
400
200
0

Figure 5.30: Results, run 13 – standard run, year 2. $\text{Log}_{10}(x+1)$, where x is the monthly average of surface CV and adult individuals.

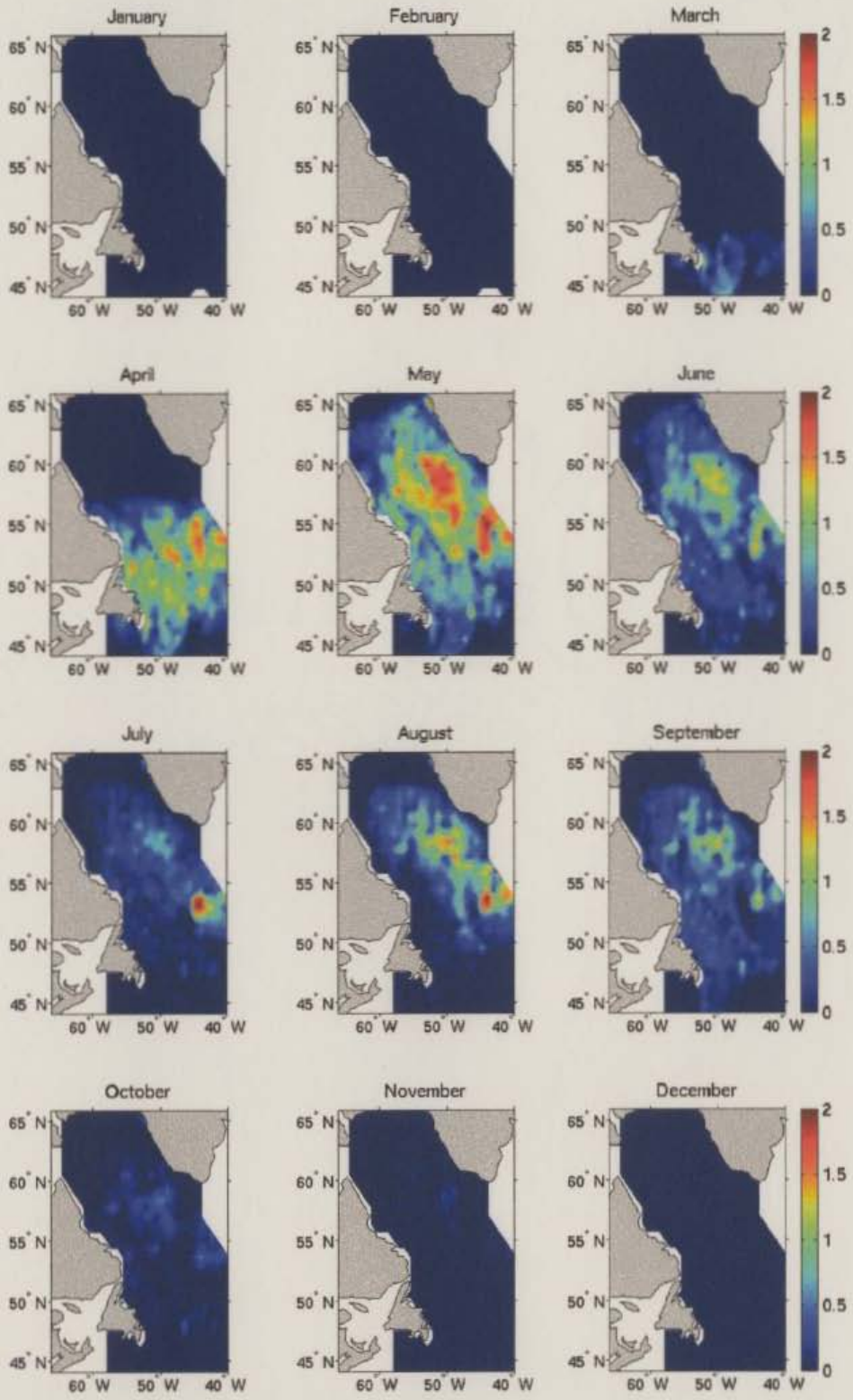
January
February
March
April
May
June
July
August
September
October
November
December
65° N
60° N
55° N
50° N
45° N
60° W
50° W
40° W
2
1.5
1
0.5
0

5.15 Model Results, overall productivity

Figure 5.31 compares the percentage change between final and initial diapausing populations in selected model runs.

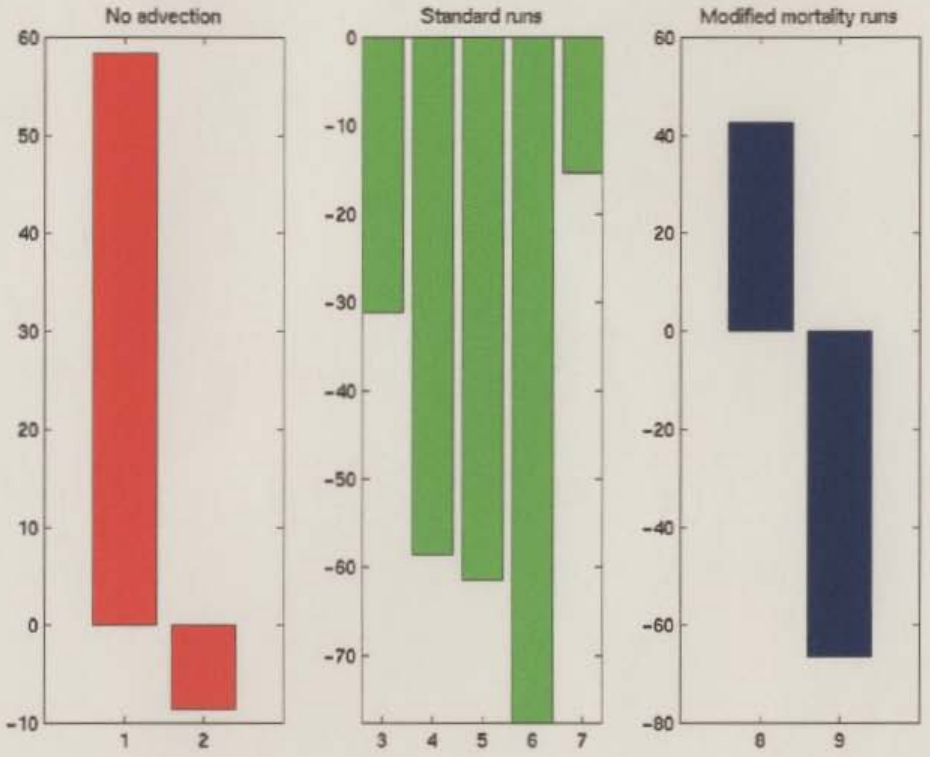

Figure 5.31: Percentage change in diapausing individuals over annual (1) No advection, lat. dependant emergence. (2) No advection, bilatitudinal emergence. (3) Standard, lat. dependant emergence. (4) Standard, simultaneous emergence. (5) Standard, bilatitudinal emergence. (6) Standard, early bilatitudinal emergence. (7) Standard, latitudinal emergence, year 2. (8) Mortality – 10%. (9) Mortality +10%.

5.16 Discussion

5.16.1 Model runs without advection

The model runs without advection are useful for assessing relative regional productivity. Figure 5.2 shows that the region most favourable for the growth of the population is located in the southeast, and this is confirmed by Figure 5.4. An interesting aspect of both Run 1 and Run 2 is that the productive southeast locations are at the same latitude as the least productive regions to the south of Newfoundland. Since at the same latitude the growth and diapause parameters are the same, growth (and hence productivity) is a function of food availability and temperature (in the modelled system).

The low-productivity southern regions have a high-phytoplankton signature from February to April. The spring bloom thus comes relatively early in these regions. The high-productivity south-eastern region has a lower food availability for much of the period of surface *Calanus finmarchicus* activity than the low-productivity regions (Figure 3.4). The difference would therefore seem to be attributable to temperature. The waters are much warmer in the south-eastern region (e.g. 10°C and warmer all year round at SE Flemish Cap), but much cooler in the south-central region (e.g. Avalon has the following temperatures: Winter -1.10°C, Spring 2.93°C, Summer 11.45°C, Autumn 6.42°C). The cooler temperatures can cause a significant delay in growth, especially in the southern regions where most surface *Calanus finmarchicus* have returned to depth by the time that the water has warmed in the summer.

The fact that productive areas do not match precisely to bloom areas could be attributable to two possible causes; (1) the modelled diapause function is incorrectly timed and thus individuals do not surface to match the spring bloom, or (2) temperature plays a more significant role relative to food when determining growth rate in the model. Since the same productive region is observed in both Run 1 and Run 2, and the model has been tuned to match diapause emergence timings to observed data in both cases, it seems more likely that food plays an important role when limiting (as in Chapter 4), but that otherwise temperature is the more important factor in determining productivity. This would appear to be confirmed by the fact that the most productive regions are not those of high food availability; they are those with high temperatures.

The entire western portion of the model, from the Davis Strait down the coast of Labrador to the coastal seas off Newfoundland and further south, is less productive than the rest of the model region. This is likely due to cool mixed layer temperatures; there is a significant spring bloom at 62°N on the east coast of Labrador in July, but this region is still underproductive. Figures 5.2 and 5.4 show the slow development in this location during May; this would seem to be due to a cooler water temperature than surrounding regions.

When comparing Run 1 and Run 2, it can be seen that most individuals emerge earlier in Run 2, especially south of 50°N, and towards the northern parts of the Labrador Sea. The relatively lower productivity in Run 2 (Figure 5.31) is probably due to

emergence into cooler waters - some with lower food availability due to mismatch with the timing of the spring bloom - thus limiting growth and development.

5.16.2 Standard model runs

Run 3 clearly shows the influence of advection. Figure 5.6 indicates the regions in which diapausing individuals show high concentrations in the Labrador Sea, and those of low concentration. The G1 generation can be seen to appear in the southern regions first, and spread northwards (Figure 5.7). By the end of the model run, individuals have reached most regions of the model - including shelf and slope regions in which they were not originally located (for the 200m isobath see Figure 1.5). The final population in Figure 5.6 (b) shows the effect of the current patterns; regions which were not particularly productive in the non-advective model run now end up with large numbers of individuals, whereas the productive southern regions have had their population advected away.

The slice at 53°N latitude (Figure 5.6 (d)) indicates that the model appears to be functioning correctly with regard to depth positioning; all diapausing individuals are in the deepest possible water in their location.

Figure 5.8 presents the results in a fashion that bears easy comparison to the data from Planque (1997); a key test for model validity. Though the scaling used in the model is different from that of Planque, the relative abundance between locations should be

similar. In Planque's data set, individuals are present at the surface to the south of Newfoundland somewhat earlier, with individuals at the surface during most of the year, and beginning to appear in numbers during February. The model does not mimic the surface activity during the early winter, as individuals emerge around one month later, during March. However, the model does indicate that surface activity in the southern regions is reduced beginning in May, and is almost over by September; this is somewhat similar to (though earlier than) Planque's data, in which surface activity is very much reduced from June to October.

In the data set of Planque *et al.* (1997), individuals begin to appear at the surface of the southern part of the Labrador Sea in March, with May through to September showing the most activity. In the model, individuals do not appear in numbers until April, but then match the data very well, with May through to September / October being the months with the most individuals at the surface. The lack of individuals at the surface from October through to March fits well with Planque's data (November through to February). The model also matches the spatial structure of Planque's data reasonably well, having the largest concentration of individuals located in the central and southern Labrador Sea, and to the south of Greenland. The population maximum appears to extend further north in the model, into regions in which there are no CPR data (e.g. Figure 5.6c).

Run 3 does not match the timing of Matthews (1968) and Miller *et al.* (1991) very well, with emergence from diapause being too late in all regions except those at the same latitude as the Flemish Cap (Figure 5.8).

The other standard runs (with differing diapause functions) have a similar final spatial structure for diapausing individuals on day 365, with differences lying in absolute numerical values. This suggests that advective properties function essentially similarly within the separate emergence schemes, and that differences in productivity occur from variance in the match or mismatch of emergence timing to warm waters and food availability (Figures 5.6, 5.9, 5.12 and 5.15).

The simultaneous emergence scheme, Run 4, matches fairly poorly with Planque's data; emergence is too late to the south of Newfoundland, and too early in the north (Figures 5.10 and 5.11). The numbers of CV's and adults peak too early. Run 5 is a slightly better fit to the data, with earlier emergence in the southern regions, and March-May being the months with most CV's and adults present at the surface (Figures 5.13 and 5.14). This is somewhat early, but there is little activity in northern regions from October to February, which is a better fit to Planque's data than Run 4. Run 5 matches well with the emergence timing in Matthews (1968) and hypothesised in Head *et al.* (2000) with emergence occurring earlier, in general, than Run 3, and especially so to the south and east of Newfoundland.

Run 6, bilatitudinal emergence that is one month early, is a poor fit to all data sets since emergence in central and northern regions is too early. The overall match is the worst of any of the standard runs (Figures 5.16 and 5.17).

The production of a second generation within the area covered by the three-dimensional model is a matter of some debate; there appears to be no or little second generation in the Labrador Sea (Kielhorn, 1952; Head *et al.*, 2000), though copepodites are found at the surface during late autumn and early winter (Huntley *et al.*, 1984). Model output matches this well, but copepodites that appear at the surface during the winter months appear to be slow-developing or late-spawned G1's rather than G2 individuals. This may indeed be the case within the data of Huntley *et al.* (1984). To the south of the model region, off Nova Scotia, there are two generations per year in some regions (McLaren & Corkett, 1986), though once more the second may contribute little in annual production. It thus seems reasonable to assume that if a second generation does appear within the model region, its effects on annual productivity would be low.

Planque's data also shows that the central/southern Labrador Sea tends to have more surface individuals than the areas to the south and west of Newfoundland. All of the model runs replicate this central/southern Labrador Sea surface population maximum, though the timing is a little different in each model run. Since the model runs without advection do not demonstrate this concentration of individuals, it would seem that the current patterns in the region are responsible for this structure, as it is present in every

standard run in which there is advection. In the model runs without advection, the most productive regions are in the south-east, so it would appear that individuals in these locations are advected to different regions, or out of the model entirely; advective processes thus have an important effect on population abundance, even when there is no incoming flux of individuals.

The model therefore seems to reproduce the timing of *Calanus finmarchicus* activity in the Labrador Sea more precisely with latitudinally dependant emergence (hypothesis 1), except for south of 50°N where the bilatitudinal scheme (hypothesis 2) appears to be a better fit when comparing to Planque (1997). When comparing to the timing of Matthews (1968) and that which was suggested in Miller *et al.* (1991) and Head *et al.* (2000), the bilatitudinal emergence scheme produces the best results. Thus different diapause emergence schemes can be used to match different data sets.

Model run 3 is the most productive of all the standard runs (Figure 5.31). This may be due to the fact that most individuals emerge later relative to the other standard runs, and thus encounter warmer water, while matching the timing of the spring bloom in many regions (Chapter 4). It is worth noting, however, that the early bloom that Head *et al.* (2000) considered could be a regular feature of northern and eastern regions of the Labrador Sea does not appear in the three-year compiled SeaWiFS data set. Runs 4-6 may have been more productive had this feature been present; as it stands, the bilatitudinal emergence scheme contains a greater mismatch between the timing of

emergence and the onset of the spring bloom than the latitudinally dependent emergence scheme.

The standard runs have a population decrease by the end of the year, but not enough to prevent the region being near sustainability with a slightly changed parameter set. In fact, the standard run with slightly reduced mortality has a greater number of diapausing individuals at the end of the year than the start (Figure 5.31). Thus a slightly different parameterisation may lead to a self-sustaining population in the Labrador Sea; even if this is not the case, the population appears to be declining at a relatively slow rate, even though many individuals are advected out of the model boundaries (Runs 3-6, mostly G1 generation from the eastern boundary). An alternative interpretation may be that the modelled population is only stable for a narrow range of the morality parameter space, although there may be stabilizing feedbacks in the model that only become evident after a number of years. Further multi-year model runs would be necessary to distinguish between these possibilities.

Running the population model for a second year produces results that appear to be very similar to the run from the first year (Figures 5.6 and 5.29). In fact, the largest observable difference is that surface activity seems to be much reduced in the month of April. This is because diapausing individuals are not present in such numbers in the more southerly regions (having been advected elsewhere, or out of the modelled region entirely), and hence do not spawn in as great quantities. The reduction in the number of

individuals between years 1 and 2, and years 2 and 3 is similar, though there is a smaller decline in the second year. The population thus follows a similar pattern for two years of gradual decline.

Within all of the standard model runs, individuals are present on most shelf and slope regions at the end of the annual cycle (e.g. Figure 5.6c). Dispersal onto these regions occurs mainly during the spring/summer with the G1 generation, as the surface currents are much faster than those at depth and relocate individuals much more rapidly. This is an important result; if *Calanus finmarchicus* overwinter in the open ocean, then they can be transported onto the food-rich shelf regions by rising to the mixed layer. Utilisation of surface currents may therefore place the G1 generation into a more food-rich environment.

Comparison of these runs with those in which advection is turned off shows a very different picture of final populations (e.g. Figures 5.2 and 5.6b). The advective processes would therefore seem to be very important in determining the spatial population structure of the region. The productive regions in the southeast that appear in the non-advective runs are not present in those with advection; consequently, it appears that individuals in these regions are advected either to another location or, more likely given the placement of the region, the final population numbers, and the model exit statistics, out of the modelled region entirely. All the model runs seem to indicate that

there are both surface and sub-surface population maximums in the central regions of the Labrador Sea; a good match to Planque (1997).

5.16.3 Model runs with modified mortality parameterisations

The model runs with modified mortality parameterisations produce spatially very similar results to the standard run. Differences lie in the absolute productivity of each region, whereas inter-regional relative productivity remains essentially the same. The change in population size is very similar to that in the one-dimensional modified mortality runs (see Chapter 4). Modification of the mortality parameterisation would seem to have a similar effect on the final density regardless of the spatial structure of the population.

5.16.4 Tracer model runs

The tracer model runs give an informative picture of the advective processes in the region. Figure 5.21 shows the development of a population started at Bravo. The population remains relatively fixed in position while in diapause (January – April), indicating that the currents at depth are relatively weak. Once individuals ascend to the surface, population dispersal is increased dramatically, with most individuals proceeding northwards, though there is movement in every direction. By the time individuals return to diapause, they cover a much larger area than the initial population. The stronger current flows at the surface clearly advect the G1 generation a far greater distance than

diapausing individuals residing at depth. The main kernel of the distribution still remains near the original seed point.

5.16.5 Flux population runs

The flux population runs are used to determine the effect of an inflowing population into the modelled region. The most likely place for this to occur is with individuals borne around the southern tip of Greenland from the Irminger Sea (see Planque, 1997), and the runs represent this by having a flux for three grid points to the south of Greenland. The boundary flux conditions at these points are set to 100 individuals. For the run at depth, these are diapausing individuals, and the flux condition operates until day 120. For the surface flux, these are CV individuals, and the flux condition operates from day 121 to 150.

Although the surface flux only operates for one-quarter of the time of that at depth, the number of individuals borne into the region is much larger – a final population which is around fifty times larger than that which occurs when the flux condition is set at depth. Consideration of the velocity fields clearly indicates why this is the case – they are much stronger at the surface (Figures 5.22 and 5.24); indeed, the surface velocity fields to the south of Greenland are some of the strongest in the modelled region as a whole. It would therefore appear that for the replenishment of the population within the modelled region that, at least on the eastern boundary, most individuals are borne inwards on the surface currents.

The western boundary of the model is closed, and the currents entering the northern and southern boundaries significantly slower than those near the eastern boundary. Within the standard model runs, most individuals are lost from the region through the eastern boundary. There is also a large population of *Calanus finmarchicus* in the Irminger Sea, to the east of the modelled region (Planque, 1997). Given the results of the flux runs, the eastern boundary may well be the most important region for both the entry and exit of individuals, and thus maintenance of population viability. Further runs and data are necessary to confirm this.

It is interesting that both the flux population runs and the Bravo runs appear to show that surface currents are very important for population dispersal and regional movement. Intuitively, this is apparent given the stronger surface currents; the magnitude of the difference between the surface and depth quite large.

5.16.6 Mid-year start model run

Figure 5.26(a) clearly shows the initial population structure, namely, a much larger population to the north of 60°N than to the south. Between August and September, there is a clear increase in the number of surface individuals, in this case CV's of the G1 generation maturing. These individuals have then almost completely entered diapause by December. Emergence begins soon after in the southern regions – January - and then spreads north until the G0 surface generation peaks in March. This G0 generation is

present on the shelves; indeed some individuals overwinter on shelf regions. The CV's and adults then decline for the rest of the run until the end of May (Figure 5.27). Surface individuals have been concentrated into two main regions – a cluster in the central Labrador Sea between 57 and 58°N, and a group on the eastern border at around 50-54°N, 44-40°W (Figure 5.26(b)).

Though there is a considerable increase in population, this figure needs to be considered with some caution – the bulk of these individuals are nauplii, which were not included at the start of the run. However, a partial explanation for the increase is that a large proportion of the initial surface individuals were present in the northern half of the Labrador Sea, where they would not have been advected out of the region within the course of a year, whereas in the standard runs a proportionately larger amount of *Calanus finmarchicus* are located in the south-east where they are advected out of the modelled system.

Chapter 6

Summary and discussion

6.1 Assessing model validity

In a model system whose scope covers an area of greater then than 1,000,000 km^2, it cannot be hoped to capture the fine, small-scale details and intricacies of zooplankton population distributions. Since the final model rests upon many interacting layers – the physical model, the biological model, the temperature and phytoplankton data sets – each of which may have their own internal inconsistencies and scales, it is important to recognise the limitations of the modelled system. However, given that the aim of this exercise is to simulate and understand the large-scale distribution patterns of *Calanus finmarchicus* in regions of the Labrador Sea, to examine physical and biological interactions within the modelled region, and to examine the effect of model parameterisations and sensitivities on population structure, these less demanding goals may be more feasible within the computational, scaling, and data constraints.

In order to achieve this result, the biological model has been constructed in such a way that it can be tested and fitted to data within the scope of a one-dimensional system, and these results then applied to the full three-dimensional scenario. Existing literature on

Calanus finmarchicus provides key data to assess the accuracy and validity of model results. The following section provides a summary of how the model fits to data, and some conclusions that can be drawn from the results.

6.2 Summary

In summary, a three-dimensional coupled model system was created to examine the population distributions of the calanoid copepod *Calanus finmarchicus* in the Labrador Sea and surrounding regions. The system consisted of a biological model, physical model, and a remotely sensed phytoplankton data set. The model was tuned in a one-dimensional setting to several key locations, and parameters were then interpolated for use within the three-dimensional setting.

Within the one-dimensional case, model sensitivities were examined. The model appeared to be quite sensitive to many parameters. However, since the *raison d'être* for the model was relative comparison between areas rather than producing absolute values for each region, this would likely not invalidate model results, especially since the model was tuned to match data at several locations, and parameters inferred and interpolated from these runs. It is important here to note the difference between the interpolation of the diapause emergence timing parameter, dt, and the food uptake coefficient, a. The diapause emergence timing parameter is used to match observed variability in the timing of diapause emergence between different locations (see Chapter 4), and quite possibly varies depending upon latitude for the observed system. The food uptake coefficient, a, is simply a mathematical construct that is tuned to provide a reasonable growth progression at different locations.

When the model was extended into three dimensions, the first model runs examined regional productivity without the influence of advection. The most productive regions were in the southeast, corresponding to areas of warm water and reasonable food supply. The entire eastern coast of Labrador was relatively unproductive.

In Chapter 5, two hypotheses were presented regarding the timing of emergence from diapause for *Calanus finmarchicus*. These hypotheses arise from integrating the available literature for the region. They are summarised in Figure 6.1.

The model fits well to observed spatial and temporal activity patterns from the CPR survey (Planque, 1997) with a mixture of hypothesis (1) and hypothesis (2); a latitudinally dependent emergence scheme for central and northern parts of the region, but earlier emergence to the south of Newfoundland. It is apparent, though, that the model system can be matched to either hypothesis by utilising different emergence schemes. The fit to the CPR survey (Planque, 1997) is reduced when using an emergence scheme derived from hypothesis (2), as is the match to the timing of the spring bloom.

The contradictions of data on emergence timing for the region are difficult to resolve. The timing of the spring bloom does appear to be somewhat different between the SeaWiFS data and that denoted in Head *et al.* (2000), but using a diapause emergence scheme based on observational evidence (Kielhorn, 1952; Anderson, 1990), individuals emerge immediately prior to the bloom in most locations. This appears to provide enough

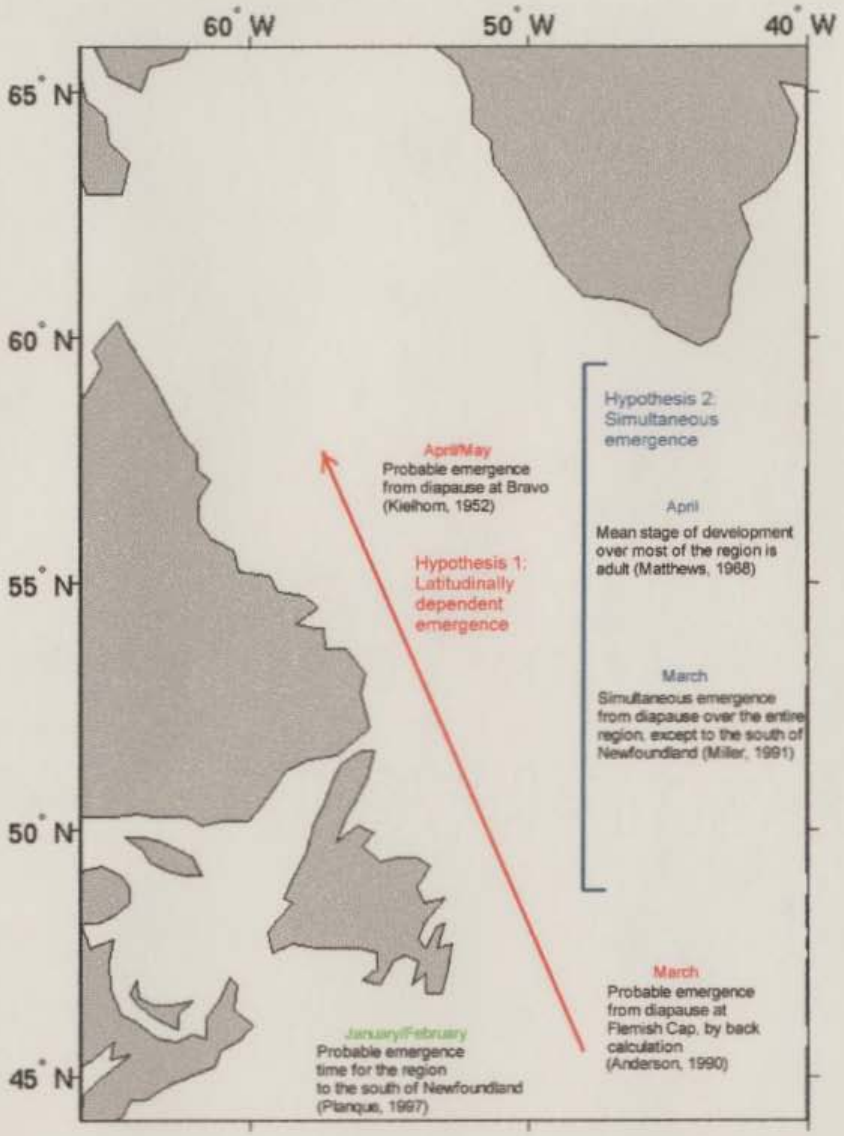

Figure 6.1: Schematic of integrated data regarding emergence from diapause and development of *Calanus finmarchicus* in the Labrador Sea and environs. Red text indicates data that fits with hypothesis 1 (latitudinally dependent emergence), and blue text data that matches hypothesis 2 (bilatitudinal emergence). Green indicates data that fits in both hypotheses.

food for a near-sustainable population in the one-dimensional model runs (Chapter 4). Utilising a diapause emergence scheme based upon bilatitudinal emergence (Matthews, 1968; Miller *et al.*, 1991; Planque 1997) decreases the match between emergence timing and the spring bloom. The bloom occurs later in more northerly regions (Figure 3.2) in the SeaWiFS data, in contrast to the data from the cruises of Head *et al.* (2000). A latitudinally dependent emergence scheme with later emergence in the north thus provides surface individuals with more food.

The modelled system explicitly shows a strong sensitivity to both food availability and temperature in a one-dimensional setting (Chapter 4); food appears to be of great importance when limiting, but otherwise temperature may be the more important factor in determining growth rates (Chapters 4 and 5).

Within the one-dimensional model runs, sensitivity to changes in mortality are more pronounced in surface individuals than those which are overwintering. This is likely due to a differential change in percentage mortality being greater with surface mortality than at depth.

The Labrador Sea, even with advective losses, produces a population that is gradually declining, but not far from stablity, over the course of an annual – or two year – cycle. The most productive regions (the south-east) do not actually contribute significantly to the overall regional production as individuals are quickly advected out of

the modelled area. Inward flux of individuals to the south of Greenland can add sizeably to the regional population, but even without this, a small parameter change in the present models would permit a population to approach stability.

A pattern is clearly observable when examining the effect of the advective field on population structure; individuals in the productive south-east regions appear to be advected out of the model system, while those to the north of this are concentrated in the central Labrador Sea. This population concentration fits well with the compiled CPR data of Planque (1997). The population maximum appears to extend into the northern Labrador Sea, an area that is not covered by the CPR surveys.

Clear evidence of transport onto shelf and slope regions (previously unoccupied in the model) is present in most model runs. Within the modelled system, a population that is started purely in deep water (> 1000m) can, in the course of a year, be advected into much shallower regions. This appears to be an effect of stronger surface currents; the G1 generation is advected much faster than diapausing G0 individuals. Confirmation of this is provided by tracer runs.

Most individuals leave the region through the eastern boundary. Individuals in the central and northern Labrador Sea would appear to have a much longer residence time than those in the southeast of the region. The fastest currents that enter the region also come from the eastern boundary, just to the south of Greenland. The flow at the surface

appears to be of much greater significance when advecting individuals into the area than that at depth.

6.3 Discussion

This thesis was begun with the intention of studying, clarifying, and understanding some of the physical and biological regulatory processes that make-up the population growth, dispersal, and spatial patterns of *Calanus finmarchicus* in the Labrador Sea and surrounding regions. While a coupled model system is particularly tricky to match to data and interpret, it is hoped that most of the intended questions have been addressed with this study. The model provided a reasonable first-order attempt at reproducing spatial and temporal population patterns in the Labrador Sea.

Utilisation of a diapause emergence scheme that is latitudinally dependent to the north of Newfoundland and provides an early emergence to the south produces a population that emerges immediately prior to the spring bloom in most locations, and matches well to the timing of Planque's (1997) data. This is somewhat counter to the 'near synchronous' emergence over much of the region that is proposed by Miller *et al.* (1991), and evidence for which appears in Matthews (1968) and Head *et al.* (2000). Fitting emergence to synchronicity produces a population that has a greater mismatch to the timing of the spring bloom, and a poorer fit to Planque (1997). The SeaWiFS-derived phytoplankton bloom (later at higher latitudes) does appear to be somewhat different to that in the ICNAF (1968) surveys and the data of Head *et al.* (2000).

In order to increase the certainty and accuracy of the model results, a number of steps are possible. Improved data on mortality and other physiological processes should aid in the setting of parameter values. Further exploration of the timing of diapause emergence would help when trying to assess latitudinal differences in productivity, together with further field data. Longer time-series for phytoplankton data, information on subsurface chlorophyll, provision of alternate food sources, and further annual time-series such as that of Kielhorn (1952) would aid in initialising and running the modelled system. Utilisation of physical (temperature and velocity field) and biological (zooplankton and phytoplankton) data from the same year would reduce the possibility that a mismatch had occurred. In order to constrain the biological model, it would also be useful to have further observations on *Calanus finmarchicus* omnivory and shipboard observations of chlorophyll concentration in parallel with SeaWiFS derived data.

The model could be further improved in several ways: a finer resolution grid, a more accurate topographic representation, a decomposition of individual stages to separate classes, and a better representation of stage-specific behaviours and physiology. A finer resolution grid or higher frequency current model would give a more accurate picture of advective effects. A three-dimensional phytoplankton field would provide a more comprehensive food source. It would be useful to have a more complete knowledge of the true diapause distribution in order to more precisely initialise model populations. The extension of the modelled geography to include the Irminger Sea would be enormously useful, since the entire proposed gyre system (Figure 1.4) would then be

included. Finally, testing the coupled system with a different biological model would help to ensure that results were model-independent.

References

Aiken, J., Moore, G. F., Clark, D. K., and Trees, C. C., 1995. The SeaWiFS CZCS-Type Pigment Algorithm. *NASA Tech. Memo. 104566*, Vol. **29**. S.B. Hooker, E.R. Firestone, Eds. *NASA Goddard Space Flight Center, Greenbelt, Maryland.* 34 pp.

Anderson, J. T., 1990. Seasonal development of invertebrate zooplankton on Flemish Cap. *Mar. Ecol. Prog. Ser.*, **67**: 127-140.

Angel, M. N., 1989. Vertical profiles of pelagic communities in the vicinity of the Azores Front (Atlantic Ocean) and their implications to deep ocean ecology. *Prog. in Oceanog.*, **22**: 1-46.

Archer, D. 1995. Upper ocean physics as relevant to ecosystem dynamics: a tutorial. *Ecological Applications*, **5**(3): 724-739

Backhaus, J. O., Harms, I. H., Krause, M., and Heath, M. R. 1994. An hypothesis concerning the space-time succession of *Calanus finmarchicus* in the northern North Sea. *ICES J. mar. Sci.*, **51**: 169-180

Balino, B. M., Fasham, M. J. R., Bowles, M.C., 2000. Ocean biogeochemistry and global change: JGOFS research highlights 1988-2000. *International Geosphere-Biosphere Programme, Stockholm.* 32pp.

Bamstedt, B., Karlson, K., 1998. Euphausiid predation on copepods in coastal waters of the Northeast Atlantic. *Mar. Ecol. Prog. Ser.*, **172**: 149-168.

Belkin, I. M., Levitus, S., Antonov, J., Malmberg, S. –A., 1998. "Great Salinity Anomalies" in the North Atlantic. *Prog. in Oceanog.*, **41**: 1-68.

Blumberg, A. F., and G. L. Mellor, 1987. A description of a three-dimensional coastal ocean circulation model, in *Three-Dimensional Coastal Ocean Models.* Edited by N. S. Heaps. *American Geophysical Union, Washington, D. C.* ix + 208pp.

Bryant, A.D., Heath, M., Gurney, W.S.G., Beare, D.J. & Robertson, W., 1997. The seasonal dynamics of *Calanus finmarchicus*: development of a three-dimensional structured population model and application to the northern North Sea. *J. Sea Res.*, **38**: 361-379.

Buchanan, R. A. and Browne, S. M., 1981. Zooplankton of the Labrador coast and shelf during summer 1979. *OLABS Program Report, LGL Ltd., St. John's, Canada.*

Campbell, R. W., and Head, E. J., 2000. Egg production rates of *Calanus finmarchicus* in the western North Atlantic: effect of gonad, maturity, female size, chlorophyll concentration, and temperature. *Can. J. Fish. Aquat. Sci.*, **57**: 518-529.

Carlotti, F., Sciandra, A., 1989. Population dynamics model of *Euterpina acutifrons* (Copepoda: Harpacticoida) coupling individual growth and larval development. *Mar. Ecol. Prog. Ser.*, **56**: 225-242

Carlotti, F., Nival P., 1992. Model of copepod growth and development: moulting and mortality in relation to physiological processes during an individual moult cycle. *Mar. Ecol. Prog. Ser.*, **84**: 219-233

Carlotii, F., Krause, M., Radach, G., 1993. Growth and development of *Calanus finmarchicus* related to the influence of temperature: Experimental results and conceptual model. *Limnol. Oceanog.*, **38**: 1125-1134

Carlotti, F., and G. Radach. 1996. Seasonal dynamics of phytoplankton and *Calanus finmarchicus* in the North Sea as revealed by a coupled one-dimensional model. *Limnol. Oceanog.*, **41**: 522-539.

Carlotti, F. and Wolf, K.-U., 1998. A Lagrangian ensemble model of *Calanus finmarchicus* coupled with a 1-D ecosystem model. *Fish. Oceanog.*, **7**: 191-204.

Carlotti, F., Giske, J., Werner, F., 2000. Modeling zooplankton dynamics. In *ICES zooplankton methodology manual.* Eds. Harris, R., Wiebe, P., Lenz, J., Skjodal, H. R., Huntley, M. *Academic Press, London.* xxi + 684pp.

Chapman, D. C. and Beardsley, R. C., 1989. On the origin of shelf water in the Middle Atlantic Bight. *J. Phys. Oceanog.*, **19**: 384-391.

Clarke, R. A., 1984. Transport through the Cape Farewell – Flemish Cap section. *Explor. Mer.*, **185**: 120-130

Clarke, R. A., and Gascard, J. C., 1983. The formation of Labrador Sea water. Part II: Mesoscale and smaller-scale processes. *J. Phys. Oceanog.*, **13**: 1779-1797.

Corkett, C. J., McLaren, I. A., Sévigny, J. M., 1986. The rearing of marine copepods *Calanus finmarchicus* (Gunnerus), *C. glacialis* (Jaschnov) and *C. hyperboreus* (Kroyer) with comment on the equiproportional rule (Copepoda). *Syllogeous Natl. Mus. Can.*, **58**: 539-546

Cuny, J., Rhines, P. B., Niler, P. P., Bacon, S., 2002. Labrador Sea boundary currents and the fate of the Irminger Sea water. *J. Phys. Oceanog.*, **32**: 627-647.

Davis, C. C., 1982. A preliminary quantitative study of the zooplankton from Conception Bay, Insular Newfoundland, Canada. *Int. Revue ges. Hydrobiol.*, **67**: 713-747.

Davis, C. C., 1986. A comparison of the zooplankton in two Newfoundland Bays with differing influences from major currents. *Int. Revue ges. Hydrobiol.*, **71**: 11-47.

Dickson, R. R., Meincke, J., Malmberg, S. –A., Lee, A. J., 1988. The "Great Salinity Anomaly" in the northern North Atlantic, 1968-1982. *Prog. in Oceanog.*, **20(2)**: 103-151.

Ducklow, H. W., Steinberg, D. K., Buesseler, K. O., 2001. Upper ocean carbon export and the biological pump. *Oceanography*, **14(4)**: 50-58

Feely, R. A., Sabine, C. L., Takahashi, T., Wanninkhof, R., 2001. Uptake and storage of carbon dioxide in the ocean: the global CO_2 survey. *Oceanography*, **14(4)**: 18-32

Frost, B. W., 1975. A threshold feeding behaviour in *Calanus pacificus*. *Limnol. Oceanog.*, **20**: 263-266.

Gallego, A., Mardaljevic, J., Heath, M. R., Hainbucher, D., Slagstad, D., 1999. A model of the spring migration into the North Sea by *Calanus finmarchicus* overwintering off the Scottish continental shelf. *Fish. Oceanog.* **8:** (*suppl. 1*), 107-125.

Harris, R. P., 1996. Feeding ecology of *Calanus*. *Ophelia,* **44**: 85-109.

Harris, R., Wiebe, P., Lenz, J., Skjodal, H. R., Huntley, M., 2000. ICES zooplankton methodology manual. *Academic Press, London.* xxi + 684pp.

Head, E. J. H., Harris, L. R., Campbell, R. W., 2000. Investigations on the ecology of *Calanus* spp. in the Labrador Sea. I. Relationship between the phytoplankton bloom and reproduction and development of *Calanus finmarchicus* in spring. *Mar. Ecol. Prog. Ser.*, **193**: 53-73

Head, E. H, Pepin, P., Runge, J., 2001. Proceedings of the workshop on "The Northwest Atlantic ecosystem – a basin scale approach". *CSAS Proceedings Series 2001/23.* 112 pp.

Heath, M., Robertson, W., Mardaljevic, J., Gurney, W.S.G., 1997. Modelling the population dynamics of *Calanus* in the Fair Isle Current off northern Scotland. *J. Sea Res.*, **38**: 381-412.

Heath, M. R., Backhaus, J. O., Richardson, K., McKenzie, E., Slagstad, D., Beare, D., Dunn, J., Fraser, J. G., Gallego, A., Hainbucher, D., Hay, S., Jónasdóttir, S., Madden, H.,

Mardaljevic, J., Schacht, A., 1999. Climate fluctuations and the spring invasion of the North Sea by *Calanus finmarchicus*. *Fish. Oceanog.*, **8:** (*suppl. 1*), 163-176.

Heath, M. R., Jónasdóttir, S. H., 1999. Distribution and abundance of overwintering *Calanus finmarchicus* in the Faroe-Shetland Channel. *Fish. Oceanog.*, **8**: (*suppl. 1)* 40-60.

Hirche, H. –J., 1987. Temperature and plankton. II. Effect on respiration and swimming activity in copepods from the Greenland Sea. *Mar. Biol.*, **94**: 347-356.

Hirche, H.-J., 1996. Diapause in the marine copepod *Calanus finmarhicus* – a review. *Ophelia*, **44**: 129-143.

Hooker, S.B., Esaias, W.E., Feldman, G. C., Gregg, W. W., and McClain, C. R., 1992. An Overview of SeaWiFS and Ocean Color. *NASA Tech. Memo.* 104566, Vol. **1**. S.B. Hooker and E.R. Firestone, Eds., *NASA Goddard Space Flight Center, Greenbelt, Maryland,* 24 pp., plus color plates.

Huntley, M and Boyd, C., 1984. Food-limited growth of marine zooplankton. *The American Naturalist*, **124**: 455-478.

Huntley, M., Strong, K. W., Dengler, A. T., 1983. Dynamics and community structure of zooplankton in the Davis Strait and Northern Labrador Sea. *Arctic*, **36**: 143-161

Huntley, M. E. and Lopez, M. D. G. 1992. Temperature-dependant production of marine copepods: A global synthesis. *The American Naturalist*, **140**: 201-242

ICNAF (International Commission for the Northwest Atlantic Fisheries), Environmental Surveys – NORWESTLANT 1-3, 1963. Special Publication No. **7**, 1968.

Jaschnov, W. A., 1970. Distribution of *Calanus* species in the seas of the northern hemisphere. *Int. Revue ges. Hydrobiol.*, **55**: 197-212.

Kaartvedt, S., 1996. Habitat preference during overwintering and timing of seasonal vertical migration of *Calanus finmarchicus*. *Ophelia,* **44**: 145-156.

Kalnay, E., Kanamitsu, M., Kistler, R., Collins, W., Deaven, D., Gandin, L., Iredell, M., Saha, S., White, G., Woollen, J., Zhu, Y., Chelliah, M., Ebisuzaki, W., Higgins, W., Janowiak, J., Mo, K. C. , Ropelewski, C., Wang, J., Leetmaa, A., Reynolds, R., Jenne, R., Joseph, D., 1996. The NCEP/NCAR 40-Year Reanalysis Project. *Bull. Amer. Meteor. Soc.,* **76**, 437-471.

Kattner, G. and Krause, M., 1987. Changes in lipids during the development of *Calanus finmarchicus* s.l. from copepodid I to adult. *Mar. Biol.*, **96**: 511-518.

Kielhorn, W. V., 1952. The biology of the surface zone zooplankton of a boreo-arctic Atlantic Ocean Area. *J. Fish. Res. Bd. Can.*, **9**: 223-264

Lazier, J. R. N., 1973. The renewal of Labrador Sea water. *Deep-Sea Res.*, **94**: 12,607-12,618

Lazier, J. R. N. 1980. Oceanographic conditions at Ocean Weather Ship Bravo, 1964-1974. *Atmos.-Ocean.* **18**: 227-238

Lazier, J. R. N. 1982. Seasonal variability of temperature and salinity in the Labrador Current. *J. Mar. Res*, **40**: 341-356

Lazier, J. R. N., 1994. Observations in the Northwest corner of the North Atlantic current. *J. Phys. Oceanog.*, **24**: 1449-1463

Lazier, J. R. N. and Wright, D. G., 1993. Annual velocity variations in the Labrador Current. *J. Phys. Oceanog.*, **23**: 659-678

Leggett, W. C., 1997. The ecology of migration. *Ann. rev. in ecology,* **8**: 285-308.

Loder, J. W., Boicourt, W. C., Simpson, J. H. 1998. Western ocean boundary shelves coastal segment (W). *The Sea*, **11**.

Lynch, D. R., Gentleman, W. C., McGillicuddy Jr., D., Davis, C. S., 1998. Biological/physical simulations of *Calanus finmarchicus* population dynamics in the Gulf of Maine. *Mar. Ecol. Prog. Ser.*, **169**: 189-210.

Mann, K. H. and Lazier, J. R. N., 1996. Dynamics of marine ecosystems: biological physical interactions in the oceans. *Blackwell Science, Boston.* 394 pp.

Marra, J. and Ho, C., 1993: Initiation of the spring bloom in the northeast Atlantic (47°N, 20°W): a numerical simulation, *Deep-Sea Res. II,* **40**: 55-73.

Marshall, S.M. and Orr, A.P, 1955: The biology of a marine copepod, *Calanus finmarchicus* (Gunnerus). *Oliver & Boyd, Edinburgh.* 188 pp.

Marshall, J., Dobson, F., Moore, K., Rhines, P., Visbeck, M., d'Asaro, E., Bumke, K., Chang, S., Davis, R., Fischer, K., Garwood, R., Guest, P., Harcourt, R., Herbaut, C., Holt, T., Lazier, J., Legg, S., McWilliams, J., Pickart, R., Prater, M., Renfrew, I., Schott, F., Send, U., Smethie, W., 1998. The Labrador Deep Sea Convection Experiment. *Bull. Amer. Met. Soc.*, **79**: 2033-2058.

Matthews, J. B. L., 1968. On the acclimatization of *Calanus finmarchicus* (Crustacea, copepoda) to different temperature conditions in the North Atlantic. *Sarsia*, **34**: 371-382.

Mauchline, J., 1998. The biology of calanoid copepods. Academic Press, San Diego, California. x + 709 pp.

McClain, C.R., Esaias, W. E., Barnes, W., Guenther, B., Endres, D., Hooker, S., Mitchell, G., and Barnes, R., 1992: Calibration and Validation Plan for SeaWiFS. *NASA Tech. Memo.* 104566, Vol. **3**. S.B. Hooker and E.R. Firestone, Eds., *NASA Goddard Space Flight Center, Greenbelt, Maryland*, 41 pp.

McLaren, I. A., 1986. Is structural growth of *Calanus* potentially exponential? *Limnol. Oceanog.*, **31**: 1342-1346.

McLaren, I. A., Corkett, C. J., 1986. Life cycles and production of two copepods on the Scotian shelf, eastern Canada. *Nat. Mus. Can. Syllogeus*, **58**: 362-367.

McLaren, I., Tremblay, M. J., Corkett, C. J., Roff, J. C., 1989. Copepod production on the Scotian Shelf based on life-history analyses and laboratory rearings. *Can. J. Fish. Aquat. Sci.*, **46**: 560-583.

Mellor, G. L., 1996. User's guide for a three-dimensional primitive equation, numerical ocean model. *Atmos. and Oceanic Sci. Program, Princeton Univ., Princeton, N. J.* 35pp.

Miller, C. B., Cowles, T. J., Wiebe, P. H., Copley, N. J., and Grigg, H., 1991. Phenology in *Calanus finmarchicus* (Gunnerus); hypotheses about control mechanisms. *Mar. Ecol. Prog. Ser.* **72**: 79-91.

Miller, C. B. and Tande, K. S., 1993. Stage duration estimation for *Calanus* populations, a modelling study. *Mar. Ecol. Prog. Ser.*, **102**: 15-34.

Miller, C. B., D. R. Lynch, F. Carlotti, W. Gentleman and C. V. W. Lewis, 1998. Coupling of an individual-based population dynamics model of *Calanus finmarchicus* to a circulation model for the Georges Bank region. *Fish. Oceanog.*, **7**: 219-234.

Myers, R. A., N. J. Barrowman, G. Mertz, J. Gamble and H. G. Hunt., 1994. Analysis of Continuous Plankton Recorder Data in the Northwest Atlantic 1959-1992. *Can. Tech. Rep. Fish. Aquat. Sci.*1966: iii + 246pp.

Oberhuber, J. M., 1993: Simulation of the Atlantic circulation with a coupled sea ice-mixed layers-isopycnal general circulation model. Part II: Model experiment. *J. Phys. Oceanog.*, **23**: 830-845.

Ohman, M. D., and Runge, J. A., 1994: Sustained fecundity when phytoplankton resources are in short supply: Omnivory by *Calanus finmarchicus* in the Gulf of St. Lawrence. *Limnol. Oceanog.*, **39**: 21-36.

Petrie, B., and Mason, C. S., 2000. Satellite measurements of sea surface temperature: an application to regional ocean climate. *Canadian Stock Assessment Secretariat Research Document 2000/061.*

Planque, B. 1997. Spatial and temporal fluctuations in *Calanus* populations sampled by the Continuous Plankton Recorder. *PhD thesis, Universite Pierre et Marie Curie (Paris VI).*

Planque, B., Hays, G. C., Ibanez, F., Gamble, J. C., 1997. Large scale spatial variations in the seasonal abundance of *Calanus finmarchicus. Deep-Sea Res.*, **44**: 315-326

Price, J.F., Weller, R.A., and Pinkel, R., 1986: Diurnal cycling: observations and models of the upper ocean response to diurnal heating, cooling and wind mixing, *J. Geophys. Res.*, **91**, 8411-8427

Runge, J. A., Castonguay, M., De LaFountaine, Y., Ringuette, M. Beaulieu, J. L., 1999. Covariation in climate, zooplankton biomass and mackerel recruitment in the southern Gulf of St. Lawrence. *Fish. Oceanog.*, **8**:2 139-149

Sameoto, D., 1988. The feeding ecology of the lantern fish, *Benthosema glaciale* off the coast of Nova Scoatia. *Mar. Ecol. Prog. Ser.*, **44**: 113-129.

Sameoto, D., 1989. Feeding ecology of the lantern fish *Benthosema glaciale* in a subarctic region. *Polar Biol.*, **9**: 169-178.

Slagstad, D., Tande, K. S., 1996. The importance of seasonal vertical migration in across shelf transport of *Calanus finmarchicus. Ophelia*, **44**: 189-205.

Smith, S. D., 1988. Coefficients of sea surface wind stress, heat flux, and wind profiles as a function of wind speed and temperature. *J. Geophys. Res.*, **93**: 15,467-15,472.

Smith, S. D., and Dobson, F. W., 1984: The heat budget at Ocean Weather Station Bravo. *Atmos.-Ocean*, **22**: 1-22.

Stuart. V., S. Sathyendranath, E. J. H. Head, T. Platt, B. Irwin. H. Maass., 2000. Bio-optical characteristics of diatom and prymnesiophyte populations in the Labrador Sea. *Mar. Ecol. Prog. Ser.*, **201**: 91-106

Sullivan, B. K., Meise, C. J., 1996. Invertebrate predators of zooplankton on Georges Bank, 1977-1987. *Deep-Sea Res. II*, **43**: 1503-1519.

Tang, C.L. and Wang, C. K., 1996. A gridded data set of temperature and salinity for the Northwest Atlantic ocean. *Can. Data Rep. Hydrogr. Ocean Sci.*, **148**: iv + 45pp.

Tang, C. L., Gui, Q., deTracey, B. M. 1999 A modeling study of upper ocean winter processes in the Labrador Sea. *J. Geophys. Res.*, **104**: 23,411-23,425

Trela, P., 1996. Effect of spatial and temporal variability in oceanic processes on air-sea fluxes of carbon dioxide. *PhD Thesis, Dalhousie University, Halifax.* xvii + 221pp.

Trela, P., deYoung, B., Evans, G., 2002. A weight-class population model for mesozooplankton with a linear weight distribution within class. *Subm. Fish. Oceanog.*

Yao, T., Tang, C. L., Peterson, I. K., 2002. Modeling the seasonal variation of sea ice in the Labrador Sea with a coupled multicategory ice model and the Princeton Ocean model. *J. Geophys. Res.*, **105**: 1153-1165

Zakardjian, B. A., Runge, J. A., Plourde, S., Sheng, J., McLaren, I., Gratton, Y., Thompson, K. R., 2002. Modelling the life-history of *Calanus finmarchicus* in eastern Canadian waters: application of a stage-based model. *Subm. Can. J. Fish. Aquat. Sci.*